Cosmic Research, Vol. 42, No. 5, 2004, pp. 435–488. Translated from Kosmicheskie Issledovaniya, Vol. 42, No. 5, 2004, pp. 453–508.

Solar and Heliospheric Phenomena in October–November 2003: Causes and Effects

I. S. Veselovsky[1], M. I. Panasyuk[1], S. I. Avdyushin[2], G. A. Bazilevskaya[3], A. V. Belov[4], S. A. Bogachev[3], V. M. Bogod[5], A. V. Bogomolov[1], V. Bothmer[6], K. A. Boyarchuk[4], E. V. Vashenyuk[7], V. I. Vlasov[8], A. A. Gnezdilov[4], R. V. Gorgutsa[4], V. V. Grechnev[9], Yu. I. Denisov[1], A. V. Dmitriev[1, 10], M. Dryer[11], Yu. I. Yermolaev[12], E. A. Eroshenko[4], G. A. Zherebtsov[9], I. A. Zhitnik[3], A. N. Zhukov[1, 13], G. N. Zastenker[12], L. M. Zelenyi[12], M. A. Zeldovich[1], G. S. Ivanov-Kholodnyi[4], A. P. Ignat'ev[3], V. N. Ishkov[4], O. P. Kolomiytsev[1], I. A. Krasheninnikov[4], K. Kudela[14], B. M. Kuzhevsky[1], S. V. Kuzin[3], V. D. Kuznetsov[4], S. N. Kuznetsov[1], V. G. Kurt[1], L. L. Lazutin, L. N. Leshchenko[4], M. L. Litvak[12], Yu. I. Logachev[1], G. Lawrence[13], A. K. Markeev[4], V. S. Makhmutov[3], A. V. Mitrofanov[3], I. G. Mitrofanov[12], O. V. Morozov[1], I. N. Myagkova[1], A. A. Nusinov[2], S. N. Oparin[3], O. A. Panasenco[1], A. A. Pertsov[3], A. A. Petrukovich[12], A. N. Podorol'sky[1], E. P. Romashets[4], S. I. Svertilov[1], P. M. Svidsky[2], A. K. Svirzhevskaya[3], N. S. Svirzhevsky[3], V. A. Slemzin[3], Z. Smith[11], I. I. Sobel'man[3], D. E. Sobolev[4], Yu. I. Stozhkov[3], A. V. Suvorova[1], N. K. Sukhodrev[3], I. P. Tindo[3†], S. Kh. Tokhchukova[15], V. V. Fomichev[4], I. V. Chashey[8], I. M. Chertok[4], V. I. Shishov[8], B. Yu. Yushkov[1], O. S. Yakovchouk[1], and V. G. Yanke[4]

[1] *Skobeltsyn Institute of Nuclear Physics, Moscow State University, Moscow, Russia*
[2] *Fedorov Institute of Applied Geophysics, Moscow*
[3] *Lebedev Physical Institute, Russian Academy of Sciences, Moscow, Russia*
[4] *Institute of Terrestrial Magnetism, Ionosphere, and Radio Wave Propagation (IZMIRAN), Troitsk, Moscow oblast, Russia*
[5] *Special Astrophysical Observatory, Russian Academy of Sciences, Nizhni Arkhyz, Russia*
[6] *Max-Planck Institut fur Sonnensystemforschung, Katlenburg-Lindau, Germany*
[7] *Polar Geophysical Institute, Kola Science Center, Russian Academy of Sciences, Apatity, Russia*
[8] *Pushchino Observatory, Astro Space Center, Lebedev Physical Institute, Russian Academy of Sciences, Pushchino, Russia*
[9] *Institute of Solar-Terrestrial Physics, Siberian Branch of Russian Academy of Sciences, Irkutsk, Russia*
[10] *Institute of Space Science, Jungli, Taiwan*
[11] *Space Environment Center, Boulder, USA*
[12] *Space Research Institute, Russian Academy of Sciences, Moscow, Russia*
[13] *Observatoire Royal de Belgique, Bruxelles, Belgium*
[14] *Institute of Experimental Physics of the Slovak Academy of Sciences, Košice, Slovakia*
[15] *Main (Pulkovo) Astronomical Observatory, Russian Academy of Sciences, Pulkovo, Russia*

Received May 19, 2004

Abstract—We present new observational data on the phenomena of extremely high activity on the Sun and in the heliosphere that took place in October–November 2003. A large variety of solar and heliospheric parameters give evidence that the interval under consideration is unique over the entire observation time. Based on these data, comparing them with similar situations in the past and using available theoretical concepts, we discuss possible cause-and-effect connections between the processes observed. The paper includes the first results and conclusions derived by the collaboration "Solar Extreme Events-2003" organized in Russia for detailed investigations of these events. As a result of our consideration, it is beyond question that the physical causes of solar and heliospheric phenomena in October–November 2003 are not exclusively local and do not belong only to the active regions and solar atmosphere above them. The energy reservoirs and driving forces of these processes have a more global nature. In general, they are hidden from an observer, since ultimately their sources lie in the subphotospheric layers of the Sun, where changes that are fast and difficult to predict can sometimes take place (and indeed they do). Solar flares can serve as sufficiently good tracers of these sudden changes and reconstructions on the Sun, although one can still find other diagnostic indicators among the parameters of magnetic fields, motions of matter, and emission characteristics.

† Deceased.

0010-9525/04/4205-0435 © 2004 MAIK "Nauka/Interperiodica"

1. INTRODUCTION

The goal of this paper is to present and discuss new observational data about various phenomena of extremely high activity on the Sun and in the heliosphere that took place in October–November 2003. Comparing these data with the facts known earlier, one can find certain features of similarity and distinction with other similar periods in several preceding cycles of solar activity. This makes it possible to consider both well established regularities and hypotheses about the nature of these phenomena, as well as about their influence on the processes in the near-Earth space.

Below, we present the information about the phenomena observed on the Sun and in the heliosphere at the declining phase of the 23rd solar cycle in October–November 2003. During this period a quick evolution of the global and local activity occurred and was observed on the entire solar surface and above it. The most significant changes and powerful active regions were concentrated mainly on one side of the Sun which was most fully turned to the Earth on October 26 and November 18. Very strong coronal mass ejections (CME) were detected in October–November, as well as numerous solar flares including those with the highest X-ray importance. Complex plasma and magnetic disturbances were formed after that in the solar wind: some of them reached the Earth and had an effect on the magnetosphere, while others passed far from it. A series of CMEs detected on October 28–30 by the instruments onboard the space observatories *SOHO* and *Coronas-F* close to the central solar meridian near the active region no. 10486 was an immediate cause of interplanetary transients and shock waves that reached the Earth in 1–2 days carrying strong electric fields and currents with them. It is precisely this fact that resulted in the development of geomagnetic storms on October 29–31 in three stages. One solar rotation later, on November 20 another strong geomagnetic storm occurred, now a single storm. It was initiated by CME generated at the same regions of the Sun on November 18 and approached the Earth on November 20. Therefore, this geomagnetic disturbance should be classified simultaneously both as recurrent and as a sporadic disturbance. Other events on the Sun in the time interval under consideration turned out to be not so efficient in the sense of generation of geomagnetic storms. This occurred either because their sources on the Sun were located far from the central meridian or because of the geometry of heliospheric magnetic fields that had at this time predominantly positive north–south component. For example, the extremely strong eruptive phenomenon on November 4, with a CME, a record X-ray burst, and a huge post-eruptive arcade on the western limb generated only a relatively weak geomagnetic disturbance. However, acceleration of charged particles to very high energies and the strong electromagnetic and neutron emission accompanying it were reliably detected for this event and some others within this time interval both on the ground and onboard various spacecraft.

The introduction, discussion, and conclusions of this paper are written by I.S. Veselovsky. The final version of the full text was prepared by him with assistance of other coauthors. The idea of establishing a collaboration to study solar-terrestrial links during the considered strongly disturbed period and to write the joint papers belongs to M.I. Panasyuk, who also convened discussions and workshops on this topic. The contents of all chapters of this paper were prepared either individually by authors and groups of authors or jointly on the basis of materials presented by different institutes. It should be particularly emphasized that the researchers of the Institute of Terrestrial Magnetism, Ionosphere, and Radio Wave Propagation (IZMIRAN) made decisive contribution to sections 2, 7, and 14. The scientists from Special Astrophysical Observatory (Nizhni Novgorod) and Main Astronomical Observatory (Pulkovo) endowed basically to section 6. It is pertinent to note that in so large and diverse paper with many coauthors one can find some results, interpretation statements, and conclusions that are not shared by all collaborators and rather represent the point of view of some authors or groups of authors. We did not consider necessary to avoid such debatable issues, moreover, we tried to elaborate a common point of view as far as it was possible. Nevertheless, the first author is responsible for all possible mistakes and inexact formulations made in the text.

2. COMPARATIVE RETROSPECTIVE DESCRIPTION OF SOLAR ACTIVITY FOR THE PERIOD UNDER CONSIDERATION

The events somewhat similar to those considered in this paper occurred also on the declining phase of the 20th solar activity cycle in August 1972. At that time four very strong solar flares (of importance 2B and 3B) occurred within a very short period (August 2, 4, and 7), and three strong interplanetary shock waves arrived at the Earth. These events were among the first detected since the space exploration era had began that were comparatively well documented. This was done using direct measurements in the interplanetary medium, including first of all the data of the satellites *Prognoz* and *Prognoz-2*, and of the *HEOS-2* and *Pioneer-9* spacecraft [1]. When the data set obtained in 1972 was analyzed, the emphasis was made on the determination of characteristics of shock waves: their shape, instantaneous and mean velocity, the character of deceleration, and the behavior of solar wind and IMF parameters on the fronts and behind them. Also, a very important achievement of this analysis was the fact that the energy (potential, kinetic, thermal, and magnetic) of each shock wave was estimated. This energy was released during the flare in the form of an ejection of a certain amount of matter into the interplanetary medium. For the flare of August 4, 1972 the record estimates were

obtained: the energy flux was about 100 erg/cm^2, ejected mass was 10^{17} g, and the released energy was about 10^{33} erg. Due to a certain malfunction of instruments onboard several spacecraft and some other limitations to make similar estimations for the events in October–November 2003 is more complicated task. The events of August 1972 were also multiple (the entire sequence of four strong flares covered an interval of three days), as the events in the end of October 2003. However, they were certainly much worse studied as far as observations of the Sun are concerned (at that time there were no observations of CMEs using the space-based coronograph, and so on). The closest analogy can be pointed out between the flare at 06:21 UT on August 4, 1972 and the flare at 10:02 UT on October 28, 2003. In the first event a shock wave arrived at the Earth in 14.5 h, after which the velocity and density of the solar wind increased up to ~2000 km/s and ~30 cm^{-3}, respectively. In the second event the shock wave reached the Earth in 19 h, and the velocity and density of the solar wind increased to 2100–2400 km/s and ~15 cm^{-3}, respectively. Further study will allow one to make this analogy deeper as far as both the solar origin of the interplanetary disturbance and its geoeffectiveness are concerned.

The solar activity in all its manifestations is subject to regular and irregular chaotic variations in quite large ranges of amplitudes, durations, and other characteristics that have revealed themselves some way in the time interval under analysis. This general rule does not exclude coronal mass ejections and flares, which represent with respect to each other not the cause and effect (sometimes, such an unjustified assumption is made), but rather two observable manifestations of a single dissipative process related to an increased transport of free energy from the interiors of the Sun outwards into its upper atmosphere and heliosphere (see, for example, a discussion and references in [2]). This free energy is redistributed in thermal, magnetic, kinetic, gravitational, and radiation forms, their relative fractions being changed from event to event depending on the situation determined by the boundary conditions and initial data.

It is well known that the periods when flare and eruptive activity of the Sun sharply increases are observed, as a rule, during the years near the solar cycle maximum determined as usual by the sunspot number. Rather frequently, it is in this time that the largest concentration of strong flares and eruptions over the entire cycle is observed. In this case, one or two powerful and quickly developed active regions used to appear, being record in producing flares and CMEs, and providing for the most powerful energy release over the entire cycle. Sometimes, these periods coincide with the first years of decrease after the solar maximum. The well-known events of November 1960 in the 19th cycle, of August 1972 in the 20th cycle, and of June–July 1982 in the 21st cycle can serve as examples. This also took place in the current 23rd cycle. But one cannot say so far about some firmly established rules without exceptions (because of small statistic of observations and a strong instability of all cyclic manifestations on the Sun). For example, the strongest flares in the 22nd cycle occurred at the phase of maximum (March 1989 and June 1991), while no flares of X class occurred at the declining phase of the cycle after November 1992.

These facts are well known, and they indicate to existence of rather strong and unstable quasi-biennial variations which lead to the non-monotone behavior and so-called Gnevyshev gap, i.e., to double-peak maxima of activity. Below, we present a somewhat more detailed comparative description of the solar flare events over the past few years in order to define the usual and specific conditions in this respect.

For the sake of comparison of the flare productivity of active regions, it would be very useful to have long series of absolutely calibrated measurements of energy and power. Since they do not exist, sometimes the index XRI introduced by P. McIntosh is used, which is determined as the total power of all flares of classes X and M in the range of soft X-rays (1–12.5 keV) (see http://www.jps.gov.au/Main.php?CatID=8). The flares of class X are taken with the unity weight (for example, a flare X1.5 gives a value of 1.5), while the flares of class M make a contribution one order of magnitude less (for example, a flare M3.2 gives a value of 0.32). Throughout the entire time of observations of the Sun in this range (from 1970 until October 2003) the largest XRI index was obtained for two active regions of the 22nd cycle of solar activity: active regions AR6659 of June 1991 (> 86.5) and AR5395 of March 1989 (>55.5). In the time interval of October–November 2003 considered here the XRI index was estimated as 5.73 for AR10484. It was within the limits from > 62.56 (taking the threshold of saturation into account) up to 73.06 (if importance is X28) for AR10486 and reached a value of 8.57 for AR10488.

It should be emphasized that the instruments installed onboard various satellites of the *GOES* series in order to measure the flux of soft X-ray emission in the above-indicated range have different thresholds of saturation. In this case, the X-ray importance is determined for flares in a somewhat conventional manner, proportionally to the time during which the instrument was blocked. Until 1976 the threshold of instrument saturation corresponded to the X-ray importance X5.1; therefore, the famous flares on August 4 and 7, 1972 had formally the importance X > 5.1. Before the beginning of operation of the geosynchronous satellite *GEOS-9* (April 1996) the threshold corresponded to the X-ray importance X12.5, and after that, in the 23rd solar cycle, the threshold has increased up to X17.5. Therefore, it would be more objective to characterize the X-ray importance of such flares with saturation not only by the threshold value of an instrument, but by the duration of instrument blocking as well. The extrapola-

tion of the X-ray flux for very strong flares with long saturation is hardly justifiable.

Nevertheless, it is quite probable that in accordance with such an estimate the X-ray flares on June 1 and 6, 1991 were the most intense throughout the entire time of observation. The time of instrument blocking was as long as 26 min, and for three more flares of the same active region it reached ≥17 min. This was well understood by the researchers who first obtained the data on these flares, and all of them were remained with X > 12.5 but specifying the time of blocking for the X-ray photometer [4]. Unfortunately, in the literature one cannot find such data for every strong flare, and in the majority of cases only the estimated X-ray importance is given for such flares.

According to its characteristics, the current 23rd cycle of solar activity belongs to the cycles of moderate intensity. In the course of 7.5 years of its development only four flares with the X-ray importance X ≥ 10 have been observed, while only in June 1991 five such flares occurred. Three out of four flares took place in the period of the strongest concentration (October 19–November 5, 2003) of flare activity of the current cycle, when at once three large flare-active groups of sunspots passed across the visible solar disk: one in the southern hemisphere (the group of sunspots no. 10486 with the largest area in the current cycle of solar activity) and two in the northern hemisphere (nos. 10484 and 10488).

The flare-active period in October–November 2003 began with an appearance (from behind the eastern limb on October 17) and rapid development during the first days of a group of sunspots AR10484 (N05L353, the second rotation of AR10464). On the second day (October 19) the first flare of importance X1.1/1N occurred in this region. Until October 26 only moderate flares of importance not higher than M were observed here. After emergence of a new powerful magnetic flux on October 26 that increased the area of AR10484 up to 1700 millionth fractions of solar hemisphere (m.f.s.h.), two more very strong flares (X1.2/2N and M7.6/2N) occurred in this region, after which it went behind the western limb of the Sun in its full development (on October 29). Observations with a sufficiently high spatial and temporal resolution carried out by ground-based and space observatories *Coronas-F* (orbit height 507 ± 21 km, inclination 82.5°, period of rotation 94.5 min), *SOHO*, and *TRACE*, and movies produced on this basis allowed one to trace the development of active regions, brightness variations, and motions in the solar atmosphere at all levels from the photosphere up to the uppermost regions of the solar corona. Powerful CMEs accompanied these phenomena and propagated into the heliosphere. The consequences of some of these events in the sense of arrival at the Earth of solar wind streams and magnetic clouds with a field orientation necessary for generation of strong magnetic storms and accelerated particles turned out to be not always so spectacular as for other similar events. This was the case for purely geometrical reasons, because of specific features in the field structure and its predominantly northern orientation at this time. However, in other cases the conditions were more favorable. Then, powerful fluxes of energetic particles and strong geomagnetic storms were observed on the Earth.

The time behavior of the short-wave emission of the Sun in the period of maximum solar activity of October 2003 is presented in Fig. 1 for three spectral ranges: 175 ± 3 Å, 8.42 Å (the data of *Coronas-F*/SPIRIT), and 1–8 Å (the data of *GOES*). The plots demonstrate a good similarity, though there are some significant distinctions. For example, the flares on October 22 and 26, detected as rather strong in the range of 175 Å, are observed as much weaker in the harder spectral region.

After the exit to the visible solar disk of the active region AR10486 (S16 L286), which developed into a large group of sunspots being still in the invisible side of the Sun, the flares X5.4/1B and X1.1/1N occurred in it already on October 23, and then a flare M7.6/1N occurred on October 24. The first observed emergence of a powerful magnetic flux occurred in this region on October 24–25, which increased the area of the sunspot group by 800 m.f.s.h. (S_p = 2200 m.f.s.h.). As a consequence, the flares X1.2/3B (on October 26), and M5.0/1F and M6.7/1F (on October 27) occurred. The emergence of the next new magnetic flux on October 27–28 increased the area of this sunspot group up to S_p =2610 m.f.s.h. (a record value in the current cycle) and allowed a flare X17.2/4B to occur on October 28. The flux of emission in the line 8.42 Å of MgXII measured by SPIRIT comprised 1.3×10^{-2} erg cm^{-2} s^{-1}. Taking into account the width of the spectral band (~5×10^{-3} Å) for observation in this channel the spectral density of the flux exceeds the value obtained by *GOES* (1.7 erg cm^{-2} s^{-1}) by almost an order of magnitude. Propagating heliospheric disturbances caused by preceding eruptive events, upon reaching the Earth, generated a magnetic storm on October 28. When the disturbance from the last CME arrived, this storm developed into a very strong (G5,$|D_{st}|$ > 200 nT) storm, one of the strongest in the current magnetic cycle. Energetic solar protons were emitted during the same eruptive flare into the interplanetary space, and they caused there a solar proton event of class S4 with intensity 29500 p.f.u. (the number of protons with energies > 10 MeV on 1 cm^2 per one second in one steradian).

The next period of strong eruptive and flare energy release in this active region began on November 2 by a flare X8.3/2B and continued on November 4 by a flare which was in the current cycle the most intensive in the flux of soft X-rays. The importance of this flare was X > 17.5/3B (τ = 12 min, calculated importance X28). These flares occurred near the western limb of the Sun. Therefore, they had no significant effect on the geomagnetic conditions, though solar proton events of S3

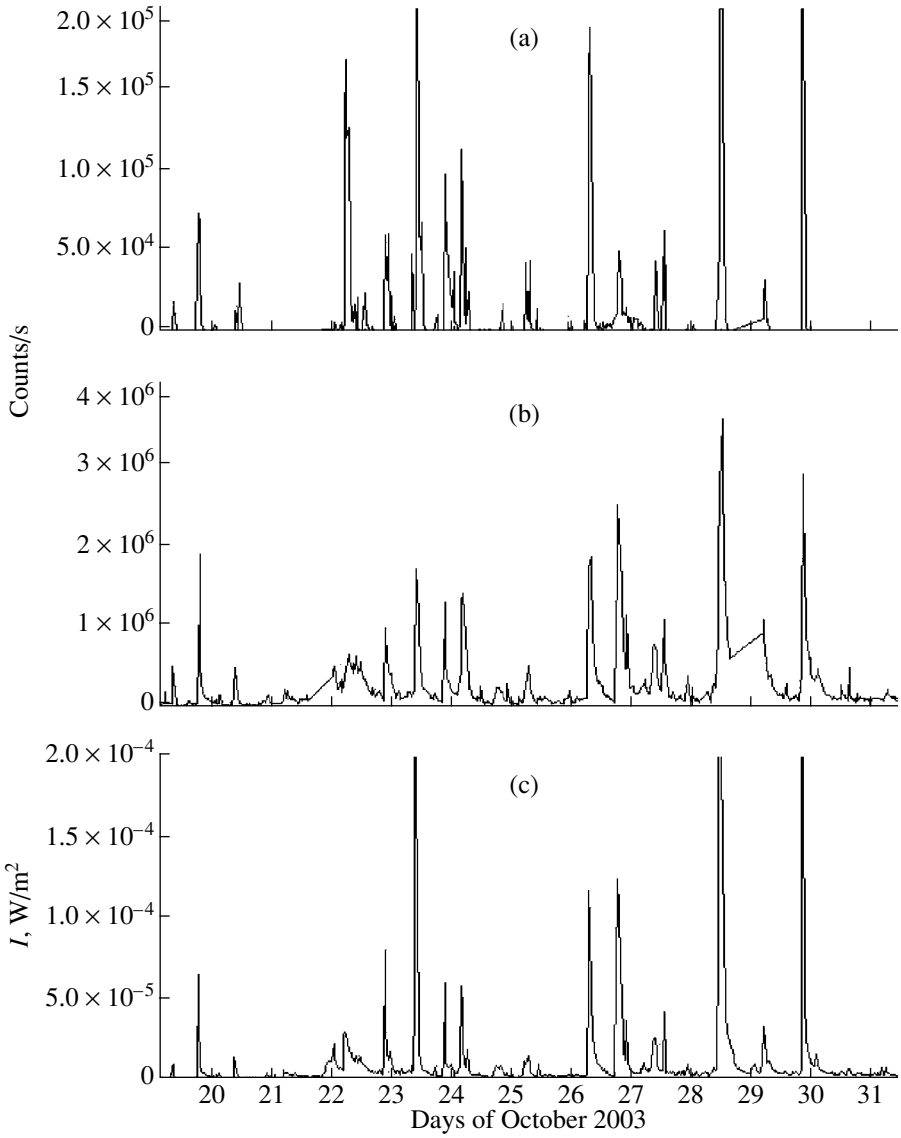

Fig. 1. Time behavior of short-wave emission in the period of strong flares of October 2003 in the wavebands (a) 175 Å ± 3 Å (*Coronas-F*/SPIRIT), (b) 8.42 Å (the line Mg XII, *Coronas-F*/SPIRIT), and (c) 1–8 Å (*GOES-12)*.

and S2 classes took place (with maximums on November 2 and 4, respectively).

The active region AR10488 (N09 L292) was formed on October 27 in the central part of the solar disk. In spite of its rapid development, it generated only modest flares, and on November 3 two flares X2.7/2B and X3.9/2F occurred in it. In total, for 16 days in 3 active regions 16 strong flares occurred, 11 of them had X-ray importance X.

The flare period in the middle of November was associated with the active region AR10501 (N05 L012, the next rotation of AR10484). It began on November 17 and continued for 94 h. In this period two strong flares and five flares of middle importance M occurred in the active region. The eruptive flare event of optical importance 2N on November 18 had the strongest impact on the near-Earth space. In the course of its development two X-ray bursts M3.2 and M3.9 with powerful CMEs took place. Reaching the Earth's vicinity the disturbances from these eruptive events generated one of the strongest magnetic storms (intensity G5) of the current solar cycle.

When considering eruptive events and solar flares, one cannot lose sight of the following circumstance. The origination and development of these strongest processes of energy release in the solar atmosphere are in the final analysis related to arrival of free energy from the subphotosphere layers and its redistribution. Observations of pre-flare situations on the Sun unequivocally indicate that frequently used conceptions of eruptive and flare events as initiated exclusively

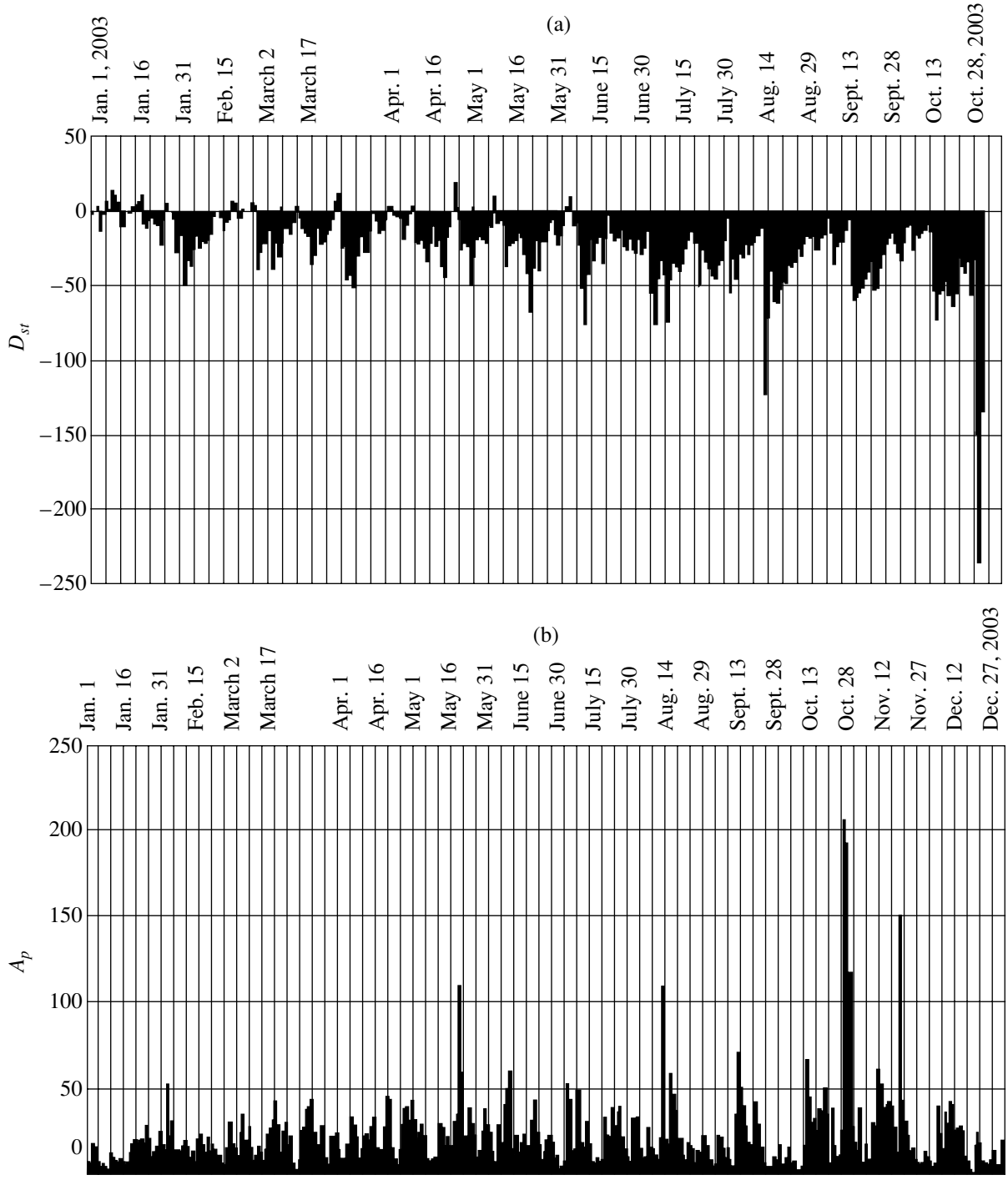

Fig. 2. Mean daily values of the D_{st} index (a) and A_p index (b) of geomagnetic activity in 2003.

by some instability and release of free energy pre-accumulated in the solar corona are insufficient.

Not denying the complexity and importance of consideration of these coronal processes, one should take into account that the strongest CMEs and solar flares often accompany each other and without exceptions take place because of and after the appearance of quite specific changes in plasma and magnetic fields at the photospheric level. This unequivocally testifies an important role of energy "signals from below." In this case the arrival of additional free energy from interior of the Sun plays a key physical role. It is quite understandable that for the most powerful phenomena both plasma and electromagnetic channels of energy release turn out to be open to one extent or another: we see both

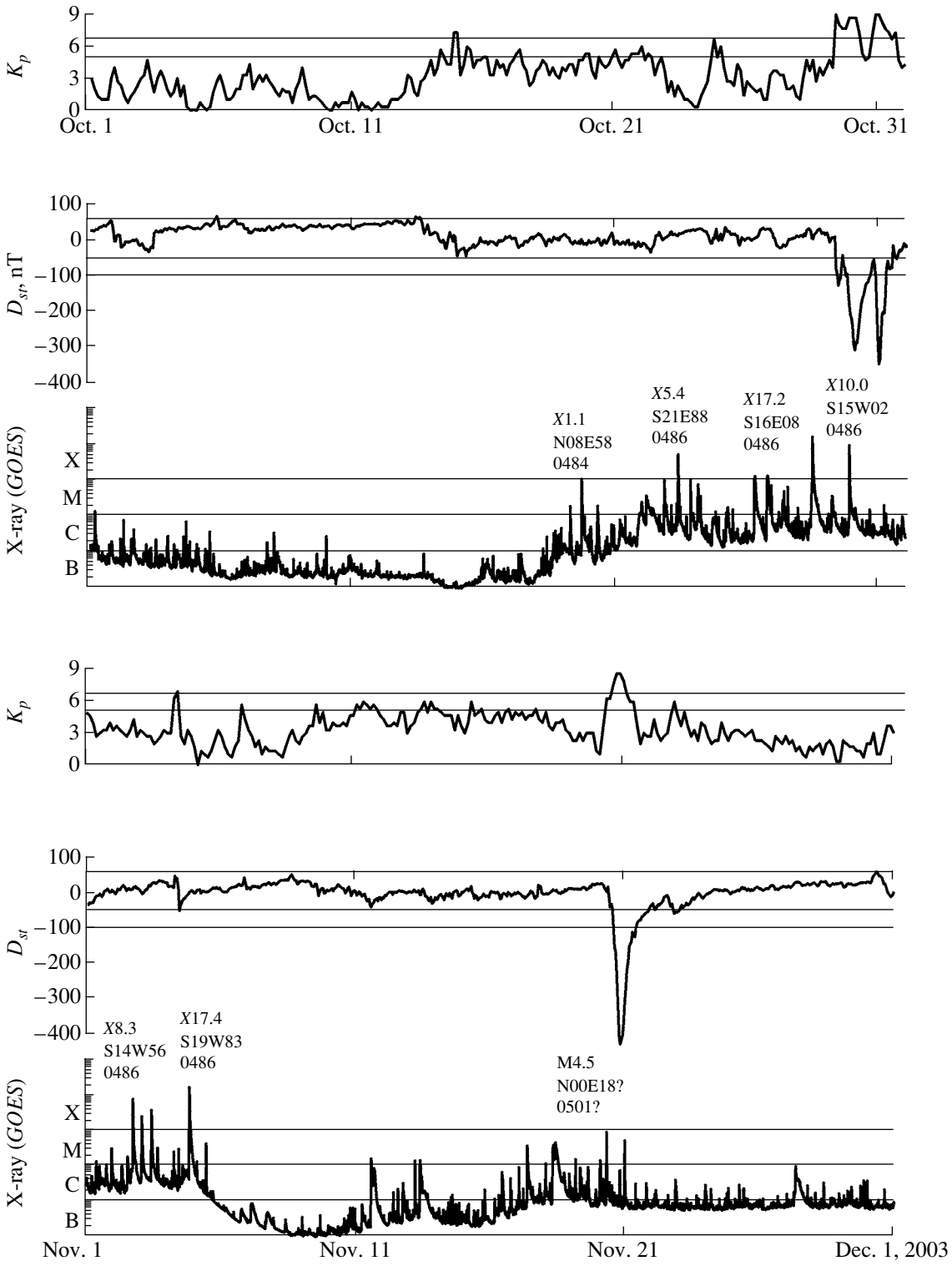

Fig. 3. The sequence of strong disturbances on the Sun and on the Earth in October (three upper panels) and November (three lower panels) 2003. From top to bottom in three panels are presented the K_p and D_{st} indices of geomagnetic activity, and X-ray emission measured by *GOES-12* (letters with figures designate the class of flares). The X-ray importance and coordinates on the sphere are given for some flares.

Table 1. The most significant and geoeffective solar flares and phenomena associated with them in the near-Earth space

Date	Onset, UT	Duration, min	Coordinates	Importance	I_{RB}	P_r p f u	I_{Pr}	Magnetic storms	I_{ms}
Oct. 19	16:29	79	N06 E58	X1.1/1N	R3				
Oct. 22	19:45	>41	S20 E90	M9.9	R2				
Oct. 23	08:17	64	S21 E88	X5.4/1B	R3				
Oct. 23	19:50	38	S17 E84	X1.1/1N	R3				
Oct. 24	02:22	66	S19 E72	M7.6/1N	R2				
Oct. 26	05:17	213	S17 E38	X1.2/3B	R3	323	S2	W Oct. 28	G1
Oct. 26	17:17	179	N02 W38	X1.2/1N	R3	466	S2	W Oct. 28	G1
Oct. 26	21:26	60	N01 W38	M7.6/2N	R2				
Oct. 27	09:21	23	S16 E26	M5.0/1F	R2				
Oct. 27	12:27	37	S17 E25	M6.7/1F	R2				
Oct. 28	09:51	>269	S16 E08	X17.2/4B	R5	29500	S4	VS Oct. 29–30	G5
Oct. 29	20:37	136	S15 W02	X10.0/2B	R4	330	S2	VS Oct. 31	G4
Nov. 2	17:03	171	S14 W56	X8.3/2B	R3	1540	S3	W Nov. 4	G2
Nov. 3	01:06	91	N10 W83	X2.7/2B	R3				
Nov. 3	09:43	>36	N08 W77	X3.9/2F	R3				
Nov. 4	19:29	80	S19 W83	X28/3B	R5	353	S2		
Nov. 5	10:46	>12	S16 W90	M5.3/SF	R2				
Nov. 18	07:16	159	N00 E18	2N/M3.2/M3.9	R1			VS Nov. 20–21	G5
Nov. 20	07:35	61	N01 W08	M9.6/2B	R2	10	S1	Nov. 22	G1
Nov. 20	23:42	.16	N00 W17	M5.8/2N	R2				

mass ejection and bright flare. The sensitivity and thresholds of their detection by corresponding instruments are such that CMEs usually look as longer events, especially if we turn our attention to images in the field of view of the LASCO/C3 coronograph within 30 solar radii. As for the flares which sometimes are seen in white light and in harder chromosphere and coronal emissions, as a rule, they look as shorter phenomena, though a somewhat subjective partition into impulsive (minutes) and long (hours) events is also used for them. Impulsive flares are more compact in space and take place usually at lower altitudes. Therefore, they are frequently not accompanied by significant mass ejections into the interplanetary space, and all motions are basically held in the gravity field of the Sun. Long events contain more energy within themselves. They are larger in occupied volume, area, and height which facilitates to overcome the gravity forces and to eject mass from the Sun. We emphasize once more that the phenomena of flares and CMEs to some extent accompany each other, but there is no physical cause-and-effect relations between them. When they are considered, it is usually difficult (and sometimes even impossible) to isolate and localize in space and time the most substantial details and to establish genetic relationships between them. This situation is generally typical for nonisolated and open physical systems which are crossed by large fluxes of energy, momentum, and mass, as is the case for the solar atmosphere at all its altitudes.

Characteristics of the most interesting flares and their geoeffectiveness are presented in Table 1. Here, speaking about the "geoeffectiveness of flares" we follow the prevalent tradition. In general, this term is true for the strongest geomagnetic storms, as was explained above. Of course, one should keenly aware that geomagnetic storms are by no means caused by optical phenomena. They result from arrival to the Earth of plasma with magnetic fields of appropriate strength and orientation, while an optical phenomenon is but a good diagnostic indicator of strong events. So called "problem storms" when rather strong geomagnetic disturbances are sometimes observed without detection of bright flare manifestations. They are never record in their strength. Physically, all of them of course are genetically connected with CMEs. But the flares in this case could be either not very bright or hidden from observations because they occurred on the invisible side of the Sun. In the future, after carrying out relevant observations, it will be possible to make these situations clear. At the moment, it is worthwhile to note that recently rather good relationships have been found between "problem storms" and visible large-scale reconstructions in the solar corona in the region of long filament channels which sometimes even cross the entire solar disk and go to the invisible side of the Sun.

Such reconstructions are caused by changes of electric currents in the solar atmosphere, and they are frequently accompanied by well seen activation of filaments and protuberances.

The duration of events is determined using flares in $H\alpha$; φ is heliographic latitude, and λ is the angular distance from the central meridian (current heliolongitude). I_{RB} is the absorption of radio waves on the NOAA scale of evaluation of the space weather phenomena. P_r is the maximum flux of solar protons in the solar units of proton flux (p.f.u.); I_{pr} is the proton flux intensity on the NOAA scale. W and VS mean weak and very strong magnetic storms, respectively; I_{ms} is the intensity of a magnetic storm on the NOAA scale.

In conclusion of this description it is worthwhile to note once more that CMEs accompany the majority of bright flares (syndrome of strong events), though generally in no way one can say about proportionality between these phenomena because of a large scatter in parameters of these events and their diversity. Rather strong CMEs are known to occur without bright flares on the visible side of the Sun. There are also flare phenomena, strong and compact in X-ray emission, which take place at relatively small heights and are not accompanied by considerable mass ejections (confined flares). They are related to the motions confined near the Sun by gravity force and magnetic fields. To make the issue about interconnections between these phenomena clear is a matter of future investigations: obviously, none of these observations are sufficient for the purpose of forecasting the geomagnetic activity. This is due to the fact that CMEs encompass on average an angle of 40°–50° and turn out to be geoeffective only in case when they have reached the Earth bearing strong and long-living southward magnetic fields (tens of nanotesla during several hours and longer). In other words, both strong solar flares and CMEs by themselves are not sufficient indicators of "geoeffectiveness" [5, 6]. In this respect, the main sufficient indicator of geoeffectiveness is a strong electric and magnetic field of appropriate direction at its sufficiently long existence in the interplanetary space. It is quite understandable that the solar wind plasma in these periods is extremely inhomogeneous and unsteady. The traces of strong solar disturbances are imprinted in it in the form of extremely large (or small) values of velocity, density, and temperature. It can also be very specific in ion composition and other characteristics. All this plays the dynamical role in the development of magnetospheric responses.

3. BRIEF DESCRIPTION OF STRONG GEOMAGNETIC AND IONOSPHERIC STORMS IN OCTOBER–NOVEMBER 2003

The response of the magnetosphere to strong solar and heliospheric disturbances in the period under consideration is discussed in more detail elsewhere [7]. Here, we restrict ourselves to only most general information, necessary in order to reveal the solar and heliospheric conditionality of observed strong geomagnetic and ionospheric storms.

Below, for the analysis of solar and geomagnetic activity we use the data presented in the following websites:

http://www.sec.noaa.gov/today.html;

ftp://ftp.ngdc.noaa.gov/STP/SOLAR_DATA/SOLAR_RADIO/FLUX/;

ftp://ftp.ngdc.noaa.gov/STP/GEOMAGNETIC_DATA/INDICES/KP_AP/;

http://sohowww.estec.esa.nl;

http://www.izmiran.rssi.ru.

In October–November 2003 two periods with very strong geomagnetic storms were observed. One of these periods with a sudden commencement at 06:12 UT on October 29 is characterized by the planetary index of activity A_p = 189 nT. The peak values of components of the geomagnetic field according to data of the IZMIRAN observatory were $Z \approx 200$, $Y \approx 600$, and $X \geq 1000$ nT. At the main phase of the storm the three-hour index of activity was K_p = 9. This storm developed in several stages. It had complicated multi-stage character and continued until October 31. In this case one can speak about overlapping of several sequential disturbances that merged in a rather long storm period. Another storm, shorter and isolated, with a gradual commencement at 15:00 (Moscow time) occurred on November 20, and its planetary index of activity was A_p = 117 nT. The peak values of components of the geomagnetic field according to data of the same observatory were $Z \approx 400$, $Y \approx 600$, and $X \approx 1000$ nT. At the main phase of the storm K_p = 8–9. The storm was observed until 06:00 (Moscow time) on November 21.

All geomagnetic storms were caused by fast and strong changes of the situation on the Sun. The development of the storms was fully controlled by parameters of fields and plasmas in the near-Earth heliosphere. The active regions observed in the period since October 19 until November 4, 2003 had a maximum area on October 30: ~5700 m.f.s.h. The evolution of one sunspot group resulted in formation of the largest flare-active group of sunspots of the 23rd solar activity cycle. The flux of radio emission of the Sun at a frequency of 2800 MHz was $F_{10.7}$ = 270 s.f.u. (1 s.f.u. = 10^{-22} W/(m^2 Hz)). In the X-ray and optical ranges a large number of flares of various class and importance were observed. The flare activity was accompanied by enhanced emission of energetic particles, ions and electrons.

Somewhat different were characteristics of those active regions that were observed from November 18 to December 1, 2003. For example, they had on November 19 the maximum area ~2140 m.f.s.h., the maximum number of sunspots comprises 209 on October 26, $F_{10.7}$ = 178. A relatively small number of flares in X-ray and optical ranges were observed in these regions. At the same time, these regions, as those described above,

were fairly geoeffective in their impact on the near-Earth space.

For comparison, under quiet conditions of the period under consideration in October-November 2003 solar-geophysical activity had the following characteristics: $A_p \approx 10$ nT, $K_p \approx 2$, $F_{10.7} \leq 100$, the sunspot number was < 50, and area < 50 m.f.s.h. Images and movies taken from high-apogee satellites during the storms show the global pattern of development of auroras which on the whole is typical for so strong disturbances. The auroral oval was subject to rapid evolution being strongly broadened and displaced to the south until middle latitudes over Europe, Asia, and America. A similar pattern of broadened polar oval was also well observed in the southern hemisphere of the Earth. Auroras were also visually and photographically detected in these regions on October 29–30 by many observers all over the world, including those in Moscow and Moscow region. In particular, beautiful amateur photos of auroras in the northern part of the sky were made over Moscow after the midnight of October 30.

According to observations from the station of vertical sounding of the IZMIRAN observatory (Troitsk, Moscow region), the development of ionosphere–magnetosphere disturbances in October–November 2003 was accompanied by a complete absorption of radio waves in the ionosphere. Considerable reconstruction of the vertical structure of the ionosphere was observed in the period of storms. The analysis of ionograms taken during this period showed that the behavior of the ionosphere over Troitsk was typical for auroral conditions: scattered reflections, complete or partial absorption of radio waves, and formation in the E-region of sporadic layers of types *a*, *s*, and *r*, which screened the above-lying region. The same conclusion can be made from local magnetic data which indicate to existence at this time of a strong auroral electrojet in the ionosphere above observers (virtually overhead). The amplitude of this magnetic disturbance is also fairly typical for strong auroral disturbances, it several-fold exceeds the values of the global D_{st} index calculated by a certain averaging of magnetic measurements over several equatorial stations.

Without doubt, the global response of the ionosphere at this time is characterized by the existence of very strong and well localized electrojets in which the bulk current flows. It is more difficult task to reveal detailed disposition and geometry of separate magnetospheric electrojets, as well as their interrelation in the global electric circuit. In particular, these events give a good opportunity to make an attempt not only to refine the distribution of electric currents concentrated inside the magnetosphere and on its boundaries, but also to discover the extent of their relation to the heliospheric current which is also strongly intensified at this time and can partially penetrate into the magnetosphere during storms and be concentrated there [8]. For the time being, when modeling the magnetosphere response, as a rule, a closed configuration of the global current circuit inside the magnetosphere is assumed [7]. However, the validity of this assumption and the extent of openness of the magnetosphere current circuit are unknown at the moment. To clarify this issue in the course of a future detailed analysis of the data would be of specific interest for physics of the heliosphere–magnetosphere interaction.

4. SOLAR AND HELIOSPHERIC PHENOMENA RESPONSIBLE FOR GEOMAGNETIC DISTURBANCES IN 2003

Figures 2a and 2b demonstrate the histograms of mean daily values of the indices characterizing the planetary geomagnetic activity in 2003. For the analysis of solar and heliospheric causes responsible for geomagnetic disturbances observed in 2003 it is convenient to use the database APEV created for this purpose (http://alpha.sinp.msu.ru/apev). By this means one can trace a wide variety of recurrent events which were repeated with every rotation of the Sun and had as usual relatively small amplitude. These events are especially well seen in Fig. 2b in the form of recurrent sequences of disturbed days at every rotation. Sporadic disturbances are overlapped on these sequences, and sometimes they are stronger, so that the repetition is not quite regular. It is worthwhile to notice well known regularity: recurrent disturbances are ordered in such a way that the amplitude of disturbances in each sequence decreases from its beginning to the end.

The explanation of this regularity lies in the specific features of heliospheric propagation of high-speed streams of the solar wind from the coronal holes. As is known, in this case they are involved in nonlinear interaction with slower streams from the rotating Sun. As a consequence, a compression of matter and intensification of the magnetic field occur on the leading edge of high-speed streams coinciding with the rotation of the Sun. This is one of the causes of the above asymmetry. Another cause is related to boundary conditions on the Sun itself. As is known, similar asymmetry is also observed there. It is connected with rotation and consists in the fact that leading (western) sunspots from sunspot groups and active regions usually are more compact than more scattered and small successive sunspots. One can also observe a peculiar oblateness of large-scale structures on leading (western) edges in the direction of rotation. As a consequence of this one should expect a certain asymmetry in relative disposition and longitude structure of active regions and coronal holes, though this issue was not studied by us in detail. It is difficult to say at the moment, which factor is predominant: solar or heliospheric, and a special quantitative investigation is necessary.

The pattern of recurrent disturbances in 2003 was rather unstable and variable. This can be explained by the causes on the Sun: emergence and disappearance of separate and relatively stable-located or drifting active

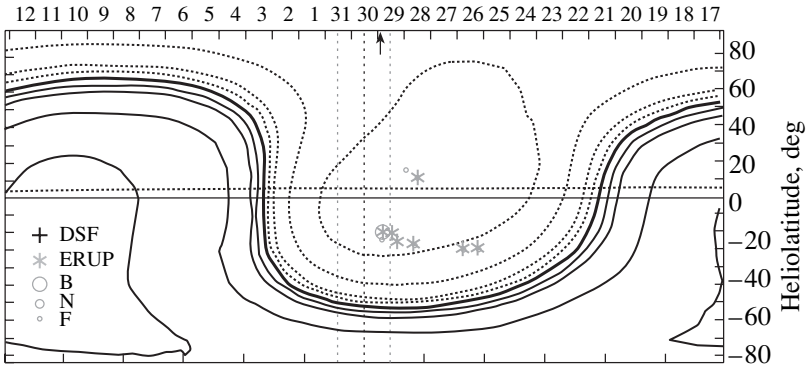

Fig. 4. The situation on the Sun having resulted in strong heliospheric and geomagnetic disturbances in October 2003. The synoptic map is taken from the database APEV 428 (http://alpha.sinp.msu.ru/apev). DSF designates disappearing filaments. The flares are marked according to the commonly used classification of optical importance: bright (B), normal (N), and faint (F). The eruptive flares are marked by asterisks.

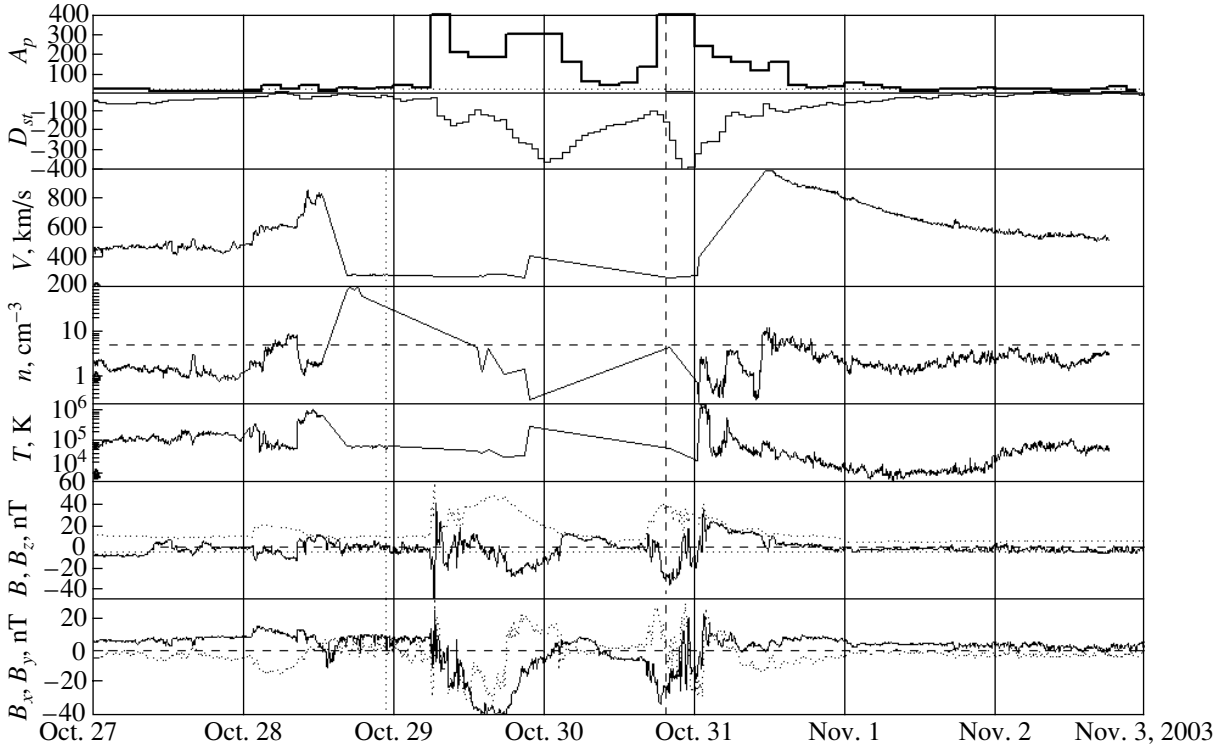

Fig. 5. The situation in the heliosphere responsible for strong geomagnetic disturbances in October 2003. The data are taken from the database APEV 428 (http://alpha.sinp.msu.ru/apev).

regions, coronal holes, and active complexes. It is clear that all this dynamics in many respects depends on the structure of flows and thermal and magnetic fields in subphotosphere region of the Sun. Corresponding boundary conditions for density, velocity, and temperature of plasma and for electromagnetic fields on the photosphere always were and remain to be important controlling factors which can be determined only from observations. At the moment they are far from being known sufficiently well. Thus, a certain upper limit is determined in time and accuracy for attempts to forecast heliospheric conditions based on the observations of the Sun.

Figure 3 illustrates the observed sequence of strong disturbances on the Sun and geomagnetic storms in October–November 2003 produced by them. Figures 4–7 present in more detail the situation on the Sun and in the heliosphere for separate most interesting time periods, and in Table 2 geomagnetic disturbances with maxi-

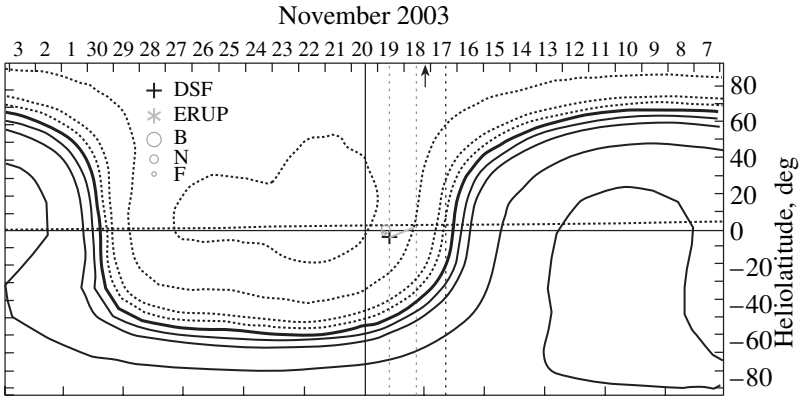

Fig. 6. The situation on the Sun that resulted in strong heliospheric disturbance and geomagnetic storm in November 2003 (see Fig. 13). The synoptic map is taken from the database APEV 431 (http://alpha.sinp.msu.ru/apev).

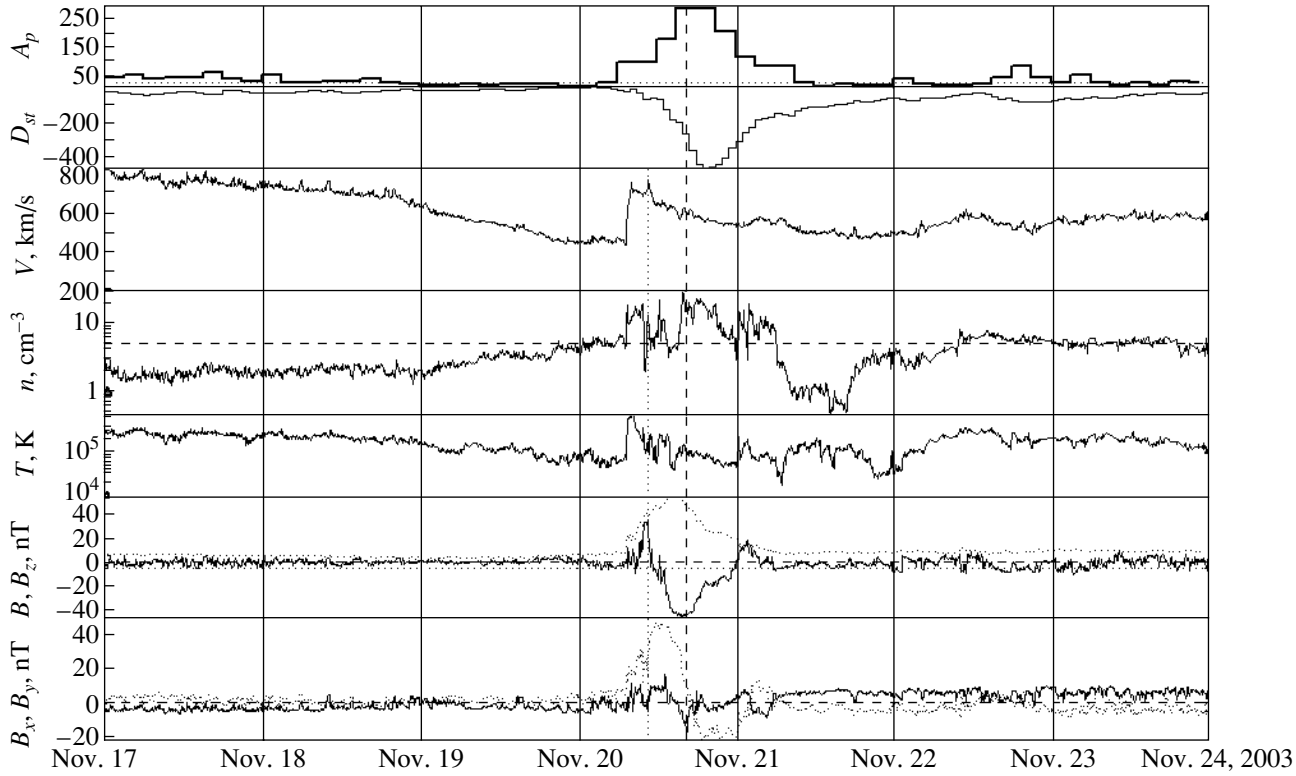

Fig. 7. The situation in the heliosphere responsible for the strong geomagnetic storm in November 2003. The data are taken from the database APEV 431 (http://alpha.sinp.msu.ru/apev).

mum three-hour index $A_p > 100$ in October–November 2003 are brought into correlation with the situation on the Sun and in the heliosphere which generated them.

Direct measurements of the solar wind parameters by spacecraft and satellites during very strong disturbances are extremely difficult and sometimes become unreliable or even impossible because of malfunctions and failures in the normal operation of instruments and their limited dynamic range, which is well seen in Figs. 4–7. It is in particular for this reason that one should be very careful when using the data (regularly published on the Internet) about the velocity, temperature, and density of the solar wind for the time period under consideration. In view of these circumstances, Fig. 8 presents a comparison of the *ACE* satellite data processed and corrected using a special program taking into account the specificity of operation of a plasma analyzer in this period (private communication by R. Skoug) with the calcu-

Table 2. Geomagnetic disturbances with maximum three-hour index $A_p > 100$ in October–November 2003, in relation to the situation on the Sun and in the heliosphere resulting in them

Storm period: Date and time (UT)	A_p	Interplanetary conditions	First appearance of CME in the field of view of LASCO C2	Onset time and source position on the Sun according to EIT observations	Maximum of corresponding flare
October 24, 2003, 15:00–18:00	111	Shock wave at ~ 15:00 on October 24 with a subsequent layer $B_z < 0$	03:54 on October 21, halo[1]	Dimmings and EIT-wave at 03:47 on October 21 on the eastern limb (future AR10486)	None[2]
October 29, 2003, 06:12–09:00	400	Shock wave at ~ 06:00 on October 29 with a subsequent layer $B_z < 0$, then a magnetic cloud with NS orientation	At 10:54 on October 28, halo, 2125 km/s	Dimmings and EIT-wave, 11:11 on October 28, AR10486	X17.2, 11:10 on October 28
Second peak 18:00 on October 29 – 03:00 on October 30	300				
October 30, 2003, 18:00–24:00	400	Shock wave at ~ 16:00 on October 30, then a magnetic cloud with NS orientation	20:54 on October 29, halo, 1950 km/s	Dimmings and EIT-wave, 20:48 on October 29, AR10486	X10.0, 20:49 on October 29
November 4, 2003, 09:00–12:00	132	Shock wave at ~ 06;00 on November 4 with a subsequent layer[3] $B_z < 0$; 25	17:30 on November 2, halo, 1826 km/s	Dimmings and EIT-wave, 17:23 on November 2, AR10486	X8.3, 17:25 on November 2
November 20, 2003, 15:00–21:00	300	Shock wave at ~ 07:30 on November 20, then a magnetic cloud ESW	08:50 on November 18, halo, 1175 km/s	Dimmings and EIT-wave, 07:58 on November 18, AR10501	M3.2, 07:52 on November 18

[1] Though the main source of this CME is located behind the eastern limb, its visible configuration has an appearance of a halo due to propagation of a disturbance and shock wave. It is difficult to estimate the propagation velocity of this disturbance.
[2] This flare was probably behind the limb.
[3] The source was located close to the western limb. Corresponding CME passed by the Earth. Only one layer was observed.

lated velocity of the solar wind. The calculation was made by A.V. Dmitriev on the basis of magnetic data from a pair of satellites *ACE–Geotail* that were in the solar wind at that time. Under the assumption of spherical symmetry the known distance between these two spacecraft was divided by the time lag in observing the magnetic structures carried away by the solar wind stream. The smoother curve corresponds to the first case, while the histogram represents the second case. A fairly good agreement is observed, within the expected accuracy of about ten percent. The reliability of high velocity values that reached ~2000–2200 km/s and of the assumptions about normal front of propagation in the Earth's vicinity during the considered strongly disturbed period is confirmed by general correspondence of two curves, including undisturbed time intervals too. The same is also confirmed by the agreement with estimated velocity of propagation of interplanetary transients. This velocity was evaluated by the time of delay of geomagnetic storms relative to CMEs observed by the *SOHO* coronograph LASCO. This time was extraordinary small: only 19–20 h.

For the larger part of the period October 10–November 30, 2003, the reliable data on the solar wind are available on the Internet. First of all, these are the data of the SWEPAM instrument onboard the *ACE* spacecraft (see Fig. 3). However, the *ACE* data open to general use are completely wrong for time interval from the middle of October 28 to the end of October 30, and throughout the day of November 3, 2003. We do not consider here the second interval. However, for the first interval one can suggest approximate estimates for two most important parameters, the velocity and density of the solar wind.

Let us discuss the available data. The data of the *Geotail* satellite (CPI instrument) and the data of the *ACE* spacecraft close to them look quite reasonable from the beginning of October 28 to 12 UT of October 28, 2003. So, these data can be taken as a basis. After 12 UT of October 28, 2003 the *ACE* data became erroneous: the velocity values are unreasonably low until the beginning of October 31. One cannot confide in these data. The data of the *Geotail* satellite look better, but in fact here there is also an instrumental malfunction caused by the arrival of energetic particles from the Sun. It occurred after an extremely strong flare (X17.2/4B) at 11:02 UT on October 28, 2003 (very strong SCR enhancement was observed by *GOES-10*). Therefore, one cannot consider the *Geotail* data for October 28–29 presented at the website GSFC as reliable, the more so that they are contradictory (as far as both instruments, CPI and LEP, are concerned).

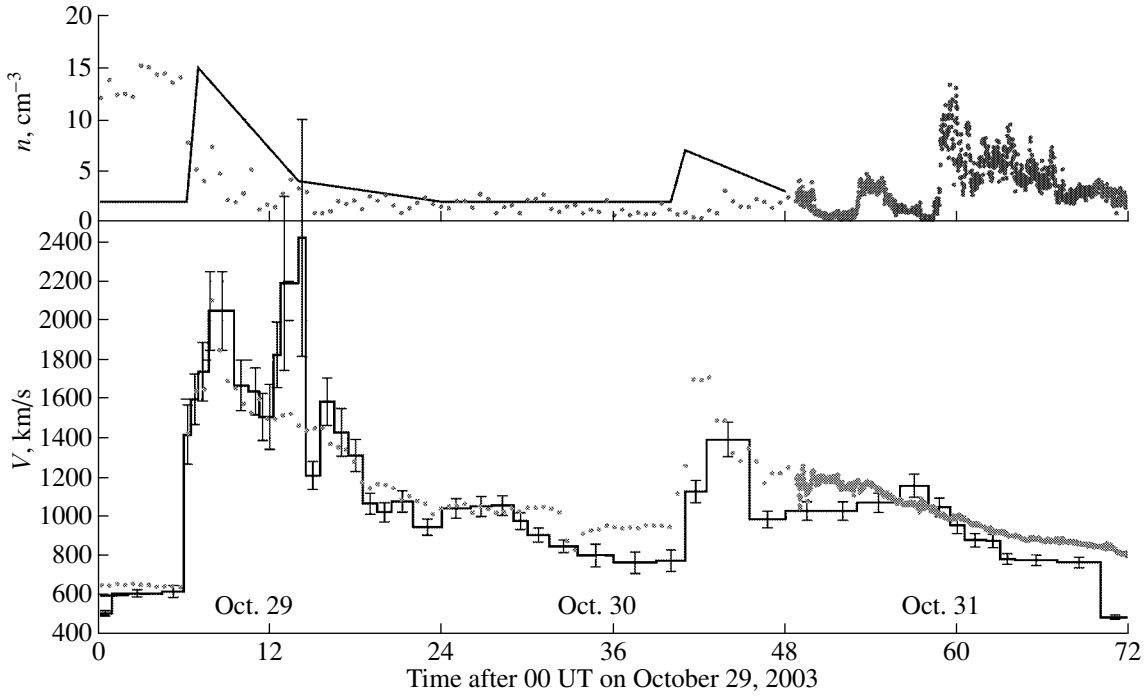

Fig. 8. The time profiles of the model density (upper panel) and velocity (lower panel) of the solar wind. The velocity and density derived from plasma data of the *ACE* satellite are shown by points. The density shown by line was estimated using the procedure described in the text. The velocity reconstructed from magnetic data of a pair of satellites *ACE* – *Geotail* on October 29–31, 2003 is presented as a histogram with estimated confidence intervals.

At the interval from 12 UT of October 28 to 24 UT on October 30 one can use the results of modeling the motion of interplanetary shock waves by a group headed by M. Dryer. Of course, they are only model estimates and not experimental measurements, but the long-term experience of this group proved rather high degree of coincidence of their estimates with reality for a variety of conditions, including extreme events. The estimate made by Dryer group for the solar wind density in the interval from 12 UT on October 28 to 24 UT on October 30 are presented in the upper panel of Fig. 8 by a solid line. Starting from ~11 UT on October 31 all three satellites (*ACE*, *SOHO*, and *Geotail*) give identical densities. It is worthwhile to note that at some instants of October 29–31 the contribution of helium to the solar wind density could be quite large. An interesting structure reached the Earth at ~11 UT on October 31, when the helium contribution increased up to 40%. This probably was a cold filament. For the solar wind velocity in the interval October 29–30 there are estimates based on fragmentary (once in 32 min) data of the SWEPAM instrument (private communication by Ruth Skoug, see Fig. 8), on the motion of magnetic irregularities (communicated by A. Dmitriev, see Fig. 8), and on the velocities of alpha-particles (the instrument SWICS on the *Ulysses* spacecraft).

Finally, we have the following pattern. For the interval from 12 UT on October 28 to 06 UT on October 29 one can only interpolate between the measured values in the beginning of this interval ($V \sim 750$ km/s and $n \sim 2$ cm^{-3}) and coinciding estimates for 06 UT of October 29 (close values for velocity and density). At 05:58 UT (according to numerous data) an interplanetary shock wave arrived at the Earth, and it generated a sharp and large growth of the density (up to 15 cm^{-3}) and, especially, velocity of the solar wind (see Fig. 8). The velocity reached 2100–2400 km/s (1950 km/s according to alpha-particle measurements). This record value is comparable only with 2000 km/s for the event of August 4, 1972. On the interval from 06 UT to 24 UT on October 29 the wind density rather quickly (in 6–9 h) dropped from 15 cm^{-3} down to ~1–2 cm^{-3}, and further it remained so low almost to the end of October 30. For the solar wind velocity there is an estimate (Fig. 8) giving a drop to the end of October 29 down to 1000–1100 km/s, very close to an estimate by the Dryer group (1100–1300 km/s), and identical to an estimate by alpha-particles (1100 km/s). Judging from the *Geotail* data the solar wind velocity drops at 18–22 UT on October 29 down to 900–1100 km/s, while the density at this time is ~2–5 cm^{-3}. Further on, after 22 UT a malfunction of *Geotail* instruments occurred again (apparently, due to the arrival of energetic particles from the flare X10/2B at 20:42 UT on October 29), and one cannot believe in their data. After ~04 UT on October 30 the *Geotail* satellite enters the magnetosheath, and yields no data on the solar wind until October 31. For October 30 there are still no data of *ACE*, and we use estimates. Accord-

ing to an estimate by the Dryer group, the solar wind density remains at the level ~2 cm^{-3} until the arrival of an interplanetary shock wave at 16:19 UT, when it increases up to ~7 cm^{-3}, and then for 6–8 h it decreases again down to ~2 cm^{-3}. Upon arrival of the shock wave the wind velocity increases (see Fig. 8) up to 1400–1700 km/s. However, there is an estimate derived from the data on alpha particles (~2000 km/s), which seems to be an overestimation in the given case for the region near the Earth, since it is valid only for the heliolatitude where the *Ulysses* spacecraft was located. After a sharp increase the solar wind velocity gradually decreases down to the value ~1200 km/s to 01 UT on October 31, where it is already consistent with regular measurements by the SWEPAM instrument. At this time the wind density comprises about 3–5 cm^{-3}.

For the sake of completeness of the picture one can remark that corresponding strong disturbances in the heliosphere propagated retaining the deviations from the spherical symmetry and "memory" about the longitude and latitude of the place of their origination on the Sun. This statement follows from a comparison with the published data of the *Ulysses* spacecraft which was located at this time at a distance of about 5.3 AU from the Sun in heliolatitude of about 5 degrees and heliolongitude with respect to the Earth about 90 degrees. The October disturbances on the Sun produced several well-pronounced fast streams of plasma and shock waves on their background, which arrived on November 6, 10, and 13. Step-like variations in the solar wind velocity took place from 400 to 500 km/s, then from 500 to 600 km/s, and from 600 to 800 km/s. All of them were accompanied by the phenomena of compression and rarefaction of plasma between them because of the difference in relative velocities of motion and dynamical processes on the way of propagation. However, the longitude of *Ulysses* corresponded to its position on the periphery of respective CMEs and shock waves. This explains the moderate value of plasma disturbances in comparison to those that were detected in these events at the Earth.

A very strong limb flare of November 4 occurred practically on the longitude of *Ulysses* location. Therefore, the plasma ejection that reached *Ulysses* in 10–12 days propagating with a velocity 950 km/s turned out to be emitted precisely in this direction, and not very strong shock was detected at the Earth. After that, an extended region of rarefaction was observed on the *Ulysses* spacecraft for about two weeks. Finally, a shock wave from the flare of November 18 came to this region on November 29. This flare was almost central for the Earth, while for *Ulysses* it was a limb flare. The solar wind velocity behind its front was equal here to 600–700 km/s, far from record values even taking into account considerable attenuation of the disturbance with moving away from the Sun. In all these cases the conclusion that the width of a "disturbed" cone of plasma was about 90 degrees in longitude seems to be quite natural and sufficiently justified.

5. GLOBAL ASYMMETRY OF THE SUN IN OCTOBER–NOVEMBER 2003

The global asymmetry of the Sun and manifestations of solar activity in October–November 2003 can be immediately traced at all level of the solar atmosphere using the published data about magnetic fields on the photosphere, data about sunspots and filaments, ultraviolet and X-ray emission, including the data obtained by *Coronas-F* (Figs. 9a and 9b), *SOHO* (Fig. 9c), and *GOES* (Fig. 3). Many other indicators can also be used, as well as indirect geomagnetic data.

The brighter side of the Sun with powerful active regions was facing the Earth from October 19 to November 4. The central dates in this respect are October 26–27. The corresponding central dates at the preceding and subsequent solar rotations are approximately on September 30 and November 28. The darker side of the Sun with weaker magnetic fields was facing the Earth on October 12 and November 11. Thus, the global asymmetry of the Sun clearly observed at the phase of growth and near the maximum of solar activity in the 23rd cycle [9] does exist at the declining phase. It is well pronounced and plays its important role during the disturbed period in which we are interested. All strongest flares and CMEs observed in October–November 2003 occurred on the bright side of the Sun. The strong geomagnetic storms on October 29–31 and November 20 were also produced by sporadic processes on the Sun in the vicinity of corresponding central longitudes. In the above sense these geomagnetic disturbances can be considered as recurrent, since it is an easy matter to find and denote the "active longitude." However, the Sun as a star in October–November substantially increased the lost energy per rotation in the ultraviolet and X-ray emission, which is well seen in the data of *Coronas-F*/SPIRIT and *GOES*, if one compares the rotations in September–December between themselves. In other words, a relatively short but significant burst of all manifestations of solar activity took place in October–November.

The observations in Lyman alpha line also confirm these conclusions about the global asymmetry of the Sun and bursts of activity (Fig. 9d). In the period of flares the immediate observations in optical range by VUSS and SUFR onboard *Coronas-F* showed no growth in the emission flux, while in the range of extreme ultraviolet emission the observations turned out to be impossible because of a sharp increase of instrumentation sensitivity in this period. However, it turns out that one can trace the variation of emission fluxes using indirect (ionosphere) data. In accordance with [10], the data on parameters of the E-layer of the ionosphere can be used as indications of a natural detector of ionizing emission, and they can also be represented in the form of an equivalent flux in the L_α line (121.6 nm). The variations of the equivalent radiation flux calculated for the period from August 2003 to January 2004 are presented in Fig. 9d. The data of the Slau

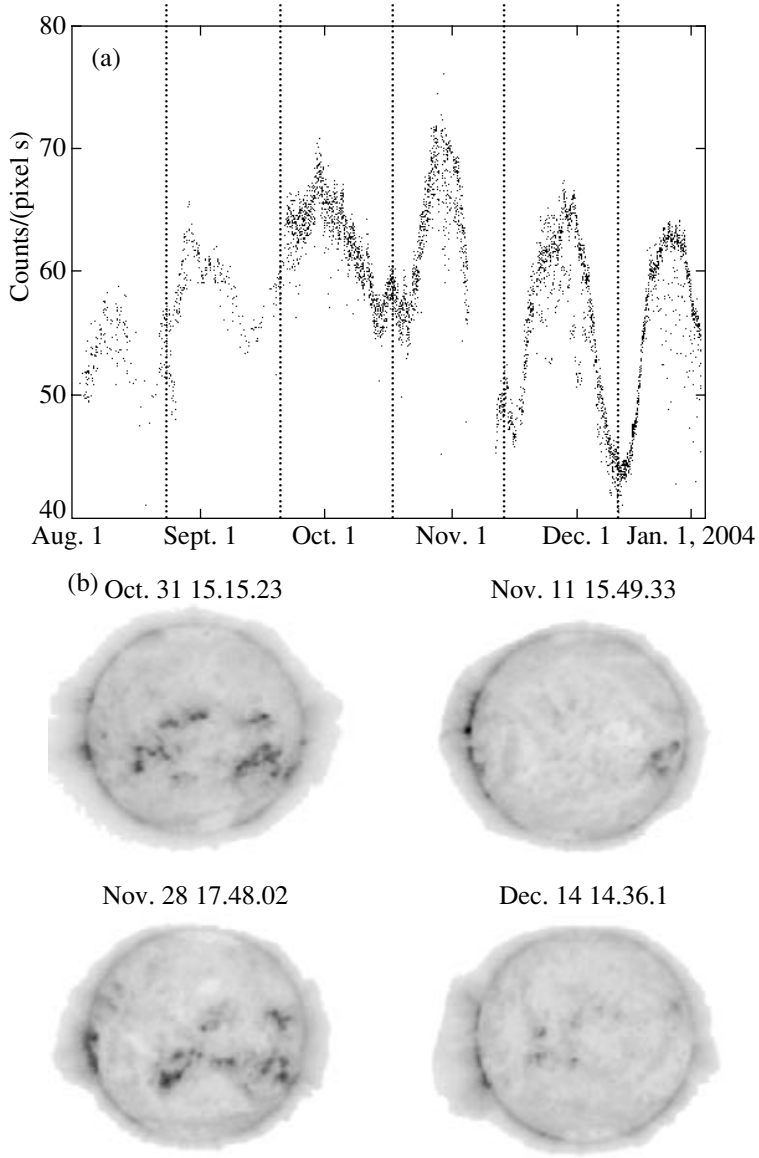

Fig. 9. The data illustrating the global asymmetry of the Sun. (a) Variation of the integral (over the solar disk) luminosity of the Sun in the range 175 ± 3 Å ($T \sim 1.3$ MK) according to the data of *Coronas-F*/SPIRIT instrument in the period from August to December 2003. Dashed lines show the minima of luminosity with a step corresponding to sidereal period of rotation (27.275 days). (b) Images of the Sun during the observed maxima and minima of integral luminosity according to the same data. (c) The global asymmetry of solar emission in the line 195 Å according to observations of *SOHO*/EIT during several rotations of the Sun in September–December 2003. (d) Model flux of solar emission in the Lyman-alpha line in August–October 2003. One can see strong sporadic variations and changes during several successive rotations. The upper row of arrows shows the moments of flares of X class, while the lower row is for flares stronger than M5.

station obtained through the World Data Center B1 are used. The arrows at the top mark the dates of the flares presented in Table 1 and some flares stronger than M1.

One can see that pre-flare situations are characterized by a considerable (by ~30%) increase of extreme UV emission, and then there comes a time when no observations are available due to strong disturbance of the ionosphere. So substantial increase is, apparently, also indicates to changes in the global characteristics of the Sun in the period before the enhanced flare activity: in particular, a prominent asymmetry is possible in the luminosity of the undisturbed (beyond active regions) solar surface in the ultraviolet range.

These phenomena can be explained by powerful intrasolar (more precisely, subphotospheric) processes that lead to temporary supply of large amount of free energy into the solar atmosphere and its dissipation there, including the corona. In particular, an important role can be played by additional fluxes of thermal energy which is transformed into the emission of

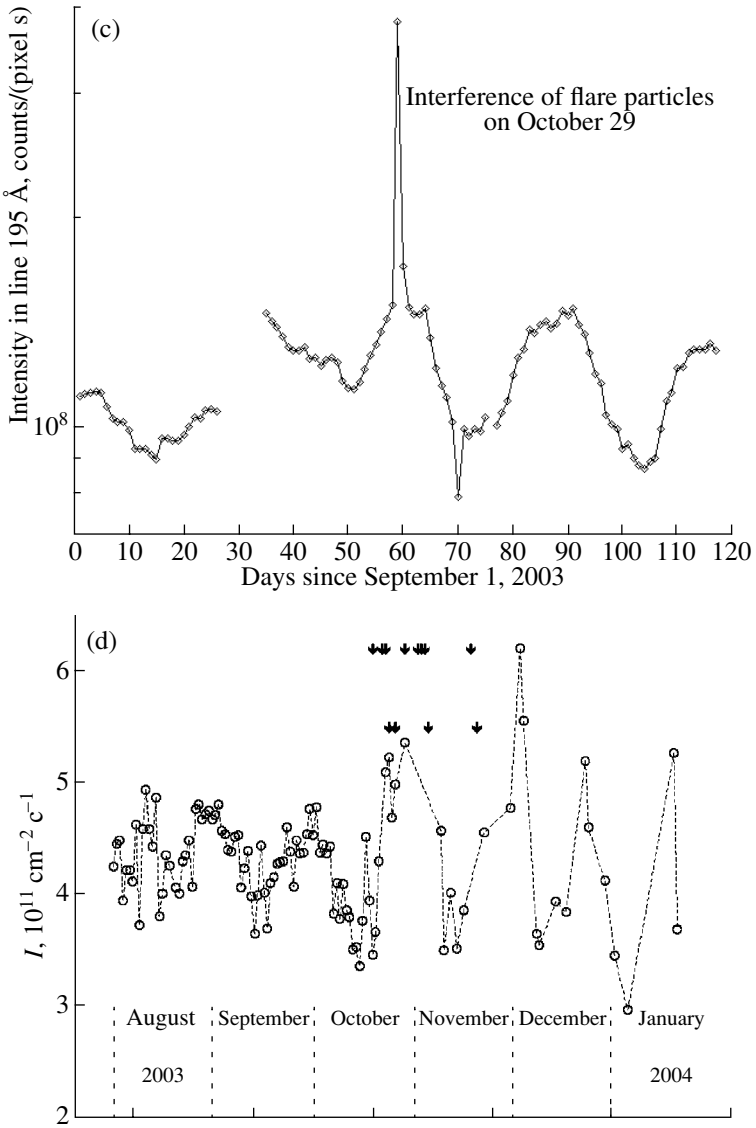

Fig. 9. (Contd.)

heated gas and other forms of energy (including magnetic energy of electric currents) in a thin subphotosphere layer. A relatively small local temperature increase (by fractions of a percent) would be quite sufficient, due to enhanced concentration and speeded up convective carry-away of energy, in order to fully support the energy balance of considered electromagnetic emission and magnetohydrodynamic processes in gravitationally confined and higher parts of the atmosphere. Generation of strong electric currents and magnetic fields, supersonic and super-Alfvenic motion of plasma, particle acceleration and accompanying hard electromagnetic and neutron emission, and radio emission in a wide frequency band easily can be a direct consequence of fast transformation of this excess free thermal energy arriving from below. The existence of heating at the photospheric level is usually seen only during the strongest flares, since in all other cases the contrast is too small. Unfortunately, such an important component as a flare in white light is insufficiently studied at the moment, and this gives birth to not fully justified hypotheses about the origin of solar flares. The estimations of energy release in white flares available in the literature are of order of some ten percent in the total energy balance. The need to be refined and can be underestimated, since only the brightest and most contrast part of this phenomenon, exceeding a very high background by tens of percent, is taken into account. May be, it is due to this reason that the visible area of white flares always seems to be relatively small even in the strongest events.

Sufficiently accurate and absolutely calibrated observations in white light and infrared range (i.e., in the region of a main maximum of emission) are

extremely complicated and so far have not been carried out with necessary precision. This will require special measurements from space, which is a matter of future experiments. These reasons do not exclude the important and well established role of stored free magnetic energy in the course of these processes in the solar atmosphere. However, it is very difficult to make necessary quantitative estimates, and they are always rather uncertain, even in the order of magnitude. Nevertheless, when discussing the solar flares it should be remembered that the main energy channel of these phenomena due to the above reasons can elude observations and be undeservedly ignored. A quantitative investigation of non-local and nonlinear relations on the Sun during CMEs and flares (including white flares) remains to be one of central unresolved experimental problems. In particular, a white flare, even if unobserved because of its relatively small brightness and insufficient contrast, should be always present due to very essence of the physical phenomenon related to intensified carrying-out of energy from the open physical system, which is not limited in advance by certain parts of the solar atmosphere. Figures 10–15 present some images of the Sun in the visible and ultraviolet emissions that illustrate the said above about the distribution of activity on the Sun. Below, these observations are discussed in more detail.

6. LARGE-SCALE ACTIVITY IN EXTREME UV-RANGE

The eruptive events on the Sun considered here included the flares of extremely high X-ray importance and prominent CMEs (including those of halo type) that were detected using the white-light coronographs *SOHO*/LASCO. The flares and CMEs were also detected in the extreme UV range onboard *Coronas-F*, *TRACE*, and *SOHO*. Figure 11 presents four successive exposures from a series taken on October 28 by the SPIRIT instrument [11] onboard the *Coronas-F* satellite [12] in the channel 175 Å. One can see the changes from one exposure to another: increased and decreased brightness of separate segments of the image. The dynamics of a long flare in a complex arcade of loops of active region 10486 is most clearly traced. In addition, on a large part of the disk surface one can see (especially in the southern hemisphere) a whole system of temporarily arising regions with a decreased intensity of emission (transient coronal holes or so-called dimmings). A special difference technique applied for processing the images allows one to make these changes more contrast and better discernible. A similar picture of global and local changes in brightness was observed in four UV channels by the *SOHO*/EIT telescope. These channels matched up to different effective temperature of excitation of corresponding lines. In spite of all complexity of local changes occurring in this case, it is noteworthy that the general large-scale topology of light and dark segments is conserved before and after events under consideration. The time resolution in this case is insufficient for detailed observation of quickly variable processes, such as coronal waves frequently referred to as "EIT waves" (luminous fronts propagating over the disk from the place of eruption with a velocity of 100–200 km/s). A relatively bright structure stretched out from the eastern limb to the central meridian and further to the south (*SOHO*/EIT image at 11:12) has the features of a front of a coronal wave.

The analysis of dimmings and, partially, coronal waves was made in [13] using heliograms of *SOHO*/EIT in the coronal channel 195 Å with a 12-min interval, and in coronal channels 171 and 284 Å, and transition region channel 304 Å with a 6-h interval. The results of this analysis in the form of heliograms and movies can be found at the following website: http://helios.izmiran.troitsk.ru/lars/Chertok/0310_11/index.html. The general information about the entire active period during two solar rotations is also presented there.

During the first passage across the disk of the complex of three active regions (more precisely, until November 4) SPIRIT fixed the heliograms of the entire disk in the channel 175 Å, as a rule, with an interval of 15–45 min (taking into account the shadowing of the satellite by the Earth). Similar observations were also carried out in the channel 304 Å starting from November 11 and during the second passage. The SPIRIT heliograms with the above time intervals do not allow one to trace the propagation of coronal waves, but they are quite suitable for the analysis of dimmings whose lifetime is measured by hours. The results of a more detailed analysis are presented in paper [14], as well as their comparison with the EIT data.

The heliograms of both telescopes were processed using the method of derotated fixed difference heliograms earlier applied in [15, 16]. This method includes two stages. At first the images are matched by compensating the solar rotation (derotation), i.e., by shifting all heliograms of a particular event to one and the same time instant, usually that before the event. Then, one fixed background image before the event is subtracted from all heliograms under consideration. The fixed difference images obtained in this way give a real picture of disturbances related to CME, in particular, dimmings. They are radically different from successive difference images. The latter accentuate the changes in intensity, structure, and localization of sources occurred in time elapsed between two neighboring heliograms, i.e., the time derivative of these changes rather than their values themselves.

As an example, let us consider out of the events studied in [13] the event of October 28. The flare 4B/>X17 with a maximum at 11:10 UT occurred in the region 10486. Corresponding CME had the form of a halo with a glow around the entire occulted disk and especially intense component above the southern limb, and the velocity of its propagation in the picture plane

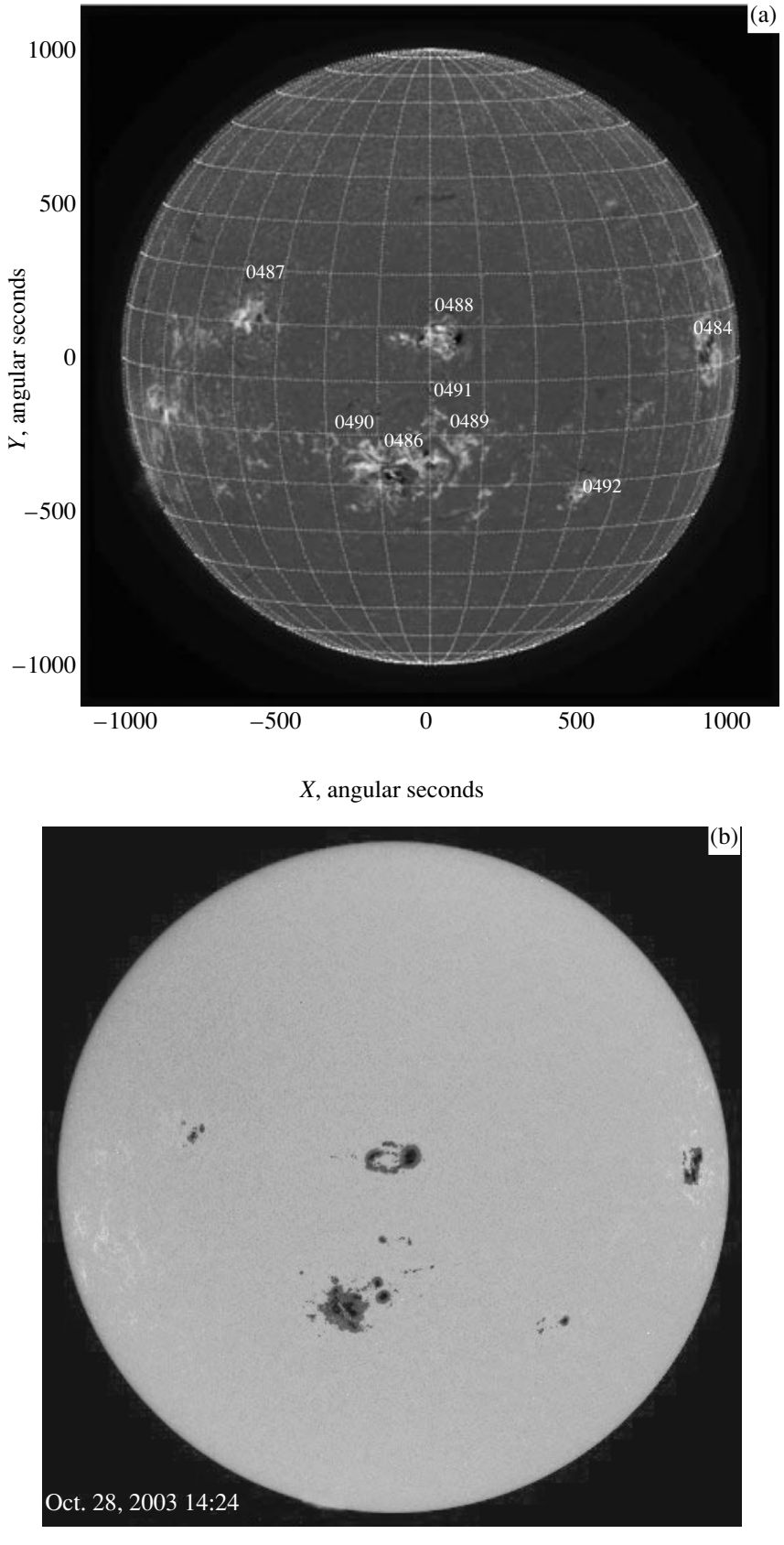

Fig. 10. The Sun image in the $H\alpha$ line on October 28, 2003. (a) is from (http://beauty.nascom.nasa.gov/arm/20031028/halpha_fd.html) and (b) from (http://www.spaceweather.com.archive).

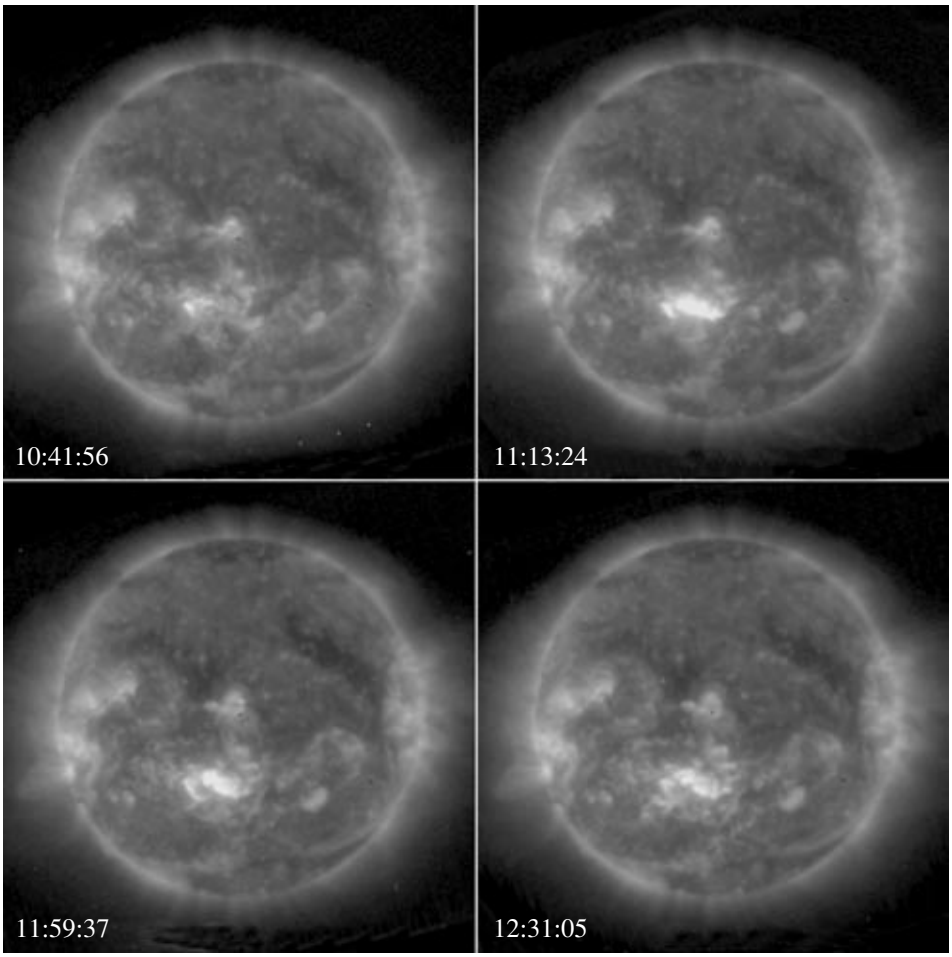

Fig. 11. The Sun images in the line 175 Å of extreme ultraviolet emission on October 28, 2003. Four sequential frames from a movie shot by the SPIRIT instrument onboard the *Coronas-F* satellite.

reached 2125 km/s. Figure 15 presents fixed difference heliograms of SPIRIT in the channel 175 Å and of EIT in the channel 195 Å. On the exposures (Figs. 15a and 15b) close to the flare maximum a bright flare region is seen. EIT shows it with substantial instrumental distortions: saturation, leakage of charge the CCD detector, and strong increase of brightness on a considerable area around this region (due to scattered light in the telescope). No such effects are observed on SPIRIT heliograms, since at a very high level of signals the detectors, in which microchannel plates are used, go into the nonlinear mode. As a result, the level of saturation for SPIRIT exceeds the EIT's limit of detection considerably. This also allows one to see on SPIRIT images more complete and distinct pattern of dimmings at the instant of maximum of the strongest flare. Both EIT and SPIRIT data show that already at this stage the dimmings covered nearly all southern half of the disk and an adjacent part of the northern hemisphere. In this case, not only three main regions AR10484, 10486, and 10488, in which the strongest flares took place during the period under consideration, were connected by dimmings, but at least two other distant regions that were located on October 28 not far from the eastern limb. The extended dimming structure seen in the southern near-polar zone is also noteworthy. The fact that dimmings in the northern half of the disk were very weak is explained by the existence here of a large coronal hole.

All dimmings described above survived for several hours and at 12:46–12:48 UT they had the shape shown in Figs. 15 c and 15 d. These and subsequent images of EIT turned out to be more and more covered by "snow," i.e., by bright points appearing as a result of impact on the detector of a powerful flux of energetic particles generated in the event and arriving at the telescope. As for the SPIRIT heliograms, they remained clear throughout the event, since *Coronas-F* was orbiting relatively low inside the Earth's magnetosphere, so that it was partially protected against penetration of these particles.

The heliograms SPIRIT 175 Å and EIT 195 Å presented here correspond to close temperatures of the coronal plasma of about 1.3 and 1.5 MK, respectively. A similar analysis of this event carried out in [11] using the data of four channels (304, 171, 195, and 284 Å)

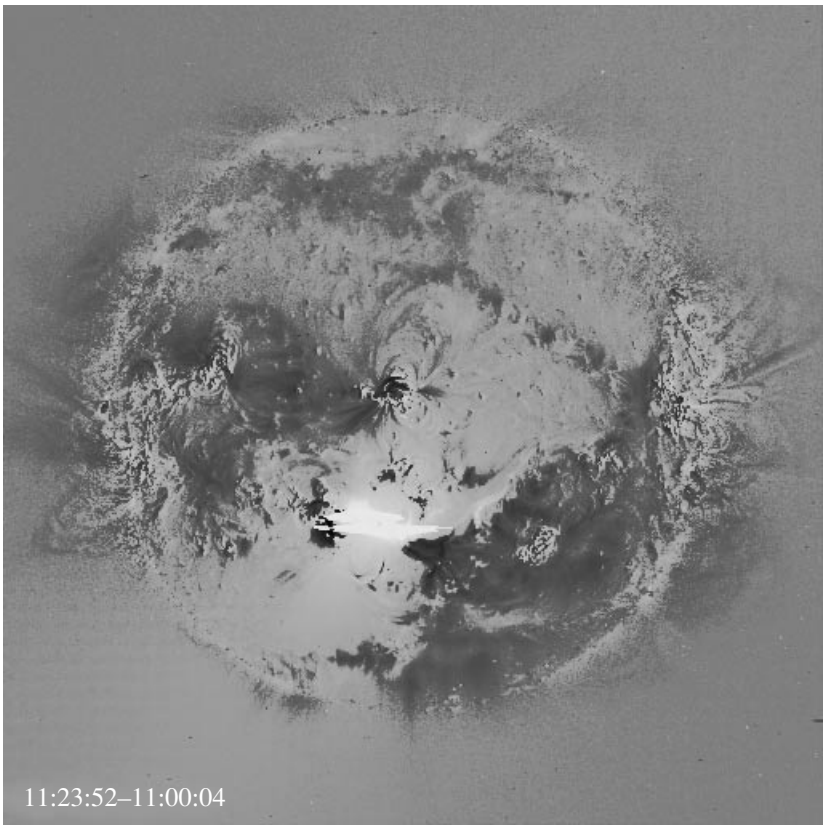

Fig. 12. An example of constructing a difference image of the Sun in the line of extreme ultraviolet emission on October 28, 2003. The image is obtained by subtraction of two successive frames of a movie shot by the EIT telescope onboard the *SOHO* spacecraft. The image at 11:00:4 is subtracted from that at 11:23:52.

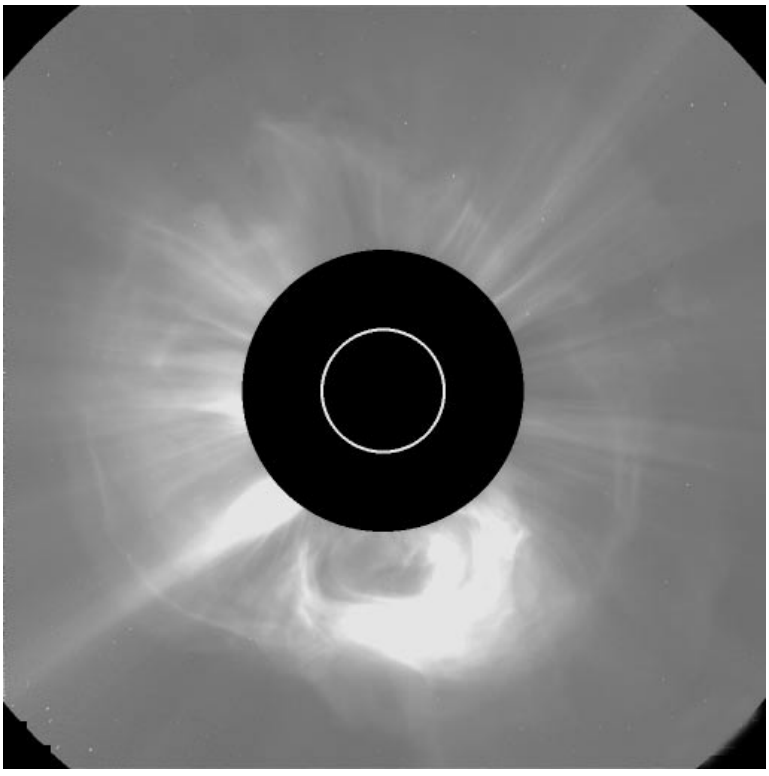

Fig. 13. The image of the solar corona in white light on October 28, 2003. An exposure from a movie of the LASCO C2 coronograph onboard the *SOHO* spacecraft.

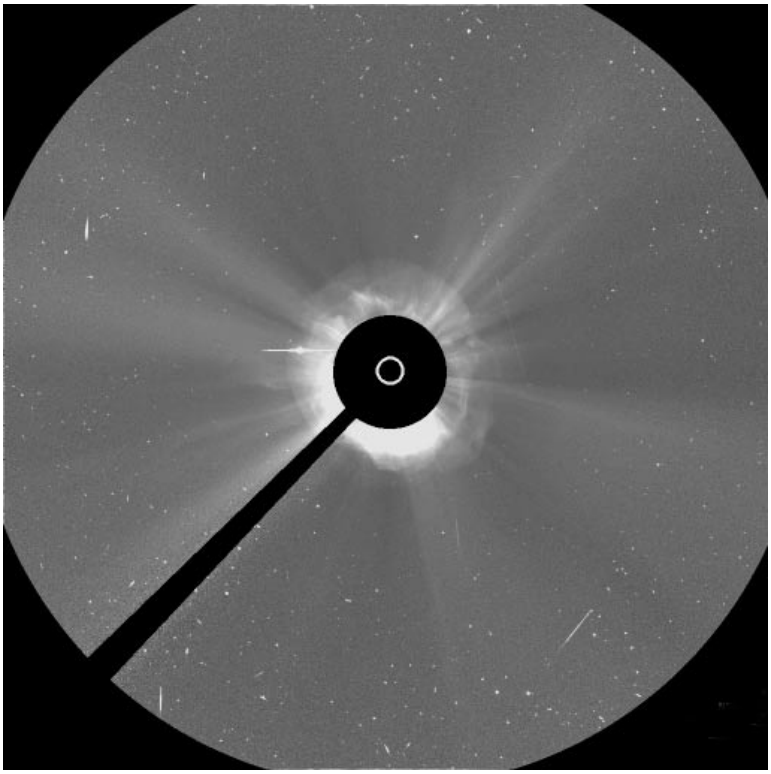

Fig. 14. The image of the solar corona in white light on October 28, 2003. An exposure from a movie of the LASCO C3 coronograph onboard the *SOHO* spacecraft.

representing essentially different temperatures of line excitation from 0.05 to 2 MK showed that basic dimmings were similar and coincided to a large extent in all above channels. This observation fact is indicative of the existence on the line of sight of densely located structures emitting all this set of lines. The global character of dimmings in this and other events of a given series means that a considerable part of the solar atmosphere was involved in the process of CME eruption. It is remarkable that the pattern of dimmings was in many respects repeated form event to event, including the above-mentioned structures between the remote active regions and in the southern near-polar region. This indicates to homology of eruptive events under consideration, i.e., CME eruption every time involved approximately the same structures, which, apparently, had time to regenerate their magnetic field and luminosity between events.

7. DEVELOPMENT OF ACTIVE REGIONS ACCORDING TO RATAN-600 DATA

The RATAN-600 observations in centimeter wavelength band of active regions in October–November 2003 give valuable experimental data for studying the spatial distribution of emission sources over the solar disk and their altitude profiles. One can also search for possible precursors of powerful process of energy release in the solar corona using the data on intensity, spectra, and polarization of this radio emission.

During the last three years, a new mode of observations was applied at RATAN-600, which allows one to discover and study the features of radio emission of flare-productive active regions (FPAR) generating extremely strong flares [17]. These features look in the centimeter waveband as sharp spectral irregularities in a polarized emission. Such phenomena take place in a wide range of radio emission fluxes (0.05–200 s.f.u.) and in a relatively narrow range of wave lengths (2–5 cm). They are detected in the time interval from a few hours to several days before a strong flare, and also during the flare. Frequently, these events forego CME and the fluxes of energetic particles (protons) that upon reaching the Earth's magnetosphere cause its disturbances. Below, we analyze the events associated with the strongest flares that occurred on October 29 and November 4. The most powerful active regions of the 23rd cycle (AR10484, AR10486, and AR10488) started at RATAN-600 only since October 25 (a delay was due to a technical interruption). The time intervals when RATAN-600 observations were carried out, from October 30 to November 5, are shown in gray color in Fig. 16. They are overlapped on the plots of time behavior of the X-ray emission intensity according to *GOES* data.

In order to study dynamics of the active region we used regular spectral polarization measurements. The

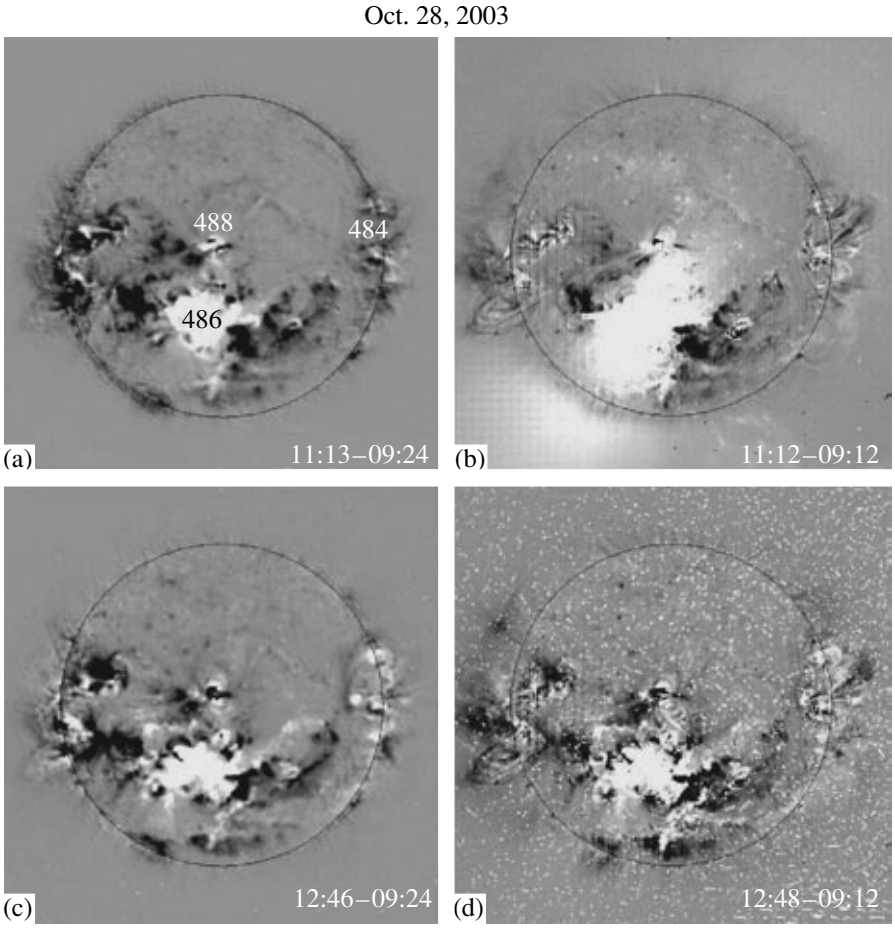

Fig. 15. Fixed difference heliograms of the eruptive event on October 28, 2003 according to the data of two telescopes of the extreme ultraviolet waveband: *Coronas-F*/SPIRIT in 175 Å channel (a, c) and *SOHO*/EIT in the line 195 Å (b, d).

radio telescope has such parameters that allow one to perform measurements already at early stages of FPAR development. In this case, the most important property of this instrument is a combination of the instantaneous frequency spectrum from 1 to 16 GHz (in this work we used the range 4–16 GHz) with a frequency resolution of about 5–7%, at a high sensitivity to measurements of small degrees of circular polarization (about 0.05%) and high sensitivity of measuring the emission flux, reaching a few jansky (1 Jy = 10^{-26} W m^{-2} Hz^{-1}). Such a high sensitivity is reached owing to a broad band of received frequencies (200–600 MHz), a parallel analysis of the spectrum, and a large collecting area (600–1000 m^2). The RATAN-600 radio telescope has a modest spatial resolution in the horizontal plane (<15″ at the wave 2 cm) and a low resolution in the vertical plane (about 15′ at the wave 2 cm). The dimensions of the directivity diagram of the instrument vary proportionally to the wave length. Observations were performed regularly both in the mode of single scanning (3–5 observations per day) and in the mode of multiple scanning (60 scans per day with an interval of 4 min during 4 h). Such scans with a fairly narrow diagram frequently repeated for 4 h allow one to identify clearly the emission from particular details of the active region structure (local sources above sunspots, interspot sources, flocculi, etc.).

As is seen from radio observations presented in Figs. 16–17, both active regions AR10484 and AR10486 had specific features of the structure in polarized emission (Fig. 17, on the left), which allows us to classify them as flare-productive regions. As is known [17], such regions generate several strong flares of M and X classes as a minimum. In the polarization spectrum (Fig. 17) for the group AR10484 a growth of the polarized flux is observed at short waves 2.03, 2.24, and 2.32 cm, while a complex nonuniform structure is observed at longer waves from 2.74 to 3.21 cm. For the group AR10486 located in the eastern hemisphere of the solar disk, a complex structure in polarized emission (with multiple changes in the polarization sign) is observed in the range from 3.21 to 7.59 cm.

Let us discuss the properties of the spectra presented in Fig. 18. In the polarization spectrum of this region one can see already on October 30 the existence of an excess of emission with negative (right circular) polar-

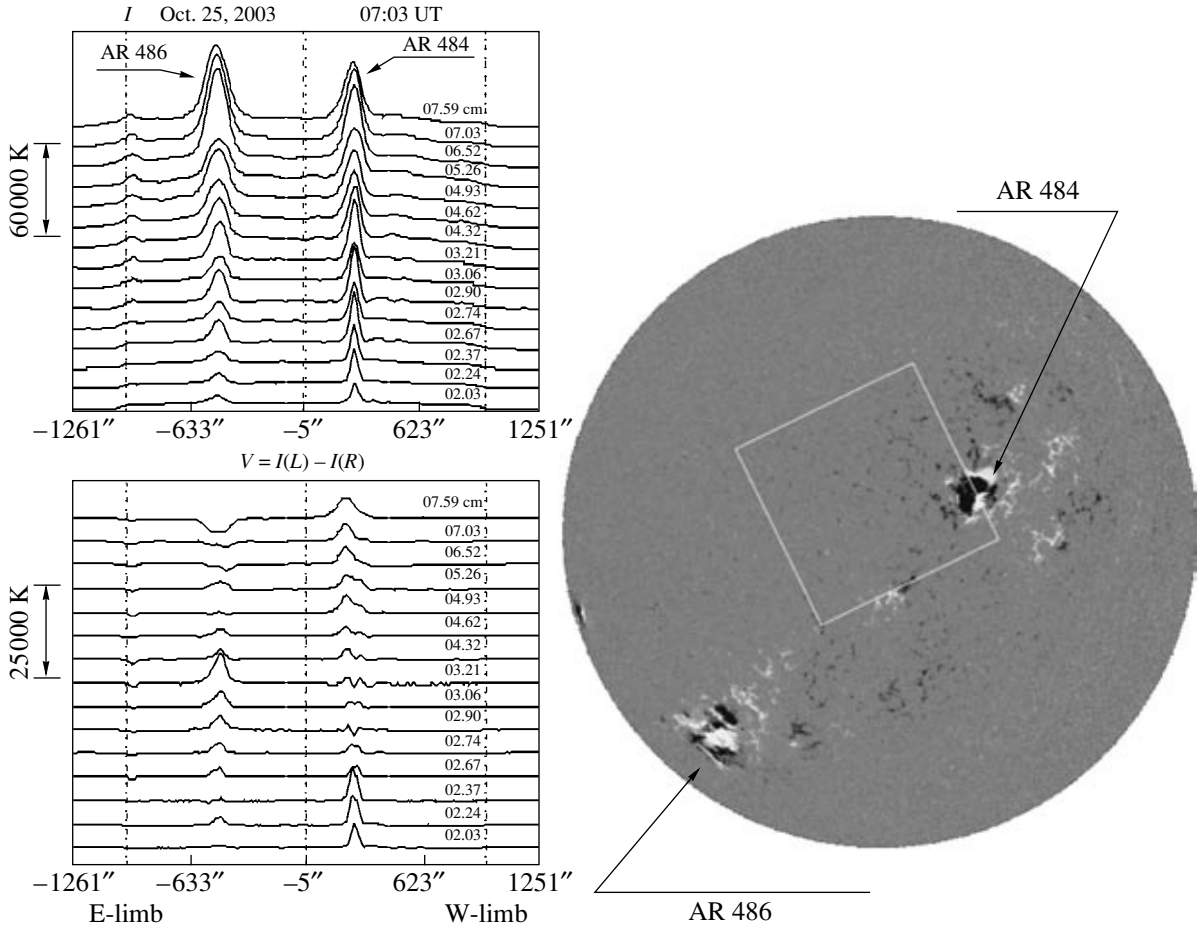

Fig. 16. Demonstration of the situation on the solar disk on October 25, 2003. A magnetogram based on the data of *SOHO* MDI is given on the right. Both active regions AR484 and AR486 have a complicated configuration of magnetic fields. On the left are multiwave one-dimensional scans of RATAN-600 for the intensity $I = I(L) + I(R)$ (at the top) and for circular polarization $V = I(L) - I(R)$ (at the bottom). The left polarization has a sign "plus." The frequency bands for both AR in which the structure is inhomogeneous due to pre-flare processes are marked in the polarization scans by dashed lines.

ization in the frequency band 12–14 GHz. This gives evidence of the appearance of emission associated with an emergence of the magnetic field of northern polarity. The intensity spectrum for October 30 also shows a break in this band. In the subsequent days of October 31 and November 1 an excess of right polarization gradually drifting to the longer wave range is also seen in the spectrum. This effect is interpreted as heating of higher layers during the emergence of a new magnetic flux. However, starting from November 2 and on subsequent days (November 3 and 4) a stable increase of the polarized emission of left polarity was observed at short waves (from 10 GHz to 17 GHz), which corresponded to the emergence of a magnetic flux of southern polarity. Apparently, it is this process that resulted in a powerful energy release caused by the emergence of a new magnetic flux and violation of stability of the active region magnetosphere. After generation of a strong flare the magnetic structure in the active region became stable. The excess of polarized emission at short waves (in the frequency band 10–16 GHz) disappeared (Fig. 18), and the form of the intensity spectrum (Fig. 18, right bottom panel) became typical for stable active region, determined by thermal emission of plasma.

Thus, it is shown by considering the spectral-polarization properties of radio emission of powerful active regions which existed on the solar disk in the period from October 18 to November 5, 2003 that these regions belong to a class of flare-producing regions. They possess typical properties of such regions: a growth of polarized flux at short centimeter waves (1.7–5 cm), multiple inversions of polarization in this range, and substantial variability of emission both at the preliminary and main stages of a strong flare.

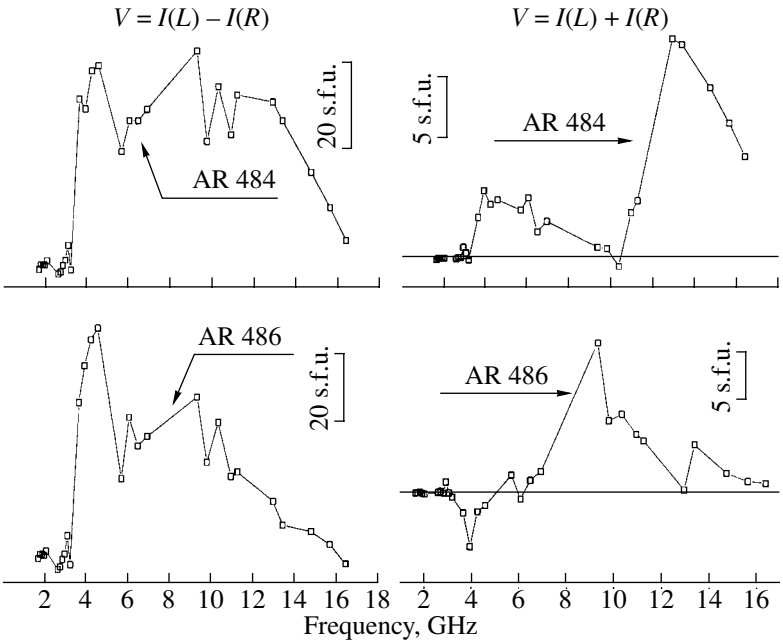

Fig. 17. The spectra of emission of active regions existing on the Sun on October 25, 2003 (intensity on the left and circular polarization on the right). A growth of the polarized flux spectrum at short waves is characteristic for AR484, while for the group AR486 a change of the sign of circular polarization is observed in the 6 cm wavelength band. Both phenomena allow one to classify these regions as belonging to the FPAR class.

8. MICROWAVE AND METER-WAVE RADIO BURSTS: IZMIRAN DATA

Observations of the radio emission of the Sun were carried out by the IZMIRAN instrumentation complex in the mode of everyday monitoring in the intervals 06–12 UT in October and 07–12 UT in November. The complex includes radiometers at fixed frequencies 3000, 204, and 169 MHz, and radio spectrographs of the frequency band 270–25 MHz [18, 19]. The latter allow one to obtain dynamic spectra at various time scales, i.e., both time-compressed spectra over the entire interval of observations to study large-scale phenomena and spectra with high temporal resolution to analyze the fine structure of radio emission. The review everyday dynamic spectra, as well as detailed spectra and time profiles of separate outstanding events, are presented on the website http://helios.izmiran.troitsl.ru/lars/LARS.html.

The passage in October–November of rapidly developed large active regions AR10484, AR10486, and AR10488 across the solar disk was accompanied by high activity in the radio range. This was the result of many CMEs, high flare activity, and the evolution of these regions. For example, during the first passage in the period October 19–30 an intensive noise storm was observed in meter waveband, with strong continuum and numerous bursts. This gives evidence of permanent acceleration of electrons in the lower and middle corona above these regions up to energies of tens of keV. We succeeded in detecting a series of powerful radio bursts against the background of a noise storm. They were associated with flares of X-ray class X and CMEs of the halo type. One of the strongest events of October 28, 2003, can serve as an illustration of this activity.

The flare 4B/>X17.2 occurred in the active region AR10486 (S16 E08) with a maximum in the soft X-ray range at 11:10 UT. According to the data of the *SOHO*/LASCO coronograph in this event at first (since 10:54 UT) a large CME was observed above the southeastern limb. Then (in the interval 11:06–11:30 UT) one more (still larger) CME of halo type began, with a homogeneous glow around the entire occulting disk of the coronograph. The average velocity of the main CME front in the picture plane was 1785 km/s at small altitudes, while at distances $>5R_s$ it reached 2125 km/s. As is shown in the lower panel of Fig. 19, the microwave radio burst at a frequency of 3000 MHz is characterized by a complex profile. In the interval 10:20–11:00 UT the flux density was up to 2500 s.f.u. This burst was associated with a remarkable activity of AR10486. Apparently, it corresponded to the first of above-mentioned CMEs. A much more intensive burst began at about 11:00 UT. At 11:03 UT the radio emission flux reached its first maximum with an intensity of about 10000 s.f.u. Then, after a certain decrease, a new component of the burst was observed, powerful and long, with a smooth time profile. Its intensity for 4 min (11:12–11:16 UT) exceeded the maximum threshold of detection 13000 s.f.u.

Judging from the compressed dynamic spectrum (the upper panel of Fig. 19), continuum emission with

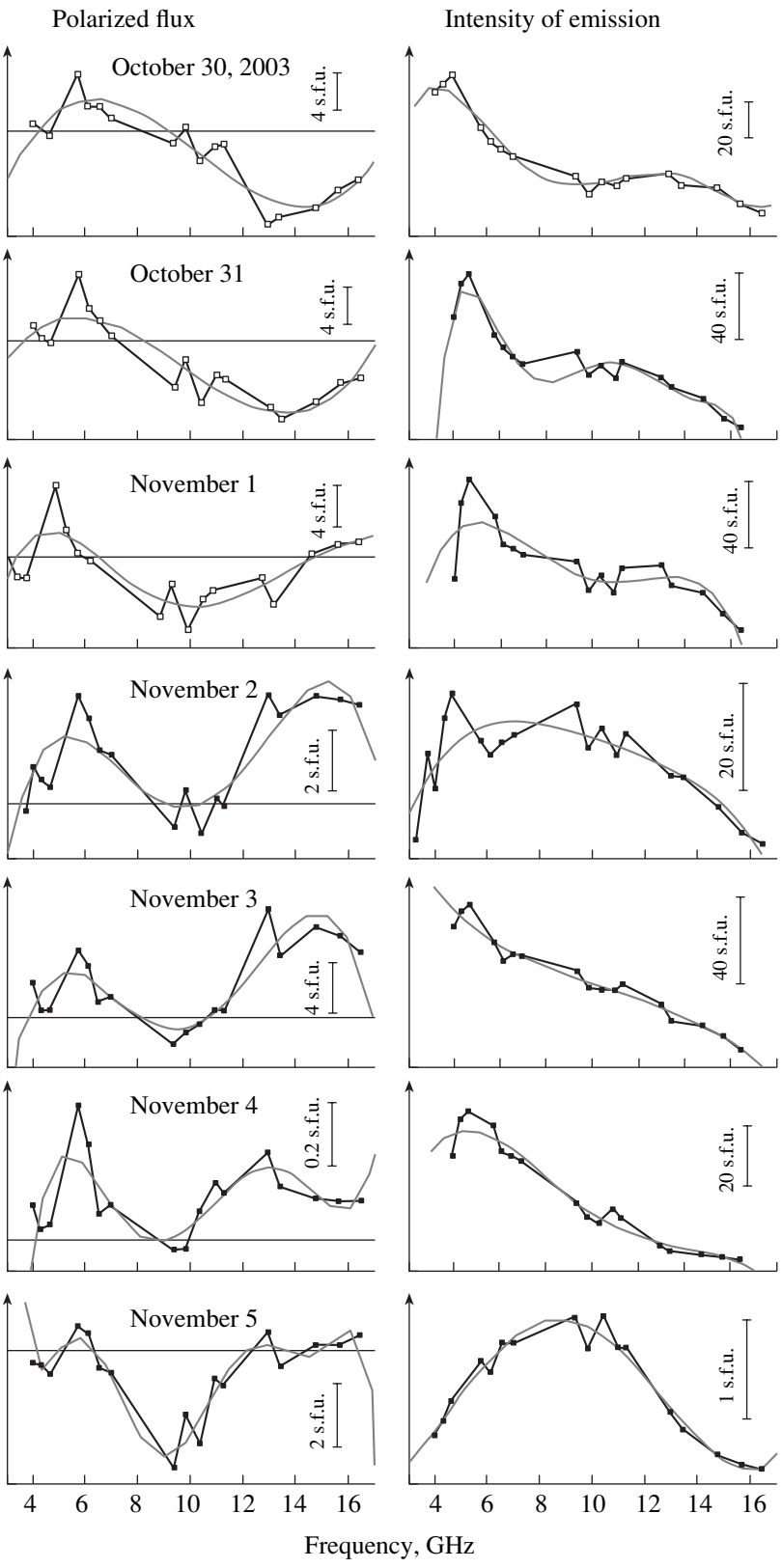

Fig. 18. Broadband spectra of a polarized flux of the microwave radio emission (left) in the period from October 30, 2002 to November 5, 2003 and the intensity spectra in the same period (right).

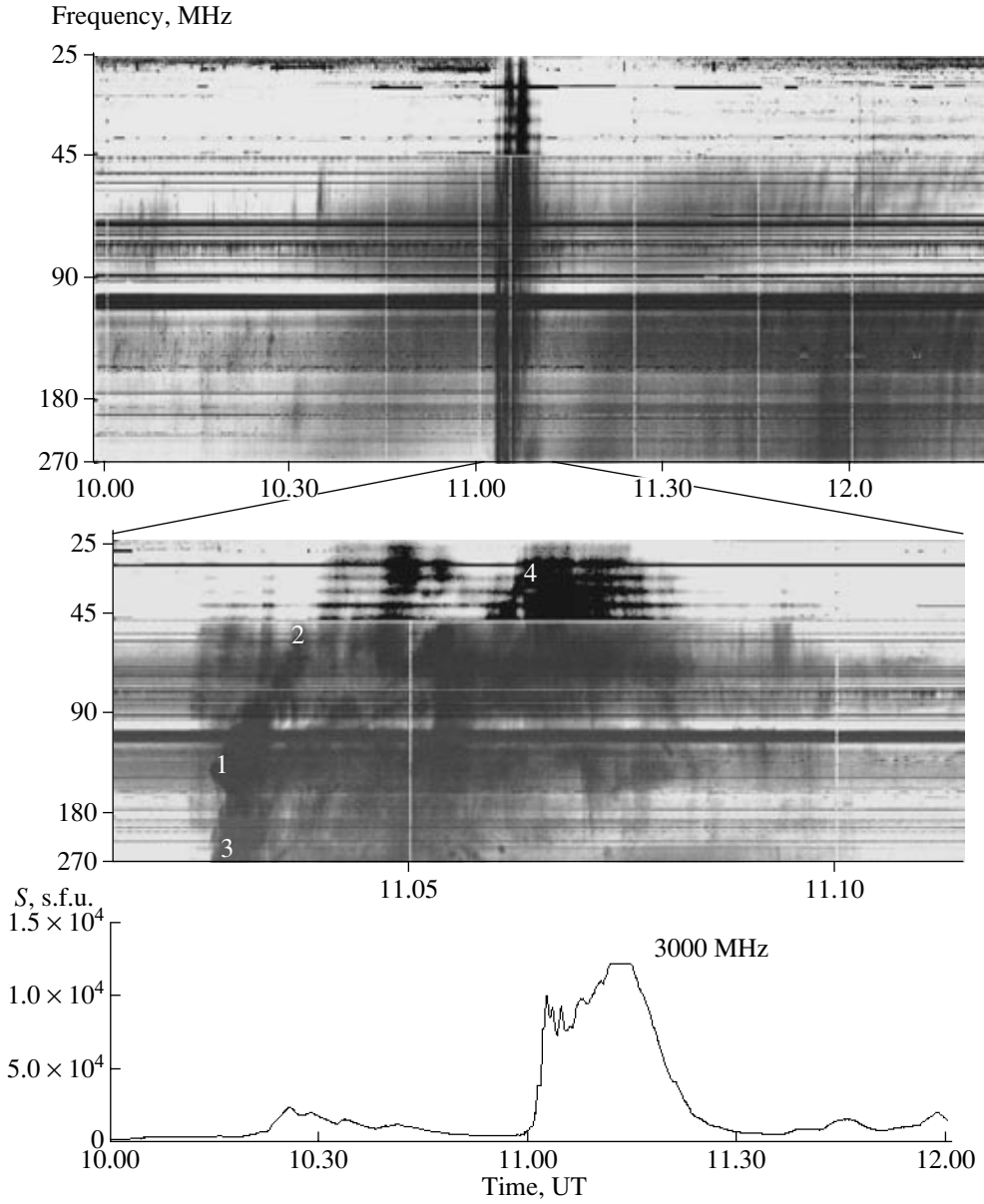

Fig. 19. Compressed (upper panel) and detailed (middle panel) dynamic spectra of meter-wave radio emission and the profile of a microwave burst (lower panel) in the event of October 28, 2003 according to IZMIRAN data.

a slow drift from high to low frequencies corresponded in the meter-wave band to the first microwave burst. The initial component of the main flare was accompanied by a powerful group of bursts of the III type. These bursts, as is known, are excited by the streams of accelerated electrons with energies of tens of keV. These electrons propagate in the corona along the open magnetic field lines. Then, in 5 min an intensive structured continuum began, which persisted until the end of observations.

More detailed spectrum in the interval 11:02–11:10 UT (the middle panel of Fig. 19) shows that a complex system of bands is observed on the background of an intense group of III type bursts. It has slower frequency drift, typical for bursts of the II type. This system includes the band 1–2 and several bands between the points 3 and 4. The complicated character of the spectrum indicates to multiple sources of radio emission and does not allow one to point at the place of generation unequivocally, identifying these bands as harmonics of the result of splitting.

The meter-wave radio bursts of II type are generated by electrons through a plasma mechanism. These electrons are accelerated on the fronts of shock waves propagating in the corona. CME can serve as a driver for these waves. According to estimates, the drift of II type bands corresponds to a fairly high velocity of the coronal shock wave: 3500–5000 km/s.

This value exceeds even the above indicated CME velocity, which is already quite large. This difference between the shock wave velocity, calculated from the drift of the II type burst, and the observed CME velocity can be associated with two factors: either with quite probable distinction of the real distribution of electron density in the corona from the model one (this can be a result of disturbances caused by preceding activity) or with a possible tilt of the emitting part of the shock wave front with respect to quasi-radial gradient of electron density in the corona.

In general, all data about the event of October 28, 2003 give cumulative evidence that the main flare included both impulsive and post-eruptive phases. During the impulsive phase a series of pulsed bursts was generated in the microwave range and the bursts of III and II types correlated with them. This means that acceleration of electrons and formation of a shock wave took place. During the post-eruptive phase the magnetic field of an extended region (strongly disturbed by CME) relaxes to a new quasi-equilibrium configuration by means of magnetic reconnections in extended current layers. This process is accompanied by long energy release and particle acceleration. It is quite probable that precisely because of this an intensive and long-living microwave component (detected at a frequency of 3000 MHz) appeared at the concluding phase of the event.

In many respects the pattern of radio emission observed in other eruptive events that we succeeded to detect at IZMIRAN in the period under study was quite similar. The relevant analysis of them is presented in [20].

9. COMPARATIVE ANALYSIS OF DYNAMICS OF SEPARATE EVENTS ON NOVEMBER 4, 2003

The X-ray flare record in its strength occurred on November 4, 2003 in AR10487 on the western limb (S21 W88). The dynamic ranges of the instruments that operated in space at that time were insufficient for obtaining high-quality images because of too large amplitudes of X-ray and ultraviolet bursts in this flare. In the movies shot by the *TRACE* satellite one can well trace the dynamics of brightening in a large arcade of loops after the flare. However, the image of the flare itself turns out to be strongly distorted in this case due to overloads of instruments and charge leakage to adjacent cells in CCD-matrices. The same picture is observed for images with lower spatial-temporal resolution of *SOHO*/EIT and, to a much lesser extent, of *Coronas-F*/SPIRIT, since the SPIRIT telescope used microchannel plates for detection of images. The development of the flare as a whole is accompanied by the appearance of a large number of fast-variable small-scale details rather than a single dominant feature like simply connected current layer, magnetic island, bright plasmoid, etc. The CME formed at large altitudes corresponds in its geometrical configuration to the elevation of twisted magnetic ropes and loops with electric current inside them, which is well traced in the character of images in the movies shot by the SPIRIT telescope.

Due to a limited dynamic range of the instruments now in use for the X-ray and ultraviolet parts of the spectrum, the large intensity of events in these and similar cases does not allow one to have high-quality images. At the most interesting phase of maximum luminosity one cannot do this because of overloads. The instruments simply were not designed to get high-quality images of the strongest (and, therefore, in many respects interesting) events. However, such events occur rather rarely. Therefore, one could recommend in the future either to provide for a possibility of automatic reduction of instrument sensitivity or to use some channels with low sensitivity. It is desirable to have something of this kind included in instrumentation, if we want to get reliable information about the strongest solar flares. In this connection, one of the authors of this paper recently made such a suggestion for the planned mission *SDO*.

Combining the exposures obtained by the telescopes EIT and SPIRIT for this and other events, one can try to improve slightly (approximately twice) the temporal resolution. The result of this procedure will be presented in a separate paper.

Practically there is no joint geomagnetic signal of this flare and an extended CME detected by the LASCO coronograph, since this powerful CME was westward-directed and missed the Earth. The same fact explains rather weak signals in neutron monitors. Thus, the X-ray flare with record parameters virtually had no effect on the solar wind parameters and the magnetic field in the Earth's orbit. It is needless to say that the ionosphere response to intensification of short-wave electromagnetic emission at this time should be also record in its value, which was indeed the case and allowed one to estimate indirectly [21] the power of X-ray emission at a level of 4.8 mW/m^2 in the detection channel of the *GOES* satellite. Formally, this may correspond to X-ray importance X48 according to the scale of comparison accepted for the *GOES* satellite. Detailed investigation of this problem is beyond the scope of this paper. However, it is worthwhile to emphasize here once again that the system of X-ray importance evaluation is very conventional, as was already discussed in section 1. One can find detailed descriptions of the situation on the Sun, in the heliosphere, and in the magnetosphere in the period under consideration on the Internet at various web-pages on solar-terrestrial physics, including those supported by prognostic centers of NOAA (Boulder, USA) and SIDC (Brussels, Belgium).

10. OBSERVATIONS OF DISTURBANCES IN THE SOLAR WIND BY THE METHOD OF INTERPLANETARY SCINTILLATIONS

The radio astronomy method of interplanetary scintillations is based on measurements of the intensity of emission of natural radio sources of sufficiently small angular dimensions. The intensity modulation is produced by irregularities of plasma density moving on the line of sight. Everyday observations of interplanetary scintillations of a large number (about 100) of flickering sources allow one to trace the dynamics of spatial distribution of the level of turbulence in the solar wind. In this way one can detect large-scale disturbances propagating in the solar wind. For some years the radio astronomic investigations of the solar wind are carried out in Pushchino Radio Astronomy Observatory of Lebedev Physical Institute using the Large Solar Antenna in the meter-wave band (a frequency of 111 MHz). For every source the index of scintillations m (or relative dispersion $\delta I(t)$) of time fluctuations of the intensity) is measured: $m^2 = \langle \delta I^2(t) \rangle / \langle I \rangle^2$.

The main contribution to the intensity modulation of sources in the waveband under study is made by those density irregularities with a characteristic scale of several hundred kilometers that are located in the interplanetary medium layer adjacent to the aiming point of the source's line of sight. Interplanetary scintillations have small characteristic times (of order of 1 s), which allows one to identify them against the background of comparatively slow (characteristic times of 10 s and longer) ionosphere scintillations. When disturbed regions with the enhanced (comparing to undisturbed level) turbulence level cross the line of sight, this passage is accompanied by the amplification of scintillations with respect to a calibration level known for each source. The solar wind region sounded in the meter-wave band includes a broad region of heliolatitudes, from near-equatorial to polar, in the range of heliocentric distances from 0.5 to 1 AU.

The period of high activity in October–November 2003 was also embraced by observations of the interplanetary plasma that were carried out using a prototype of 16-beam basic radio telescope. In these observations the active events on the Sun manifested themselves in the following three effects:

—powerful and long noise-like emission at 111 MHz;

—sharp intensification of interplanetary scintillations of observed radio sources; and

—sharp intensification of ionospheric scintillations of the radio sources.

The radio emission of a noise-like character and moderate strength (the flux of order of the flux of quiet Sun radio emission) was discovered already on October 18, when AR10486 had only appeared on the eastern limb. In the subsequent days until October 30 all observations of radio sources in the daytime sky were completely polluted by noise of the extremely strong radio emission of the Sun, which gave evidence about the strength of a noise storm. Relatively weak solar radio emission of the same character was detected until November 2.

In the period after October 30 the daytime sources were also observed. Substantial intensification of interplanetary scintillations (with an increase of the scintillation index by a factor of 2–3 as compared to undisturbed periods) was detected practically for all observed radio sources. An example of such intensification of scintillations due to the interplanetary disturbance produced by the October 29 flare is shown in two panels of Fig. 20. One can see in this figure how the enhanced scintillations observed on October 31 changed on November 1 into weak scintillations typical for undisturbed periods. Here, the interplanetary medium region transilluminated by the radio source 3C 352 corresponds to a distance of 1 AU from the Sun. It follows from the data on interplanetary scintillations (in particular, from Fig. 20) that the interplanetary plasma near the Earth's orbit was strongly disturbed in 40 h after the October 29 flare, and relaxation to the undisturbed state took place during the following day. It also follows from these data that the mean velocity of propagation exceeded 1000–1100 km/s for this disturbance.

During the disturbed period for all sources, even for those with no scintillations on the interplanetary plasma, a significant intensification of ionosphere scintillations was observed, which indicates to an increased level of plasma density fluctuations with dimensions of order of 1 km in the mid-latitude Earth's ionosphere.

11. HARD ELECTROMAGNETIC EMISSION AND CHARGED PARTICLES: THE DATA OF AN EXPERIMENT ONBOARD *CORONAS-F*

No solar flares of class X10 (according to the *GOES* data on soft X-ray emission) were observed on the phase of growth and in the maximum of the 23rd cycle of solar activity, and the statistics of γ-flares accumulated in this cycle was substantially poorer than in the cycles 20–22. All the more unexpected was the manifestation of extremely high solar activity on the declining phase of the 23rd cycle: in the period from October 23 to November 4, 2003, as many as 9 flares of class X occurred, including the flares X17.4 (October 28, 2003), X10 (October 29, 2003), and X28 (November 4, 2003). The instruments SONG and SPR-N onboard the space observatory *Coronas-F* (h_{orb} = 500 km, I = 82.5°, and T_{rev} = 94.5 min) have detected 7 of them, including three of four strongest flares. The data about these flares are presented in Table 3. Column UT gives the time of beginning and end of the X-ray emission with energies of 50–150 keV according to SONG data (or, in case of unavailable SONG data, of the 40–100 keV emission according to SPR-N data). For two flares where there were no *Coronas-F* data (marked by italic type) the

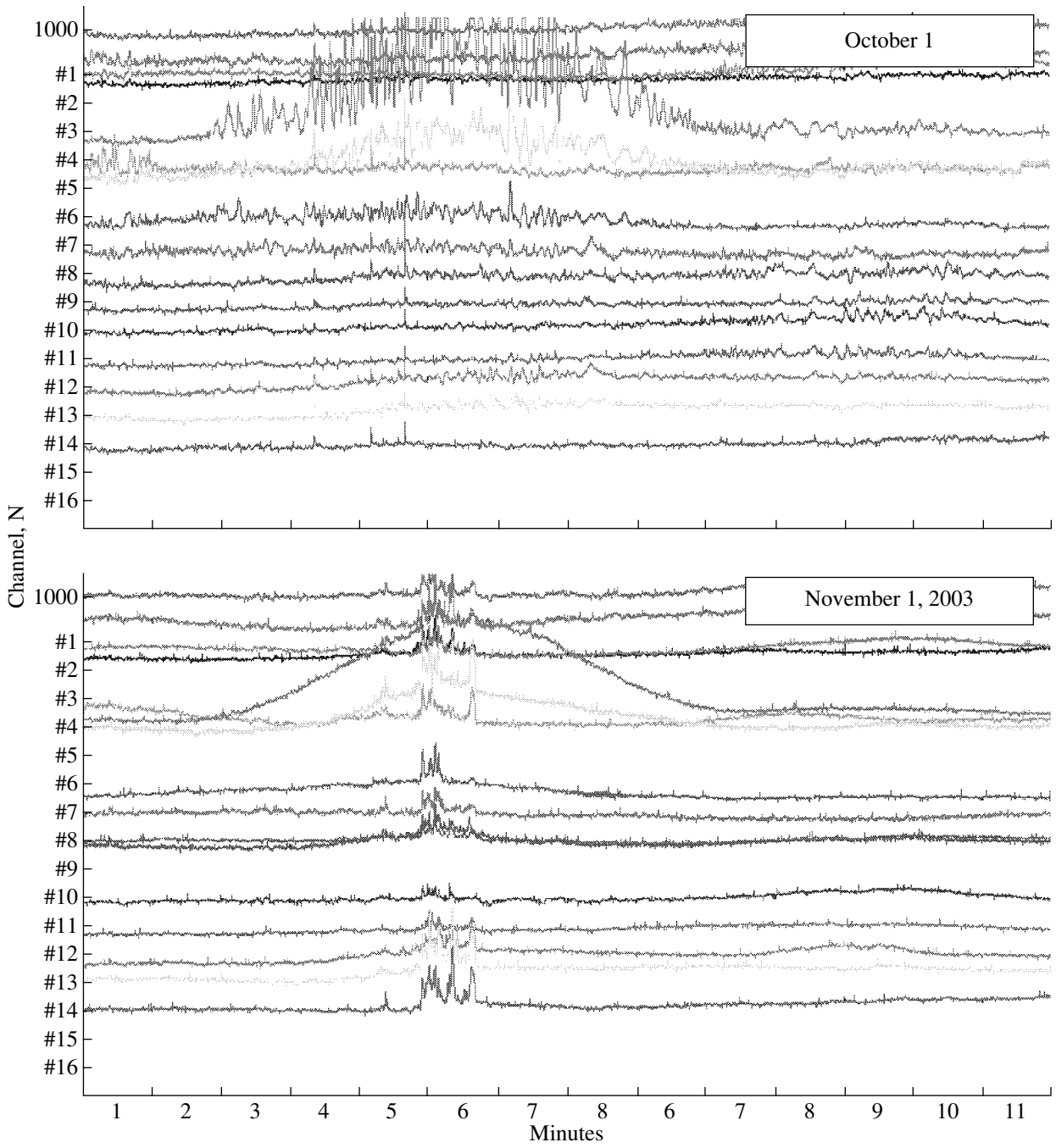

Fig. 20. An example of a sharp intensification of scintillations due to interplanetary disturbance from the flare on October 29, 2003. The source 3C252 is observed, the time of observation (at the source maximum) is 11:58 UT.

time from the flare beginning to its maximum in soft X-ray emission is given according to *GOES* data. Table 3 also presents the data on maximum energy of the neutral radiation detected in a particular event by the SONG and SPR-N instruments.

One can see from Table 3 that the NOAA region 10486 was the most productive with respect to the flares of class X: six out of nine, and precisely this region was responsible for all four flares with class higher than X8.

Figure 21 shows the time behavior of enhancements of X-ray and ultraviolet emissions measured during three strongest flares by the instruments SONG and SPR-N, as well as *GOES-12* data on the fluxes of thermal X-ray emission (SXR, 0.5–4 Å) and the time derivative of SXR. One can see from Fig. 21 that the flares of October 28 and November 4 were not only more

Table 3. The flares of the end of October – beginning of November 2003 (SONG, SPR-N)

N	Date	Time, UT	Importance	Coordinates	Active region	Maximum energy, MeV
1	October 23	08:17–08:43	X5.4/1B	S21 E88	10486	4–7
2	October 26	06:16–06:25	X1.2/3B	S15 E44	10486	0.15–0.5
3	October 26	17:21–18:19	X1.2/1N	N02 W38	10484	–
4	October 28	11:02–11:13	X17.2/4B	S16 E08	10486	60–100
5	October 29	20:38–20:55	X10/2B	S15 W02	10486	4–7
6	November 2	17:03–17:25	X8.3/2B	S14 W56	10486	–
7	November 3	01:17–01:29	X2.7/2B	N10 W83	10488	0.5–1.3
8	November 3	09:47–09:58	X3.9/2F	N08 W77	10488	0.04–0.1
9	November 4	19:32–19:57	X28/3B	S19 W83	10486	100–200

intensive in SXR, but they had much harder spectrum of γ-ray emission (up to 100 MeV). The SONG instrument detected solar neutrons ($E_n > 20$ MeV) during the flares on October 28 and November 4. Their maximum flux comprised 0.07 ± 0.02 particles per cm^2 s for the flare of October 28, which was comparable both with the fluxes measured earlier by *SMM* GSR and with the *Coronas-F* data for the flare of August 25, 2001.

Comparing the X-ray bursts in the range of tens–hundreds of keV observed by *Coronas-F* with radio bursts from centimeter to sub-millimeter waveband according to published data of ground-based observations, one can see a good synchronism of their time development in the solar flares observed. The synchronous variations of X-rays and sub-millimeter radio emission during the impulsive phase which lasted a few minutes in the flare of November 4, 2003, indicate that the energy release in these spectral ranges was simultaneous within the time resolution (it was equal to 4 s in the case of *Coronas-F* measurements of X-ray emission). The time resolution of radio observations at the Leonido station in the range 200–400 GHz was much higher and allowed one to detect strong variations on millisecond scale [22]. The physical cause of such a synchronism is the fact that both types of emission are generated by the same agents, namely, by electron beams in the solar atmosphere. One can trace in both sets of data a distinct synchronous modulation of radiation on the time scale of minutes. Nonmonotonic character of variations is associated with successive development and decay of separate discrete sources of emission in magnetic loops of the flare arcade, which can be especially well traced using the movies shot by the *TRACE* satellites during the record-strong limb flare on November 4, 2003.

12. BURSTS OF INTENSITY OF SOLAR COSMIC RAYS

Strong variations of the SCR fluxes, their anisotropy, ion composition, and energy spectra contain information about the processes of acceleration and propagation of particles on the Sun and in the interplanetary space.

The first considerable X-ray flare (X1.2/3B) occurred on the Sun at 05:57–07:33 UT on October 26 in AR10486 (S15 E44). No arrival of particles from this flare was observed at the Earth. A moderate shock wave was observed at ~05 UT on October 28. The second flare of the same day, also of class X1.2 though less intense in optics and microwave radio emission, occurred in the western active region AR10484 at 17:21–19:21 UT. The instrument SKI-3 (silicon telescope) onboard the *Coronas-F* satellite measured the fluxes of protons and He nuclei in the energy intervals 2.3–4.2 and 4.4–19 MeV per nucleon. For heavier nuclei the measurements of fluxes in two energy intervals were supplemented by measurements of energy release in three detectors, which yielded the information about charge and energy of nuclei in the range from C to Si. A significant enhancement of proton fluxes in both energy intervals was observed in the northern polar cap (NPC) already at 19:50 UT. The small time delay of particles, the steep leading edge of fluxes, considerable anisotropy, and significant dispersion in velocities correspond to fast propagation of particles in the undisturbed interplanetary space. The measured fluxes and identification of events are shown in Fig. 22.

The highest fluxes of SCR nuclei in this series arrived after the flare X17.2/4B in AR10486 (S16 E08) observed at 09:51–11:24 UT on October 28. The propagation of particles from this flare was more complicated, since the particle fluxes were modulated by a strong shock wave (SW).

The first arrival of SCR from this flare was observed in SPC at 12:46 UT for protons with energies 4.4–19 MeV. The rapid arrival of particles, distinct dispersion in velocities, and a quick buildup of fluxes indicate to a free propagation from the place of acceleration on the Sun along the IMF. However, when the fluxes reached their maximum at ~18 UT, instead of decrease, the increase is again observed. This increase

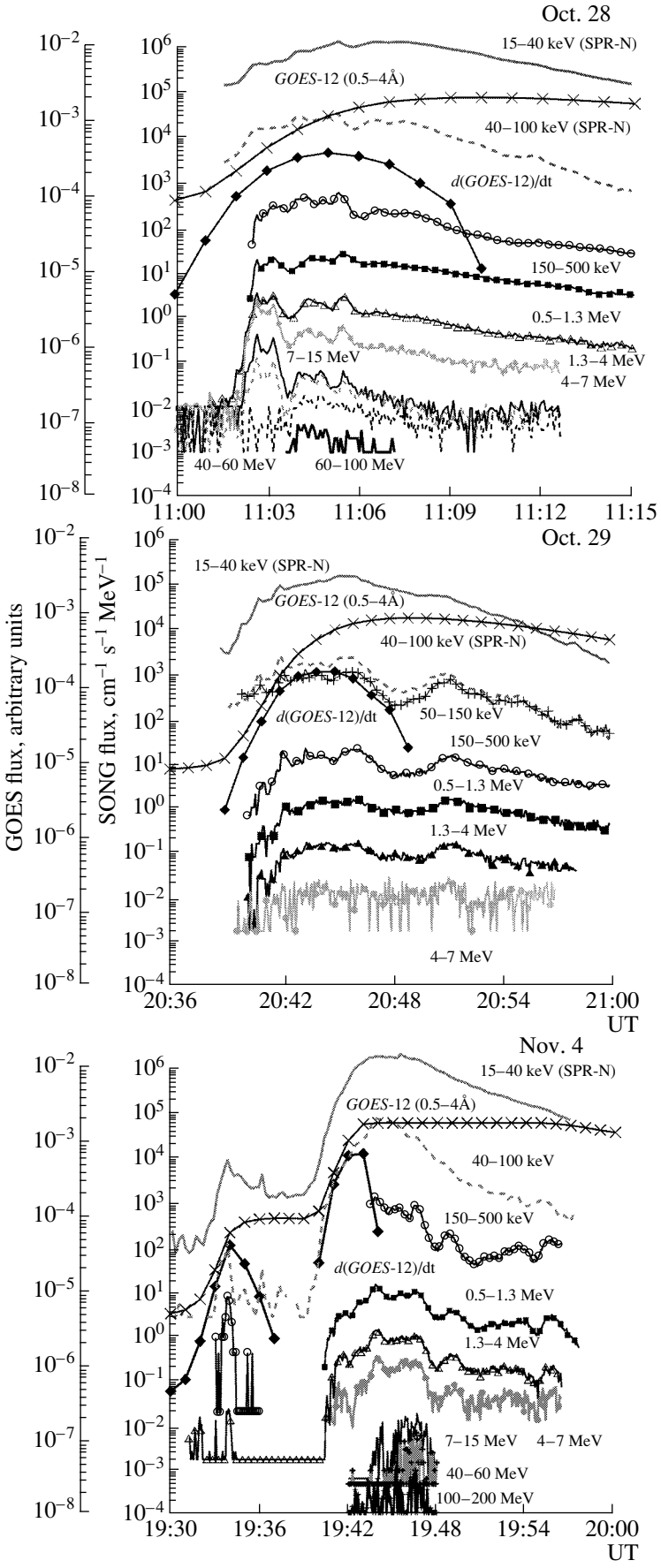
Oct. 28
15–40 keV (SPR-N)
GOES-12 (0.5–4Å)
40–100 keV (SPR-N)
d(GOES-12)/dt
150–500 keV
0.5–1.3 MeV
7–15 MeV
1.3–4 MeV
4–7 MeV
40–60 MeV
60–100 MeV
11:00
11:03
11:06
11:09
11:12
11:15
Oct. 29
15–40 keV (SPR-N)
GOES-12 (0.5–4Å)
40–100 keV (SPR-N)
d(GOES-12)/dt
50–150 keV
150–500 keV
0.5–1.3 MeV
1.3–4 MeV
4–7 MeV
20:36
20:42
20:48
20:54
21:00
UT
GOES flux, arbitrary units
SONG flux, cm^{-1} s^{-1} MeV^{-1}
Nov. 4
15–40 keV (SPR-N)
GOES-12 (0.5–4Å)
40–100 keV
150–500 keV
d(GOES-12)/dt
0.5–1.3 MeV
1.3–4 MeV
7–15 MeV
4–7 MeV
40–60 MeV
100–200 MeV
19:30
19:36
19:42
19:48
19:54
20:00
UT

Fig. 21. The review plots constructed using the data of instruments SONG and SPR-N installed onboard the *Coronas-F* satellite. In October–November 2003 the events were observed when the fluxes of hard X-ray and gamma-ray emission of the Sun strongly increased in a wide energy range indicated on the plots. The fluxes of energetic neutrons from solar flares were also detected.

is associated with SW and becomes all the more steep as it approaches. The bulk of particles arrived together with SW and behind its front. This maximum, as is usual for the events of this type, reveals itself most strongly in particles of lower energies so that the energy spectrum in the maximum is steeper than the spectrum of preceding SCR fluxes. The spectral index for oxygen nuclei in the energy range 10–37 MeV/nucleon is equal to –3.2 and –(2.1–2.3) at the maximum and before the SW arrival, respectively (Fig. 23).

The next strong flare (X10/3B) occurred in the same AR10486 (S15 W02) at 20:37–21:01 UT on October 29. It is difficult to discern visually the arrival of particles from this flare on the background of substantial SCR fluxes from the flare of October 28. However, the index of energy spectrum for the averaged flux of O nuclei was 2.1 at 02–10 UT on October 30, i.e., the same as in the first hours of enhancement from the preceding flare. The enhanced flux of nuclei after 19 UT on October 30 is due to the arrival of CME, and, as in the previous event, the spectrum for O nuclei became substantially steeper: the spectral index for O nuclei at 20–24 UT on October 30 was equal to –3.6. It is worthwhile to note also the enhanced abundance of neon ions at that time (see Table 4).

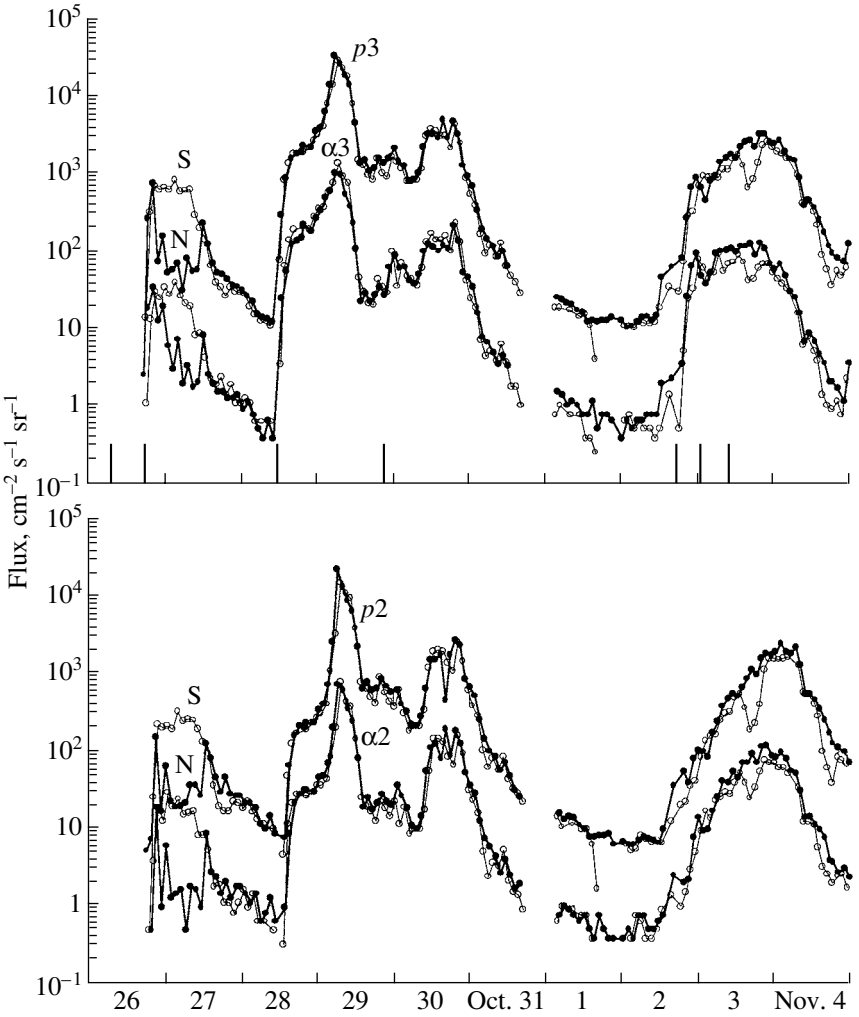

Fig. 22. The fluxes of SCR nuclei in the North and South polar caps in October–November 2003. Vertical bars on the abscissa axis of the upper panel show the instants of strong solar flares: X1.2/3B in AR10486 (S15 E44); X1.2/1N in AR10484 (N02 W38); X17.2/4B in AR10486 (S 16 E08); X10.0/2B in AR10486 (S15 W02); X8.3/2B in AR10486 (S14 W56); X2.7/2B in AR10488 (N10 W83); and X3.9/2F in AR10488 (N08 W87); p2 and α2, and p3 and α3 correspond to p and He nuclei with energies 2.3–4.2 and 4.4–19 MeV/nucleon, respectively.

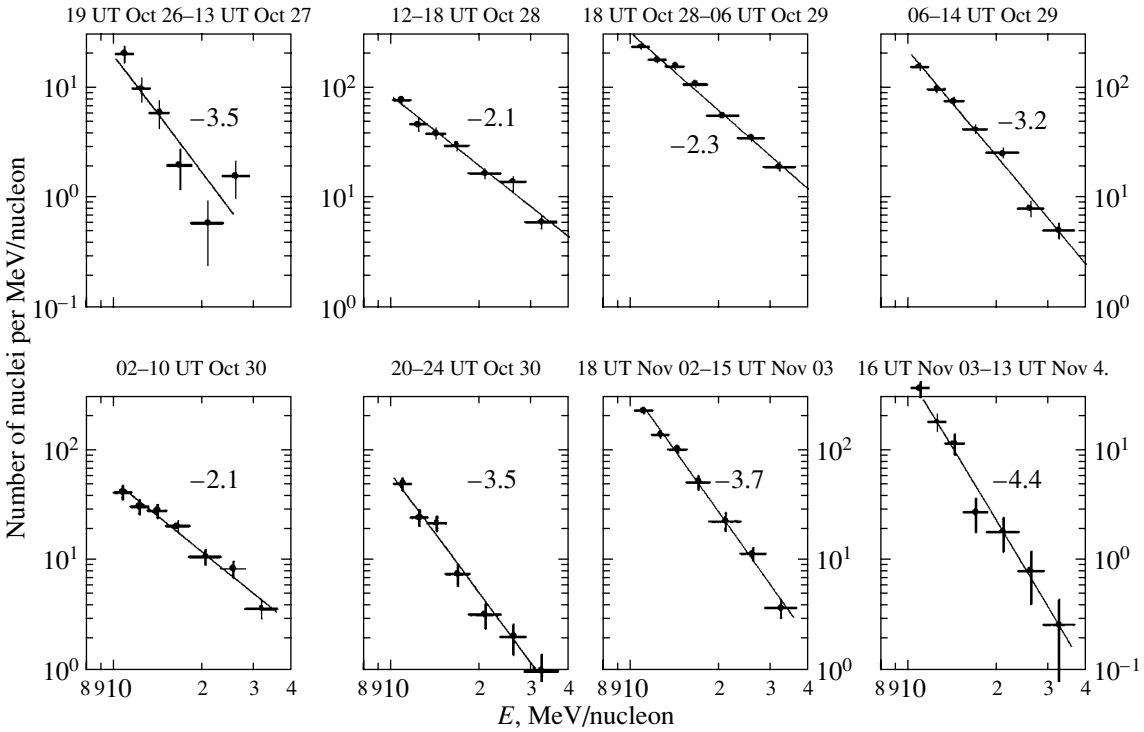

Fig. 23. The fluxes of SCR nuclei in the polar caps in the period October 26–November 4, 2003: energy spectra of oxygen nuclei.

One more sufficiently strong flare (X8.3/2B) was observed in the same AR (S14 W56) at 17:03–17:39 UT on November 2. The beginning of an enhancement of the fluxes of protons and He nuclei with energies 4.4–19 MeV/nucleon was seen in SPC at 19:45 UT. This enhancement is similar to the first one in this series of SCR events, and its character corresponds to SCR propagation in a weakly disturbed IMF. The energy spectrum index for the fluxes of O nuclei summarized over the event (until 15 h on November 3) was equal to –3.7. The enhancement of SCR fluxes after 16 h on November 3 can be due to less strong flares (X2.7/2B and X3.9/2F) observed on this date in AR10488 near the western limb and CME fluxes from the flare of November 2.

Table 4. Relative chemical composition of nuclei with energy 11.4–23 MeV/nucleon in SCR bursts from October 26 to November 4, 2003

Time, date	C	N	O	Ne	Mg	Si
19.00–13.00 October 26–27	43 ± 17	10.8 ± 7.1	100	10.8 ± 7.1	30 ± 14	24 ± 11
12.00–18.00 October 28	48.2 ± 6.7	12.0 ± 2.7	100	13.6 ± 2.9	24.4 ± 4.2	23.1 ± 4.1
18.00–06.00 October 28–29	46.5 ± 3.3	12.3 ± 1.4	100	11.4 ± 1.4	24.5 ± 2.2	21.1 ± 1.9
06.00–14.00 October 29	44.1 ± 4.8	12.6 ± 2.0	100	14.0 ± 2.2	20.6 ± 2.9	13.6 ± 2.2
14.00–10.00 October 29–30	41.8 ± 5.4	12.1 ± 2.4	100	17.3 ± 2.9	22.4 ± 3.6	19.3 ± 3.3
10.00–01.00 October 30–31	39.9 ± 5.6	14.9 ± 2.8	100	28.3 ± 4.2	30.4 ± 4.6	20.5 ± 3.5
18.00–15.00 November 2–3	33.2 ± 3.9	13.3 ± 1.9	100	13.4 ± 1.9	19.5 ± 2.5	14.9 ± 2.1
16.00–13.00 November 3–4	45 ± 13	11.6 ± 5.4	100	23.2 ± 8.6	29 ± 10	10.1 ± 4.1

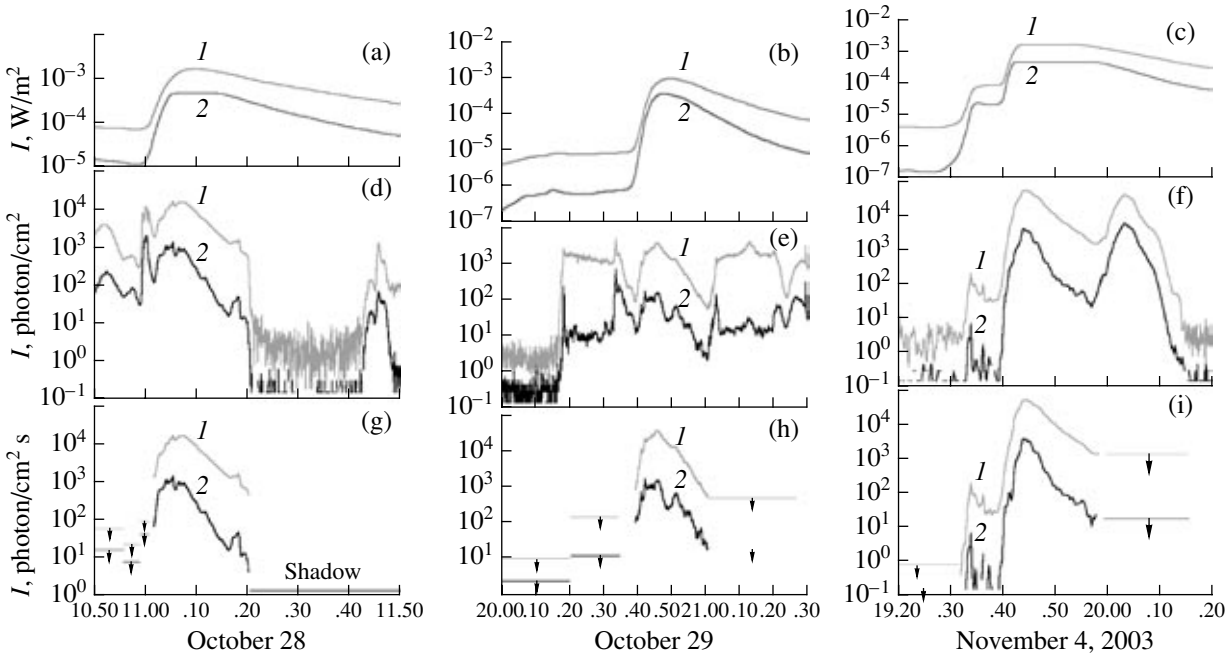

Fig. 24. The time behavior of the intensity of X-ray emission during the flares of October 28 and 29, and November 4, 2003. The data of *GOES* (a, b, and c, curves *1* and *2* correspond to channels 1–8 Å and 0.5–4 Å, respectively) are presented, as well as the data of a patrol detector of SPR-N instrument (d, e, and f, curves *1* and *2* correspond to channels 15–40 keV and 40–100 keV, respectively) and the data of SPR-N patrol detector after subtracting the background (g, h, and i, curves *1* and *2* correspond to channels 15–40 keV and 40–100 keV, respectively).

Sometimes, quite substantial anisotropy of SCR fluxes is observed, especially clearly it manifested itself on October 26–27 in different filling of both polar caps by SCR (Fig. 24). At this time the IMF was for several hours directed southward and sunward, which facilitated the formation of magnetic tubes immediately connecting the SPC with the place of particle acceleration near the Sun. The undisturbed magnetic field on the rout of particle propagation in the inner heliosphere gave a possibility for direct arrival of particles at the point of observation without significant back-scattering behind the Earth's orbit. When this time elapsed, the strong anisotropy at the Earth's orbit disappeared being changed into almost isotropic distribution. Similar pattern is also observed in the data of *Meteor* satellite. Observations of integrated fluxes (fluences) of protons with energy above 30 MeV onboard satellites of *GOES* series (http://spidr.ngdc.noaa.gov) give for the period under consideration a picture in many respects similar. As usual, the arrival of protons along the undisturbed spiral magnetic field is sometimes recorded already in several tens of minutes after a strong X-ray flare (http: //sec.noaa.gov/ftpmenu/indices/2003_events.html).

If we restrict ourselves to considering only a few or even about ten strongest events of this kind detected up to now, all of them were observed in the years that deviated by no more than two–three years from the maxima of solar cycles determined by strongly smoothed sunspot numbers. If some other indices are used in order to characterize the solar activity, for example, sunspot numbers without strong time averaging and smoothing, then one can find in them quasi-biennial variations, especially clearly seen near the maxima of 11-year cycles in the form of so-called Gnevyshev gaps. Naturally, this phenomenon can also manifest itself in the observed fluxes of protons. However, the statistics is not so large as to make some more definite and detailed conclusions about possible grouping of rare events in years of the solar cycles. It is obvious that the sunspot numbers in their very essence are not the best or single indices in this respect.

Thus, the appearance of a number of strong proton events on the declining phase of the 23rd solar activity cycle is not an extraordinary phenomenon in this sense.

13. POLARIZATION OF HARD X-RAY EMISSION OF SOLAR FLARES DURING A BURST OF ACTIVITY IN OCTOBER–NOVEMBER 2003

The degree of polarization of hard X-ray emission (~10–100 keV) of solar flares is one of the main characteristics whose measurement would allow one to judge about the flux direction of accelerated electrons generating this emission via bremsstrahlung in the solar atmosphere. However, no experimental data of this kind were so far available. The degree of polarization was measured only in a few works for several flares and only in the range of relatively soft X-ray emission (wavelengths of about 0.8 Å). The values obtained in

these experiments lie within the limits from several percent to 20–40%.

In order to measure the polarization of hard X-ray emission of solar flares the SPR-N instrument [23] is used onboard the *Coronas-F* solar space observatory. It allows one to determine the degree of polarization of X-ray emission in the energy ranges of detected photons E_γ = 20–40, 40–60, and 60–100 keV. The method of polarization measurement is based on the Thomson scattering of solar photons in beryllium plates. Five planes of metal beryllium are installed inside a hollow hexagon prism, on the faces of which six scintillation detectors are installed symmetrically. These detectors surrounding the scatterer use the phoswich from CsI(Na) and plastic scintillator (polystyrene) in order to exclude detection of charged particles. Geometrically, the area of each detector is 8 cm^2, while taking into account absorption in shielding materials, efficiency of scattering and detection the effective area changes from ~0.3 cm^2 at E_γ = 20 keV to ~1.5 cm^2 at E_γ = 100 keV.

For non-polarized emission the probability of scattering to various angles relative to primary direction of photon motion is identical, therefore the scattering should be azimuth-symmetrical, and all detectors must record the same intensity. In the case of plane-polarized emission most photons are scattered perpendicular to the plane of polarization. Considering that at the sunward instrument orientation the photons arrive at a right angle to the surface of the scatterer one can expect that the plane-polarized emission will be scattered in beryllium plates preferentially along the planes of the plates. In this case the pairs of oppositely located detectors correspond to polarization planes rotated by 60° relative to each other. Since in the case of plane-polarized emission the azimuth anisotropy of scattered photons takes place, unequal counting rates should be observed in different pairs of sensors: the largest number of counts should be in the sensors positioned maximally close (within ±60°) to the plane perpendicular to the plane of polarization. Thus, the different counting rates of detectors allow one to determine the degree of polarization P_{meas} of detected emission and, in principle, the angle φ of the plane of rotation of the polarization plane with respect to a pair of detectors.

In addition, the instrument allows one to measure in detail the time profile of the intensity of X-ray emission in the energy range 15–100 keV, to determine the flux value, and to evaluate the hardness of the spectrum in the above indicated energy range. For this purpose a narrow-angle patrol detector is used. It is manufactured on the basis of a scintillation crystal CsI(Na) with an effective area of ~1 cm^2 (E_γ = 40 keV).

The quantities P_{meas} and φ are related to the count numbers N_i (i = 1, 2, 3) of each pair of detectors measured in every exposure as

$$P_{\text{meas}} = \frac{N_i^{\max} - N_i^{\min}}{N_i^{\max} + N_i^{\min}} \frac{N_i + N_j - 2N_k}{\sum_{i=1}^{3} N_i} \frac{1}{\cos 2\varphi},$$

where $N_i^{\max}$ and $N_i^{\min}$ are the maximum and minimum count numbers for the case of detection of fully polarized emission, and $i \neq j \neq k$ are chosen so that the following inequality would be valid: $(N_i + N_j - 2N_k)/\cos 2\varphi > 0$.

In order to determine P_{meas} from measured values of N_i, the simulation of Thomson scattering in the beryllium plates was carried out for an incident plane-parallel emission. For a given value of polarization of the incident emission P_0 (which was selected in the interval from 0 to 100%) depending on the φ angle the values of $N_i/\sum_{i=1}^{3} N_i$ were calculated. The latter characterized the fraction of scattered polarized emission recorded by a specified pair of detectors in relation to the total flux illuminating the scatterer. The obtained dependences allow us to solve the inverse problem: to determine the degree of polarization P_{meas} of the incident emission using the measured quantities and taking the angle φ into account.

The polarimeter of hard X-ray emission SPR-N detected in October–November 2003 six X-ray flares, including three out of four strongest flares: on October 28 and 29, and on November 4. One and the same active region AR10486 was a source of the flares on October 29, 2003 (X10/2B) and November 4, 2003 (X28/4B). This region was located almost in the center of the solar disk on October 29 (S15 W02), while on November 4 it was on the western limb (S19 W83).

For the above flares Fig. 24 presents the time profiles measured by the patrol detector of SPR-N and by X-ray monitors of the *GOES* satellite. These dependences characterize the variations in the flux of thermal and hard (bremsstrahlung) X-ray emission during the flares. The figure presents both the original time dependences of intensity values constructed using the counting rates in the channels of the patrol detector of the SPR-N instrument and the time profiles "purified" from background variations. To this end, the values measured during the previous orbit of the satellite were subtracted from the original values of the counting rate. In this case, the points with geomagnetic coordinates closest to those corresponding to the moments of detection of the flare emission were selected on the previous orbit. When the regions of trapped radiation are crossed, because of high variability of background the error in determination of the intensity of proper flare emission is high; therefore, only upper limits are given in these cases. When the satellite entered the shadow region, no solar radiation was detected. In view of the above reasons, for all three flares the reliable data of the instrument SPR-N are available only for those time intervals in which the background was almost constant (the regions of the geomagnetic equator and polar

caps). Since for such intervals the error in determination of intensity was small (being determined mainly by statistical scatter of the counting rate values) one can trace on the time profiles of the flares the variations in the patrol detector data with characteristic times of tens of seconds, which are not of instrumental origin. They should be produced by real pulsations of intensity.

One can see in Fig. 25 a substantial increase of polarization over the background values. It is worthwhile to note that calibration of the energy thresholds of the polarization detectors was carried out using light diodes throughout the entire satellite flight. The results of this calibration show the stability of threshold adjustment within the accuracy of a few percent. The same is confirmed by practically invariable background counting rate of the channels of polarization detectors detected in the geomagnetic equator region. The level of this background should vary but slightly, since it is produced mainly by local and induced gamma rays originating as a result of interactions of high energy cosmic rays whose intensity can be considered to be constant.

Nevertheless, for more accurate determination of the degree of detected polarization we carried out a normalization of the data of polarization detectors in order to exclude possible difference in the number of counts due to different efficiency of operation of phoswich circuits (i.e., selection of events detected by plastic scintillators). In this case, it was assumed that polarization should be negligibly small at the final stage of a flare [24]. The data of individual detectors of polarization were normalized to their own data at the end of the flare. In addition, for reducing the statistical error the time profiles were smoothed by the method of sliding average over 5 successive exposures. The data were accumulated during 4 s for each sequential time interval with duration of 14 s, i.e., the exposure duration was 4 s at the on-duty factor $4/14 \approx 0.28$. Thus processed data of polarization measurements are also presented in Fig. 25 along with the data of the patrol detector.

In particular, Fig. 25 presents the time behavior for the quantities characterizing the relative contribution of separate pairs of polarization detectors to the total number of counts for all detectors. These quantities represent the ratios $N_1/\sum_{i=1}^{3} N_i$ and $(N_1 + N_2)/\sum_{i=1}^{3} N_i$, which show how far the number of counts recorded by a given pair of detectors deviates from the levels 0.33 and 0.67 corresponding to equal counting rates as should be the case for unpolarized emission. One can see the qualitative difference in the time behavior of the quantities $N_1/\sum_{i=1}^{3} N_i$ and $(N_1 + N_2)/\sum_{i=1}^{3} N_i$ in different energy ranges. Within the errors, in the channel 20–40 keV a smooth decrease of the quantity $N_1/\sum_{i=1}^{3} N_i$ takes place down to the level corresponding to detection of unpolarized emission. At the same time in the channels 40–60 keV and especially

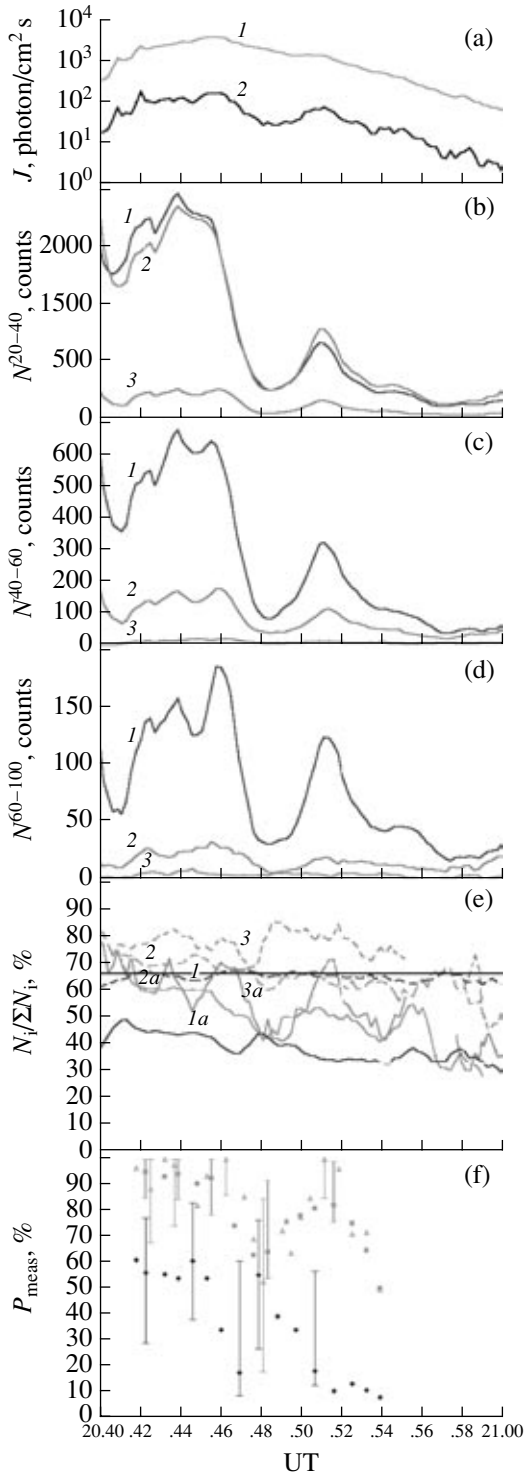

Fig. 25. The data of the SPR-N instrument during the flare of October 29, 2003. The time behavior of the intensity in the patrol detector channels (*1* and *2* correspond to 15–40 keV and 40–100 keV, respectively) (a); the number of counts during exposure 4 from three pairs (*1*, *2*, *3*) detectors of polarization in channels 20–40 keV (b), 40–60 keV (c), and 60–100 keV (d). The curves in panels b, c, and d are smoothed by the method of sliding average over 5 successive exposures. The time behavior of relative contributions of the first pair of detectors (*1*a, *2*a, and *3*a correspond to 20–40, 40–60, and 60–100 keV, respectively) and a sum of the first and second pairs of detectors (*1*, *2*, and *3* correspond to 20–40, 40–60, and 60–100 keV) to the total number of counts of polarization detectors (e) is shown together with the time behavior of the degree of polarization P_{meas} (f).

60–100 keV the time behavior of the ratios under consideration is inhomogeneous: the values of $N_1/\sum_{i=1}^{3} N_i$ and $(N_1 + N_2)/\sum_{i=1}^{3} N_i$ most strongly deviate from the levels 0.33 and 0.67 at the instants ~20:42, ~20:44, ~20:46, ~20:51, and ~20:56 UT, i.e., when the local maxima of intensity were observed. All this gives us grounds to believe that the hard X-ray emission was polarized in the flare on October 29, and the degree of polarization could be very high, especially at the maxima of intensity.

The values of P_{meas} for the flare of October 29 presented in Fig. 25 were obtained for independent points of measurements (i.e., separated from each other by the interval of averaging exposures). The error in determination of P_{meas} can be caused by two factors: statistical scatter of the number of counts during exposure and systematic error in determination of normalizing coefficients. For the flare of October 29 the normalizing coefficients were determined using the interval 20:57–20:59 UT (later the instrument data were distorted due to possible contribution of bremsstrahlung of electrons from the radiation belt into which the satellite entered). However, generally speaking one cannot state that the conditions of complete thermalization of electrons in the chromosphere plasma are fully met for this interval, i.e., with some probability the detected emission could include a polarized component. Therefore, the selected values of normalizing coefficients may be considered as maximal and corresponding values of P_{meas} as the lower limit. As minimum values of normalizing coefficients one can take the values determined using the flares whose concluding thermal stage was identified in the detector data more or less reliably. Based on such values of normalizing coefficients, the upper limit of P_{meas} for some exposures turned out to be close to 100% in the channels 40–60 and 60–100 keV. The error in determining the normalized values of the number of counts of polarization detectors (hence, in determining P_{meas}) exceeds the statistical error considerably due to the systematic scatter of values of the normalizing coefficients. As one could expect, the strongest polarization takes place at the higher energies.

At the initial phase of the flare the degree of polarization was 50–60% in the channel 20–40 keV and 70–100% in the channels 40–60 and 60–100 keV. Then, the degree of polarization decreased in the channel 20–40 keV almost monotonically (within the accuracy of measurements) along the entire time profile of the flare. As for the channels 40–60 and 60–100 keV, the variation of the degree of polarization (as one can see in Fig. 25) correlates with the time behavior of intensity: it takes on the largest values at the maxima of intensity and is minimal between the peaks.

For the flare of October 28 and the initial increase of the event of November 4 there are no indications that the emission was strongly polarized. We can give only the upper limits for the degree of polarization: for the events of October 28 $P_{meas} < 20\%$ (20–40 keV), $P_{meas} < 20\%$ (40–60 keV), and $P_{meas} < 25\%$ (60–100 keV). For the event on November 4 in all energy ranges we have $P_{meas} < 40\%$.

The dynamics of the degree of polarization of hard X-ray emission in the flare of October 29 gives evidence that the observed time structure in the form of separate enhancements of hard emission intensity correlated with variations of the polarization degree can be associated with bremsstrahlung of strongly collimated beams of accelerated electrons with energies higher than 50 keV. At lower energies the contribution of thermal unpolarized emission is substantial, its fraction was constantly increasing with the flare development, and this was revealed as a decreasing degree of polarization in the range 20–40 keV.

One can assume that in this event the beams of accelerated electrons well collimated along horizontal segments existed on the tops of the magnetic arcs and loops. If this is indeed the case, then precisely these relatively high segments should make the main contribution both to intensity and polarization of the hard X-ray emission in the energy range under consideration for a time of order of ten minutes. In this case the polarization plane should be parallel to the direction of beam propagation. Determination of the plane of polarization requires an additional analysis of the available experimental data and is a subject of a separate study which is now in progress. If this plane turns out to be coincident with the direction of the principal axis of the arcade, this may serve as an indication that there exists induction acceleration along the strong horizontal electric field which exists here and provides for upward plasma ejection due to magnetic drift in the crossed fields. If this plane rather turns out to coincide with the direction of individual loops in the arcade, then this can be an indication to the role played by acceleration in the field-aligned electric fields along the magnetic fields of separate loops, which has nothing to do with the plasma drift. The difficulty to choose between these and other possibilities lies in the fact that there are no images of the flare in hard X-ray emission. Under these conditions the real geometry can be determined only indirectly and very approximately. The penetration of the beam deep into the chromosphere would result in a strong scattering of electrons, beam destruction, and mainly unpolarized X-ray emission from these regions near the feet of magnetic loops. Let us note that the cyclotron acceleration or any other type of turbulent mechanisms of acceleration hardly can provide (without some special additional conditions) for the anisotropic angular distribution of accelerated electrons which is required to explain polarization. Without having the necessary and sufficient data, one can only assume, based on the most general considerations, that the flare process can develop in different manner according to one or another theoretical scenario depending on the altitude in the solar atmosphere and some other free parameters.

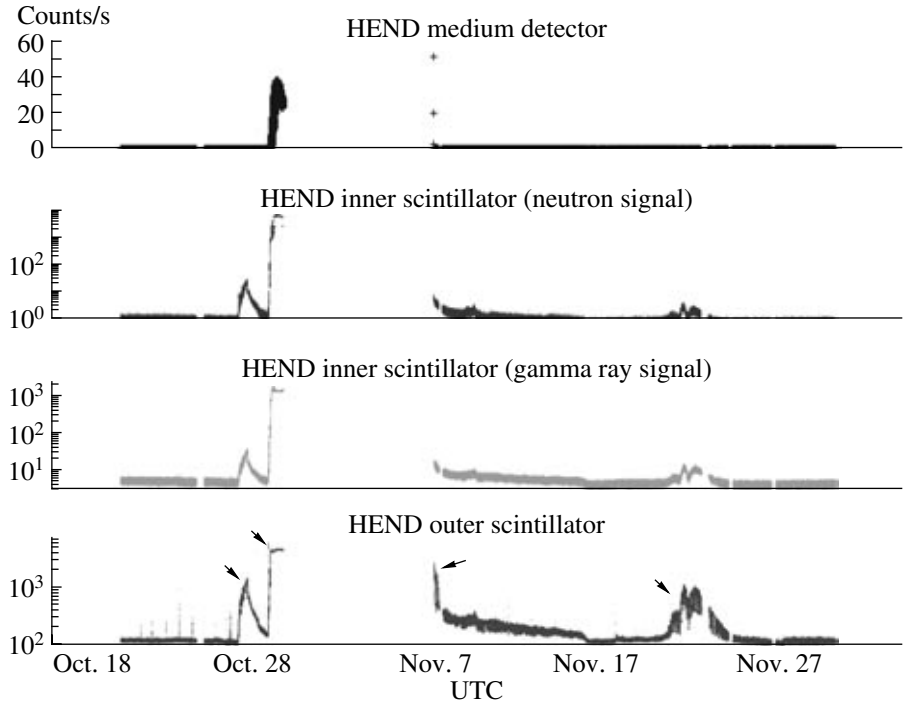

Fig. 26. The fluxes of hard electromagnetic emission and neutrons measured in several energy channels by the HEND instrument onboard the *Odyssey* artificial satellite of Mars in October–November 2003. For notation see [27].

It should be also emphasized that the strong polarization of hard emission generated in the flare processes inside astrophysical objects is not an exotic phenomenon in view of recent discovery by the *RHESSI* space observatory of the extremely high (at a level of 80%) degree of polarization in the emission of a space gamma ray burst [25].

14. SOME IMPACT EFFECTS IN THE INTERPLANETARY SPACE, FAILURES AND MALFUNCTIONS IN OPERATION OF SATELLITE INSTRUMENTS

There are several tens of communications about various manifestations of the considered phenomena of the space weather in the operation of satellite instruments. Some of them were completely or partially damaged, switched off, or transferred to the safe mode of operation (see, for example, [26]). As is usual in such cases, certain scientific measurements carried out at that time onboard satellites and spacecraft turned out to be complicated and distorted, or even impossible altogether due to the effects of saturation and interference in the sensors. A whole number of astrophysical observations were interrupted because of this. Numerous failures were found in the elements of semiconductor electronics, including errors in memory and malfunctions in onboard computers, some cases of lost telemetry, reduced power of solar batteries, breaks of the attitude control systems, occurrence of high electric potentials and interference, and blackouts of radio communication and global positioning systems. There were communications about cuts in some systems of electric power supply in Sweden and about some regional problems in power networks of the USA at that time, though the association with the space weather factors is not quite obvious from these communications. The astronauts on the ISS were evacuated to the compartment protected against radiation. The announcements were made about radiation conditions on the airplane routs, and the routs of some transatlantic flights were shifted to lower latitudes in order to avoid the zones of penetration of energetic particles into the atmosphere. In this communication we do not consider the conditions inside the Earth's magnetosphere and present only some results concerning the conditions beyond it in the heliosphere.

The *Odyssey* spacecraft in the period under consideration was located in the orbit of a Martian artificial satellite. Mars itself was at that time at an angle of about 23° to the east of the Sun–Earth line. The events which we are interested in were detected by the instrument HEND (High Energy Neutron Detector) installed onboard this spacecraft [27] in various energy channels for hard electromagnetic emission and neutrons from a few fractions of an electronvolt up to 15 MeV, as is shown in Fig. 26a. A large gap in the data corresponds to the time period October 28–November 6, when the instrument was switched off in order to avoid damaging due to high radiation fluxes after the flares. Physically, the signals of October 27–28, October 28–29, November 6, and November 21–22 (Fig. 26) are associated

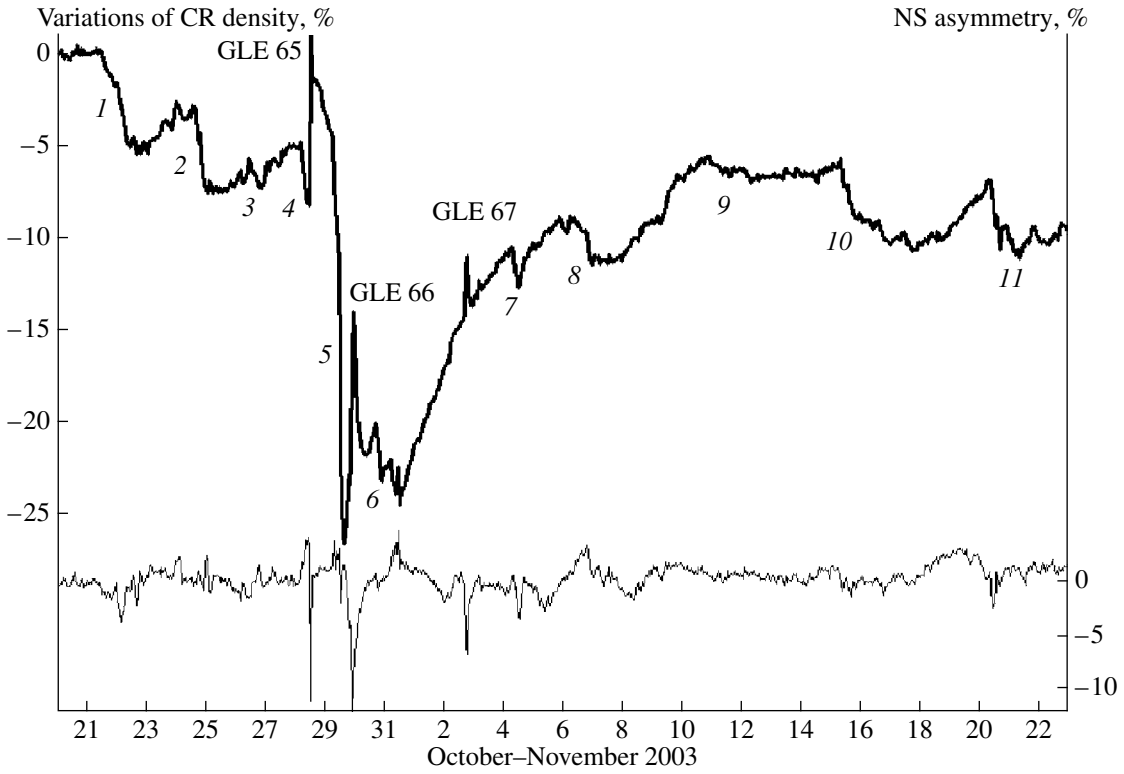

Fig. 27. The behavior of CR density and anisotropy observed by near-polar neutron monitors in October–November 2003.

with the solar events taking place several days before them. It is this time of flight that is typical for propagation of the solar wind. However, identification with particular phenomena on the Sun is not quite obvious and not so simple because of multiplicity of events during this time of flight. The fluxes are strongly enhanced in the periods under consideration and modulated with a period of satellite orbiting around Mars.

When comparing the conditions near Mars and the Earth after the flare disturbances one should take into account their different heliocentric and angular positions in the heliosphere, which gives an opportunity of partial reconstruction of the geometry and the velocity of propagation of interplanetary disturbances. The time delay and differences in strength and shape of the disturbances on Mars in comparison with the Earth are due to these circumstances. The detailed analysis of the shape of signals detected by the HEND instrument is of interest by itself, and it will be carried out and presented elsewhere.

Evaluation of the fluences, peak values, and spectra of radiation in the heliosphere along the rout of a transfer to Mars is of considerable interest for the development of strategies for future missions. Relative contributions of galactic, heliospheric, and solar populations to the total spectra during different phases of the solar cycle are known so far not very reliably, therefore, various model extrapolations and calculations should be considered with some caution. In particular, to solve the important practical problem of choosing the safest period from the standpoint of radiation environment one has to consider complicated multi-parameter problems with a large number of various additional criteria including the specific technological and biological requirements. Without these considerations the formulated problem has no simple and unambiguous solution, since the galactic component decreases in the maximum of the solar cycle, while two others are increasing with strong variations in power, energy distribution, and particle composition.

15. THE EVENTS OF OCTOBER–NOVEMBER 2003 IN GROUND-BASED OBSERVATIONS OF COSMIC RAYS

The period from October to November 2003 turned out to be the richest in the number and strength of events detected by ground-based neutron monitors in the 23rd cycle of solar activity. One can get a general impression about these events from Fig. 27 where the data of near-polar neutron monitors are presented from October 20 to November 22. The beginning of this period coincides with the appearance on the solar disk of a sunspot group 10484, while its end approximately corresponds to return of the group 10486 to the disk during the next rotation.

Figure 29 is constructed on the basis of data of near-polar neutron monitors of the Thule and McMurdo sta-

tions in the northern and southern hemispheres. Since the variation δ of the counting rate of near-polar neutron monitors is determined basically by density variations and by the north-south anisotropy of cosmic rays (CRs), the half-sum of variations $(\delta_{thul} + \delta_{mcmd})/2$ for the stations located in the opposite hemispheres demonstrates the behavior similar to that of CR density variations. The difference of these variations $\delta_{thul} - \delta_{mcmd}$ gives the information about the behavior of the north–south CR anisotropy. Exactly these values of the half-sum and difference are shown in Fig. 29. One should have in mind that the variations presented here correspond to the effective rigidities of primary particles 10–15 GV and 3–5 GV, if one considers effects in galactic and solar cosmic rays, respectively.

Neutron monitors have detected on October 28 and 29, and on November 2 three ground level enhancements (GLEs) of solar CRs, which became recorded as events 65, 66 and 67 of this type in the history of ground-based observations of CRs: they are marked by these numbers in Fig. 27. Thus, in a weak at once three events were added to the list of ground level enhancements of the 23rd cycle, so that their total number in the cycle became equal to 13. Let us recall that in the nineteenth, twentieth, twenty first, and twenty second cycles the numbers of recorded GLEs were 10, 12, 13, and 15, respectively [28]. The last November enhancement occurred exactly in 11 years after November 2, 1992, when the last GLE of the 22nd cycle was observed. It is quite possible that we will not observe in the current cycle new ground level enhancements any more. However, it is already clear that the 23rd cycle has no big difference with the preceding cycles as far as the number of GLEs is concerned. So, it can be characterized as a typical cycle. One should take into account that the number of GLEs given for the 19th cycles is almost inevitably underestimated. The low statistical accuracy of the first-generation neutron monitors and their absence in the near-polar regions limited substantially the capabilities of detecting small ground level enhancements at that time. Taking this circumstance into account it becomes more obvious that the number of GLEs in the last five cycles very slightly varied from cycle to cycle. It is of interest to see whether this tendency will be conserved in the next cycles.

Figure 28 presents the 5-min data of some neutron monitors obtained during the last ground level enhancements. All three enhancements have common features. They were a result of sporadic phenomena in one and the same active region 10486 and were observed after extremely strong X-ray flares (X17.2/4B, X10.0/2B, and X8.3/2B). This is the first series of three GLEs in the cycle, though previously pairs of GLEs were observed twice (in May 1998 and April 2001). All three enhancements turned out to be sufficiently prominent being inferior to only one event in the current cycle (April 15, 2001). The first of them (October 28) was the largest among the three being close in strength to

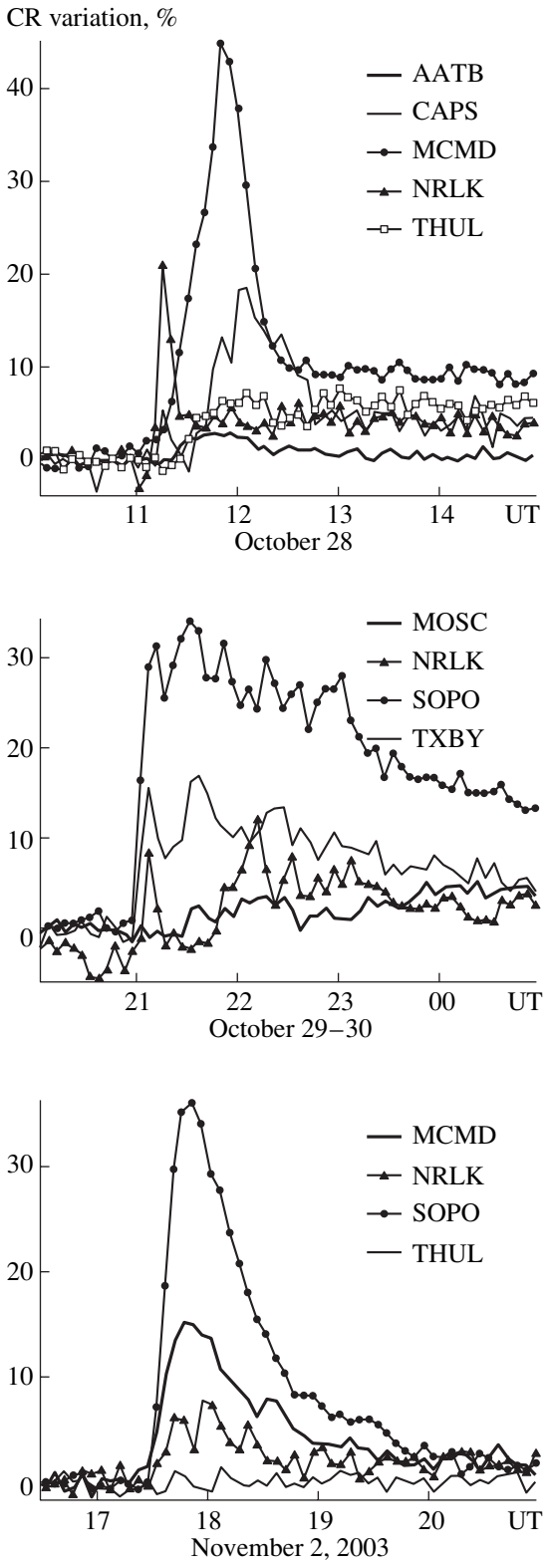

Fig. 28. Counting rates of some neutron monitors during ground level enhancements of solar cosmic rays in October-November 2003. Standard abbreviations are used for station names: AATB (Alma-Ata, 3350 m a.s.l.), CAPS (cape Shmidt), MCMD (McMurdo), NRLK (Norilsk), SOPO (South Pole), THUL (Thule), and TXBY (Tixie bay).

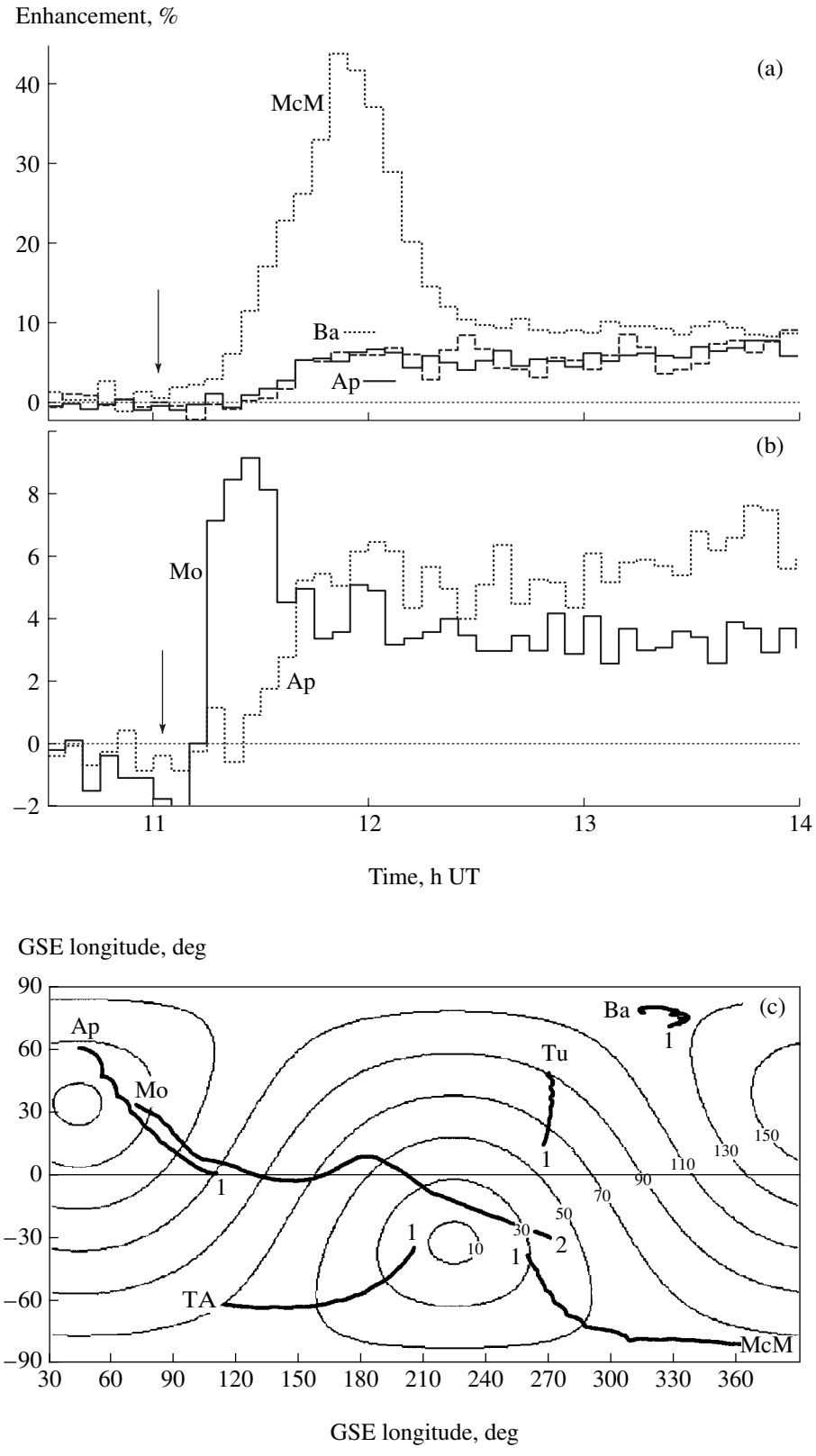

Fig. 29. Ground level enhancement of SCR on October 28, 2003 according to the data of neutron monitors (a) McMurdo (McM), Barentsburg (Ba), and Apatity (Ap); and (b) Moscow (Mo). Vertical arrows show the presumed time of generation of particles on the Sun. (c) The map with asymptotic cones of acceptance for neutron monitors Terra Adelie (TA) and Thule (Tu). Figures on the asymptotic cones designate rigidities in GV. The lines of equal pitch-angles are drown relative to the direction of the interplanetary magnetic field (the data of *ACE* spacecraft) at 12 h UT.

another famous event of the cycle, July 14, 2000. The large and prolonged anisotropy of the flux of solar particles was observed in all three events. The fluxes detected in the southern hemisphere of the Earth exceeded the fluxes observed by the northern stations substantially. This specific feature is well seen both in Fig. 27 and in Fig. 28. It is quite consistent with the fact that all flares associated with relativistic protons occurred in the southern part of the solar disk and had coordinates from S16 to S14, and with the fact that the Earth during this season is turned to the Sun by its southern side. Notice that the anisotropy of the same sign was found in filling the Earth's magnetosphere with solar cosmic rays of lower energies (measurements during successive passages of the *Coronas-F* satellite over the polar caps) which was already discussed in section 11. More detailed analysis of these data can be used for diagnostics of the heliosphere as a medium for propagation of energetic particles.

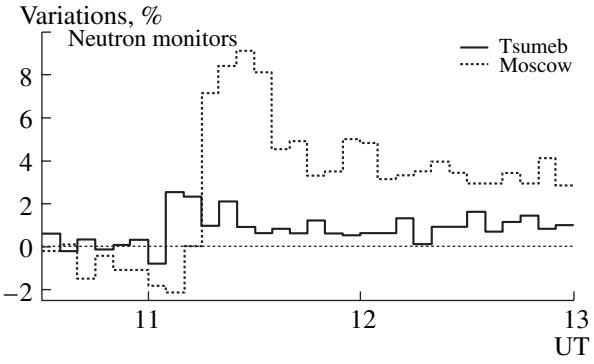

Fig. 30. The enhancement of October 28, 2003 in neutron monitors of Moscow and Tsumeb stations. A small peak of intensity of the Tsumeb neutron monitor can be associated with solar neutrons since protons have arrived later (profile of the Moscow station).

The existence of strong anisotropy in the flux of relativistic SCRs in the SCR event of October 28, 2003 demonstrates Fig. 29a, where the enhancements on neutron monitors of Apatity and Barenzburg (Spitsbergen) are shown in comparison with the McMurdo station in Antarctica. The vertical arrow marks the time when the of radio emission of II type started (presumed moment of generation of relativistic SCRs). The long delay of the beginning of enhancement with respect to the instant of generation engages our attention. On the contrary, the station Moscow detected rapid arrival of solar particles, so-called "fast component" of relativistic solar particles (RSP). It is remarkable that the value of enhancement is larger in Moscow than in Apatity in spite of higher geomagnetic threshold (Fig. 29b). In this case the Apatity station detects only slow, delayed component of RSPs. This and other features of the event of October 28, 2003 can be explained with the help of an analysis using calculated asymptotic directions of arrivals for protons in the range of rigidities from atmospheric cutoff ~1 GV (430 MeV) to 10 GV (boundary rigidity in the spectrum of solar cosmic rays). The calculation was carried out by integrating the equations of motion of a particle with negative charge and proton mass. These particles with a given rigidity were vertically released upwards at an altitude of 20 km over the given station [29]. The altitude 20 km was chosen as a mean altitude of generation of secondary neutrons which give contribution to the counting rates of neutron monitors [29]. Integration of the equations of motion was performed by the Runge–Kutta method of order of 4–5. The magnetosphere model Tsyganenko-2000 was used in the calculations.

Thus obtained map of asymptotic cones (ACs) is shown in Fig. 29c in the solar-ecliptic coordinates (GSE). The cones were calculated for some stations at the moment 12 h UT, close to the maximum of enhancement (Figs. 29a and 29b). Each point on the AC curves corresponds to the arrival direction of a proton with a given rigidity on the boundary of the magnetosphere (this proton then is detected by a given station from the vertical direction). The AC calculation is one-dimensional because only vertical directions of incident particles are considered. The CR intensity for particles arriving at some angle to the vertical is strongly attenuated due to absorption in the atmosphere. After taking into account inclined trajectories with different azimuth angles the AC curves would have a finite thickness. The map (Fig. 29c) presents also the lines of equal pitch-angles with respect to the IMF (estimates using the data of the *ACE* spacecraft located at the time of event occurrence at the libration point at a distance of 1.5 million km from the Earth). The maximum SCR flux arrived from the direction $\Phi = 215°$; $\theta = -35°$, as one can judge from the data of the stations McMurdo (Fig. 29a) and Terra Adelie whose asymptotic cones are oriented close to this direction (Fig. 29c). The station accepting the particles with large pitch-angles (Thule) and from the anti-solar direction (Apatity and Barentsburg) detected a small enhancement whose onset was delayed by 15 min relative to the direct flux. The fact that the Moscow station detected the fast component, while McMurdo and Terra Adelie did not, can be explained by the narrow directivity and hard spectrum of the fast component. One can see in Fig. 29c that the McMurdo and Terra Adelie stations could detect from the directions with small pitch-angles only low energy particles whose number is always small in the fast component. On the contrary, at the same stations the effect in the soft slow component which had a broad pitch-angle distribution was significantly stronger.

Thus, while the fast component had the hard energy spectrum and narrow pitch-angle distribution, the slow component was bi-directional. The fluxes of particles were observed from two opposite directions, though they were not equal. The bi-directional anisotropy in the event of October 28 which occurred during Forbush-effects is, presumably, associated with a loop-like structure of the IMF. This structure is caused by the coronal mass ejections responsible for the Forbush

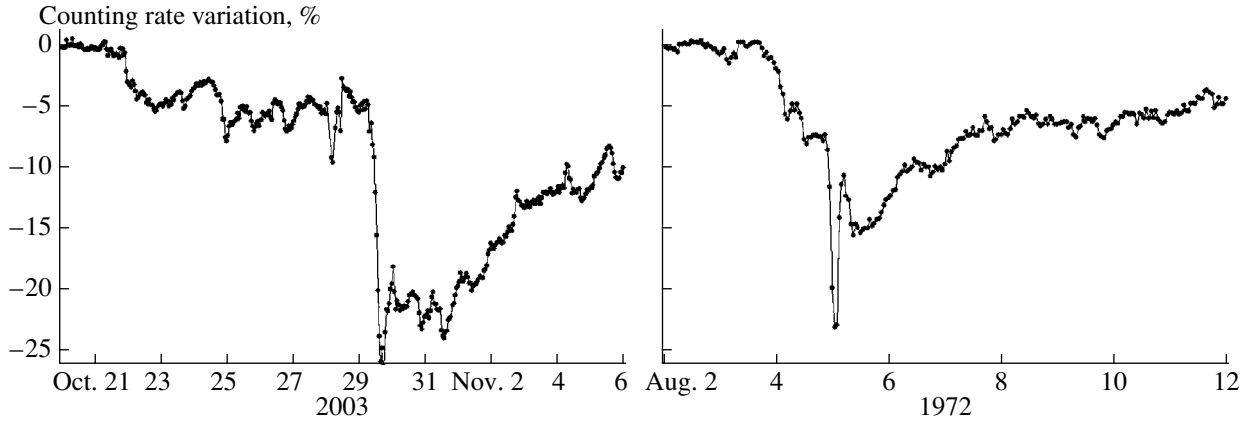

Fig. 31. Variations of cosmic rays as detected by the neutron monitor of Moscow station in October–November 2003 and in August 1972.

decreases. The injection of particles to both feet of the loop-like structure in the solar corona from an extended source (coronal shock wave) or from separated local sources can be a cause of the bi-directional anisotropy.

According to one preliminary interpretation, relativistic solar neutrons were probably detected by the neutron monitor Tsumeb (Fig. 30) in South Africa. This neutron monitor (S 19.2°, E 17.58°) with $R_c = 9.21$ GV is located at an altitude of 1240 m above sea level, and during the flare it was not far from the noon point. According to this interpretation, a small impulsive enhancement in the period from 11:10 to 11:15 UT can be associated with solar neutrons. Figure 30 presents the data of this instrument during the events of October 28, 2003 in comparison with the Moscow station data. At this time RSPs did not yet arrive at the Earth (the profile of Moscow station, 2.4 GV), while according to the data of *Coronas-F* the gamma ray emission (an indicator of generation of neutrons) was observed from 11:04 to 11:12 UT. According to another possible interpretation, in this event the generation of SCRs with energies up to 10 GeV took place on the Sun, while the delay of signals at various stations is due to specific features of the pitch-angle distribution of energetic particles accelerated in the flare and due to differences in accepting cones of these stations. In order to prove the validity of one or another interpretation, a more careful quantitative analysis is required.

Considerable differences are also seen between GLEs 65, 66, and 67. The time profiles of the first two are very complicated. It is enough to call attention to the data of the Norilsk station, which contain clear-cut peaks (with approximate duration of 10 min) of CR intensity in the very beginning of both events. These peaks strongly exceed in their values the effect of solar CRs for the stations with similar characteristics. Two largely separated maxima of intensity were observed in the profiles of October GLEs at some other stations. The time profile of the third (November) enhancement is much simpler. However, in this case a great surprise is practically complete absence of the effect at the northern near-polar station Thule. This enhancement remained essentially isotropic during the entire time of its observation (2–3 h). This, probably, indicates that interplanetary scattering of relativistic solar particles is extremely inefficient on November 2.

The differences in observed ground level enhancements should be explained by considerable difference in the location of the source of accelerated particles, and in the interplanetary and magnetosphere conditions. Table 5 presents heliolatitudes of the solar flares which are associated with ground level proton enhancements, maximum values of the solar wind velocity (measurements of *ACE*/SWEPAM and *ACE*/SWICS), maximal strength of the interplanetary magnetic field near the Earth (*ACE*/MAG), maximum K_p index of geomagnetic activity, and minimal value of the D_{st} index in the hours of observation of solar CRs by neutron monitors.

Table 5. Differences in the conditions of observing GLE 65, 66, and 67

GLE	Day	Hours	Maximum effect	Heliolongitude of flare	SW velocity, km/s	IMF strength, nT	K_p-index	D_{st}-index, nT
65	October 28	11–13	45%	E08	790	11.0	5_-	–37
66	October 29	21–24	35%	W02	1100	29.3	9_-	–345
67	November 2	17–20	36%	W56	536	5.2	4_+	–23

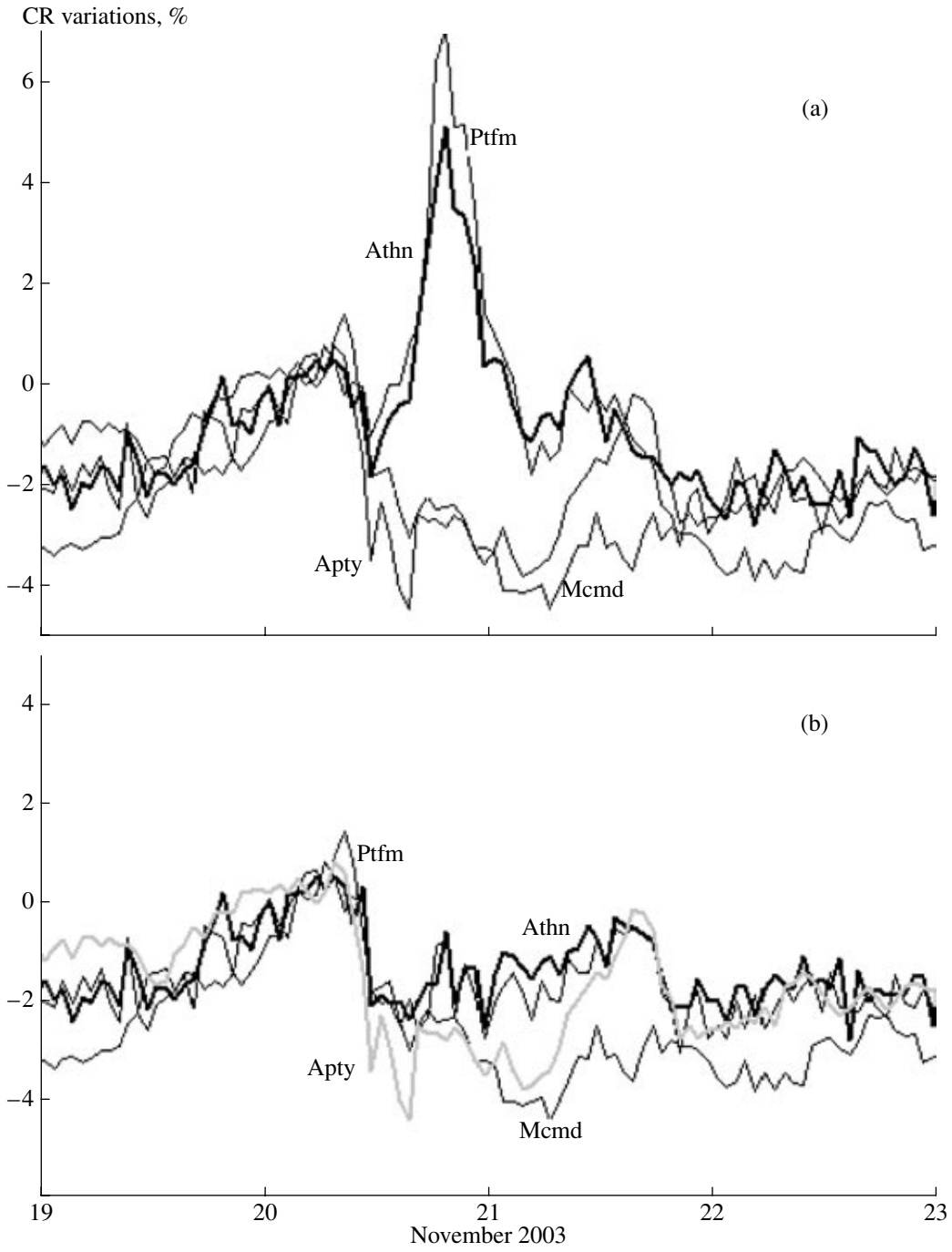

Fig. 32. Variations of cosmic rays, uncorrected (a) and corrected for the magnetospheric effect (b), detected by mid-latitudes neutron monitors of stations Athens (Athn) and Potchefstrom (Ptfm) and by high-latitude monitors of stations Apatity (Apty) and McMurdo (Mcmd).

The indices of geomagnetic activity presented in Table 5 and the data about the solar wind and interplanetary field characterize adequately the degree of disturbance of the heliosphere only in the local vicinity of the Earth rather than along the entire path of propagation of considered cosmic ray particles. Unfortunately, as usual, there are no direct data about this. The indirect data indicate that the heliosphere was strongly disturbed both as a whole and in its separate longitude and latitude segments inside and outside the Earth's orbit in the above indicated periods because of extremely high eruptive activity of the Sun for a number of days. One can judge about this from observations of strong variations in the solar corona activity by the data of instruments onboard *Coronas-F*, *SOHO*, and *GOES* space observatories. Nevertheless, one can see from these

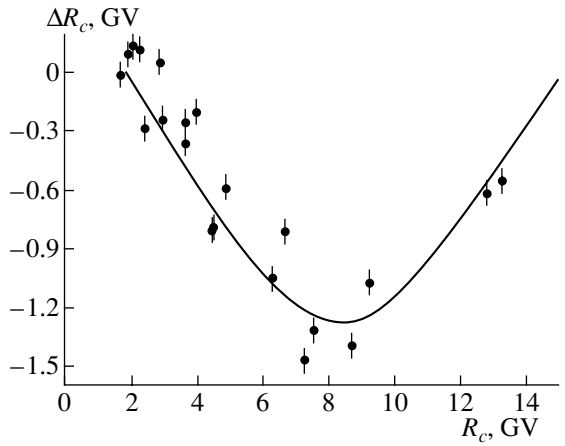

Fig. 33. An example of latitude distribution of variations of geomagnetic cutoff rigidities at various points at 20 h on October 20 when the D_{st} index dropped down to –465 nT.

data that the event 67 was associated with much more conveniently located (western) flare. This was also the only event among others that was observed in the relatively quiet interplanetary conditions near the Earth's orbit, and not during magnetic storms. The GLE 65 was observed on the background of disturbed solar wind, during a Forbush decrease and a developing magnetic storm. Especially complicated local conditions took place for GLE 66: a strong interplanetary disturbance, extremely strong magnetic storm, and a giant Forbush effect. All this, undeniably, will complicate the analysis of this event. Even on November 2 the geomagnetic conditions remained to be disturbed. The solar wind was at this time relatively quiet only in the Earth's vicinity, while the situation in the heliosphere was fairly complicated.

15.1. Forbush Decreases (FDs)

The series of FDs observed in the end of October was the most significant over the entire current solar cycle, surpassing the series of July 2000 and March–April 2001. Separate FDs are numbered in Fig. 27 in chronological order. The Forbush effects FD-1 and FD-2 were caused by activity in the group 10484 and by the eastern solar mass ejections. FD-3 is the smallest event in the series, but it is of special interest as the first manifestation of activity in the group 10486. The flare X5.4/1B on October 23 occurred near the limb (S21 E88) and was accompanied by a fast CME with so large angular size (full halo) that the interplanetary shock wave from this source (very remote in longitude) reached the Earth. The events from FD-4 to FD-8 were basically caused by the activity of the same group 10486 and around it. The last of these events took place after the record flare X28/3B occurred near the western limb (S19 W83) on November 4. Again, rather remote position of the source did not hamper the observation of a full halo and the arrival of a shock wave at the Earth. The events from FD-8 to FD-10 turned out to be related (in full or partially) to high-speed solar wind streams from coronal holes, thus reminding us that exactly the low-latitude coronal holes were a main source of recurrent interplanetary disturbances in 2003.

FD-5 observed on October 29 (Fig. 31) deserves, without doubt, a separate consideration. During the central flare X17.2 which was already mentioned in connection with generation of ultra-relativistic solar protons an extremely fast CME was observed whose velocity was evaluated from the *SOHO*/LASCO data as somewhat higher than 2100 km/s. The mean velocity of propagation of this disturbance between the Sun and the Earth turned out to be approximately the same. Upon its arrival at the Earth (SSC at 06:11 UT on October 29) in a bit

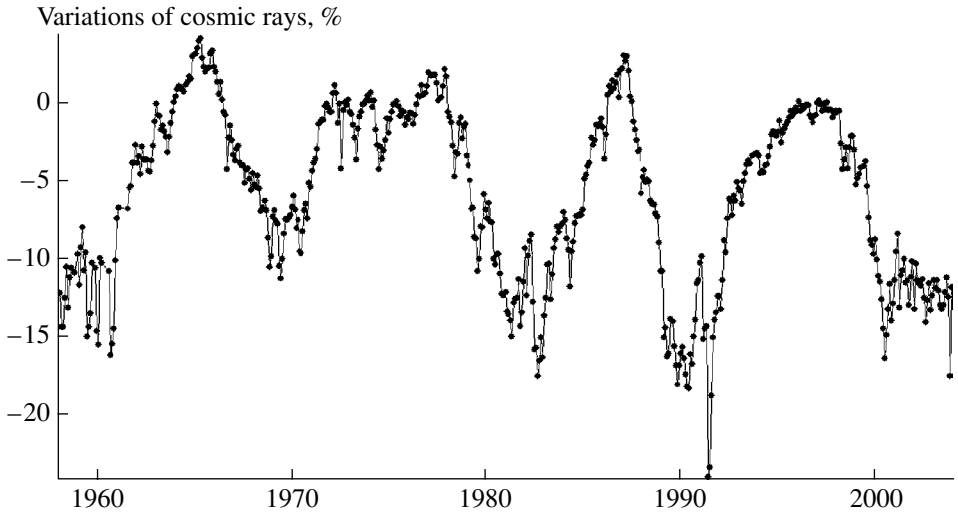

Fig. 34. Long-periodic CR variations observed by the neutron monitor of the Moscow station.

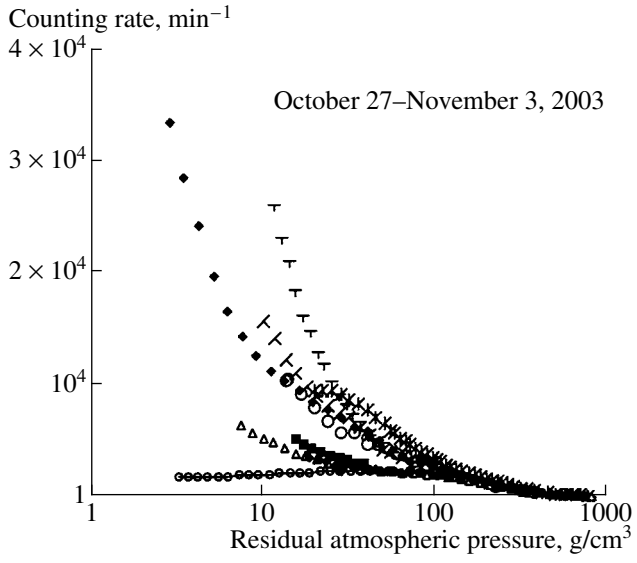

Fig. 35. The results of balloon measurements of the fluxes of charged particles in the stratosphere of Murmansk region. Different symbols correspond to different launches of radiosondes. The lower curve represents the background particle fluxes measured on October 24, 2003.

longer than nineteen hours, this disturbance became the event with the fastest propagation of interplanetary disturbance since August 1972. According to the data of *ACE*/SWICS (http://www.srl.caltech.edu/ACE/ASC/SWICS.html) the solar wind velocity in the first hours after the shock wave arrival varied from 1700 to 1900 km/s, while the intensity of the interplanetary magnetic field reached 46.5 nT according to the data of *ACE*/MAG (http://www.sec.noaa.gov.ace/). It follows from an empirical dependence derived on the basis of several thousand FDs [30] that the interplanetary disturbance with such characteristics should produce an FD with a value of 17.5% for particles with rigidities of 10 GV. The effect observed on October 29 turned out to be even larger. The variations of counting rates reached 25% at some stations. One can state with assurance that this event is among the largest FDs throughout the entire history of observations. It exceeds the values of all FDs of the current solar cycle at least twice. Our database includes almost 4000 FDs accumulated for complete 30 years. The largest (25.0% for 10 GV) is the well known event of August 4–5, 1972. Figure 31 shows that at least the neutron monitor of Moscow station observed on October 29 the stronger CR modulation than in August 1972. The separation of contributions of solar and galactic CRs seems to be very challenging problem. Another factor complicating the analysis of CR variations is the magnetic storm which coincided in time and strongly changed the state of the magnetospheric field.

The basic drop of intensity (by ~20%) proceeded on October 29 during 6 hours, at some hours the intensity dropped by 5% and more. It follows from such a rate of dropping that the gradient of CRs with energies of 10–15 GeV was at that time no less than 100% per astronomical unit in the leading part of the solar wind disturbance. Such a gradient should result in a large anisotropy of galactic CRs, and this is confirmed by Fig. 27. However, the preliminary analysis shows that CR anisotropy in this event was still considerably smaller than in FDs of August 1972 or February 1978. At certain moments of the period under consideration a bidirectional anisotropy of large amplitude (tens of per-

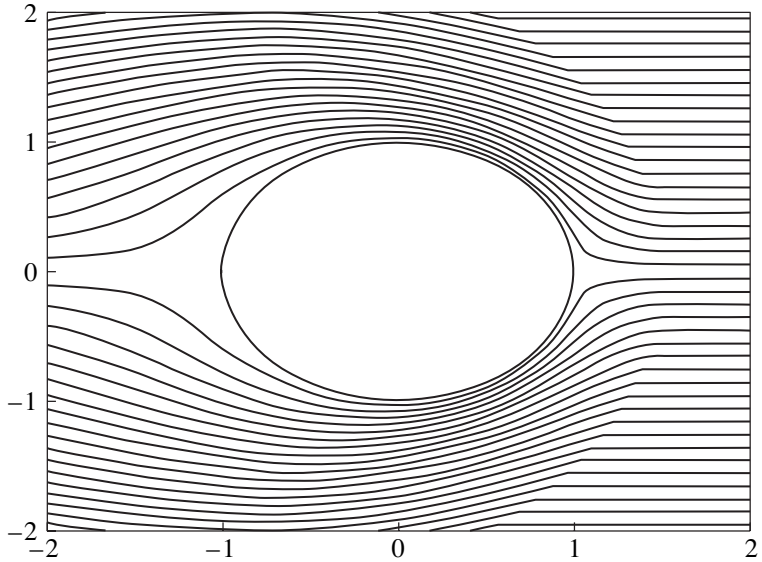

Fig. 36. The distortion and amplification of interplanetary magnetic field by a fast supersonic cylindrical cloud moving to the right along the horizontal axis. The cylinder radius is taken as a scale unit. The amplification factor can reach 5–6, i.e., if external undisturbed field was ~5–10 nT, on the flanks of the cloud the disturbed field can be as strong as ~25–60 nT, which is quite sufficient in order to generate a strong geomagnetic storm.

cent) is observed in the angular distribution of particles, which indicates, first, to carrying-out of magnetic clouds and loop-like structures of the interplanetary magnetic field (IMF) by coronal mass ejections and, second, to a high degree of regularity of the IMF in these structures. The maximum amplitudes of bi-directional anisotropy were observed on October 29 and November 1 (~60%), and on November 2, 20, and 23 (~40%) for particles with rigidity $R = 4$ GV.

Detailed investigations of the events described above were also carried out by V. M. Dvornikov *et al.* (http://www.iszf.irk.ru/documents/events/oct_nov.php), 2004 using the data of satellite and ground-based measurements of cosmic rays. Here, an original approach was used, applying a special expression for power-law rigidity spectrum of galactic CRs in a wide energy range. This expression describing the CR spectrum was based on the assumption that the variation of CR intensity in the interplanetary space took place due to energy changes in regular electromagnetic fields of the heliosphere in accordance with the Liouville's theorem, i.e., under the condition of constant particle density along the trajectory of motion in the phase space [32]. Using the method of spectrographic global survey [33] for the data of the global network of neutron monitors, the information was obtained about variations of the angular and energy distribution of primary CRs beyond the Earth's magnetosphere (isotropic CR component and anisotropies of the first and second orders), and also about changes in the planetary system of geomagnetic cutoff rigidities for every hour of observations. The preliminary results show that the CR intensity variations (within the framework of model used) proceed, first, because of time variations and space inhomogeneity of the potential of induced electric field, second, due to particle acceleration in the loop-like structures of coronal and interplanetary magnetic fields that are time-variable, and, third, because of acceleration of background particles by polarization electric fields that are generated during the propagation in the inhomogeneous heliosphere fields of particles accelerated in the solar corona and interplanetary space. In this case, the magnetic field strength in these structures changes with respect to background by a factor of 2–3 due to time variations, and the squared ratio of the intensities of polarization electric and magnetic fields varies within the limits from ~0 to ~0.9. The dimensions of the regions with non-steady electromagnetic fields (converted to the Earth's orbit) are 10^{10}–10^{11} cm in accordance with the values of parameter R_0. The potential of the induced electric field decreased almost to zero values and increased by a factor of ~1.5 relative to the background values.

The interpretation of cosmic ray events described above and the attempts to establish on this basis some cause-and-effect relationships on the Sun and in the heliosphere are strongly complicated in the given case by multiple character of disturbances and by impossibility to consider them as linearly independent. Figuratively speaking, the transfer function for the "solar signal" turns out to be nonlinear due to its large amplitude in the parameters of the heliosphere field and plasma. Therefore, for the time period under consideration it is invalid to speak about individual undistorted "signals," events, and phenomena, trying to seek out the ephemeral space and time boundaries between them which sometimes can be nonexistent. It is more reasonable to analyze a strongly disturbed situation on the Sun and in the heliosphere with nonlinear relations. Such "situation" approach seems to be much more adequate than the "event" approach in the given complicated case. Indeed, all plasma and magnetic disturbances were so strong and densely located in space and time that not only their linear superposition in the heliosphere took place (though one should primarily have this in mind at any qualitative estimations and discussions taking into account the main factor: supermagnetosonic character of the solar wind expansion). The nonlinear character of the heliosphere response to solar disturbances also revealed itself notably in all characteristics of FDs and GLEs discussed above.

In essence, the distinction between "situation" and "event" approaches lies in the necessity of considering and taking into account longer time intervals and larger space regions on the Sun and in the heliosphere in order to describe strong multiple disturbances with different scales as compared to simpler one-scale events. In a sense, the analogy with turbulent and laminar states is appropriate here.

15.2. Geomagnetic Effects in GCR Modulation on the Earth's Surface

Three extremely strong magnetic storms occurred in October–November 2003, may be the strongest in the current solar cycle. In the first of them on October 29–30 the K_p index of geomagnetic activity increased to the maximum possible value 9_0, while the D_{st} index dropped down to –363 nT. The same values for the storms of October 30–31 and November 20 were 9_0 and 401 nT and 9 and 465 nT, respectively. Only two preceding storms of this cycle can be compared with the 2003 storms: on July 15, 2000 when the extreme values of the K_p and D_{st} indices reached 9_0 and 300 nT, respectively, and on March 31, 2001 ($K_p = 9$ and $D_{st} = -387$ nT).

Earlier only once in this cycle (in March 1989) D_{st} index fell even lower than on November 20, 2003. Usually, during so strong magnetic storms the effects of immediate impact of the disturbed magnetosphere on charged particles [34] reveal themselves in ground-based CR observations. The geomagnetic effect in CRs is mainly related to changing effective rigidity of geomagnetic cutoff at the points where CRs are observed [35].

Indications to geomagnetic effects manifest themselves in large differences of CR variations at mid-lati-

tude variations from the variations at high and low latitudes, and they are seen in all three magnetic storms. The most complicated situation took place during the first magnetic storm in the night of October 29 to 30, when the geomagnetic effect coincided with variations of the density and anisotropy of galactic CRs in a giant FD and with changing flux of solar CRs in GLE66. The reduced cutoff rigidity, probably, explains the growing counting rate of the neutron monitor of Moscow station near midnight (Fig. 28, middle panel). In this unusual case the changes of cutoff rigidity influence not only galactic cosmic rays (as usual) but solar cosmic rays as well.

The largest and most obvious geomagnetic effect of CRs was observed on November 20. High-latitude neutron monitors detected on this date the Forbush decrease of ~5%. Taking into account that a record increase of the IMF intensity (up to 55.7 nT according to *ACE*/MAG) was observed at this time, one could expect even larger effect. Mid-latitude stations observed virtually no decreases, detecting instead of this considerable increases of the counting rate, as it is seen in Fig. 29a. In order to isolate and study the geomagnetic effect in this case, we have used the data of all neutron monitors, which we succeeded to find promptly (40 stations in total), and the method suggested in [36]. For each station and each hour we found the changes of geomagnetic cutoff rigidity ΔR_c and the geomagnetic effect corresponding to them. The CR variations at stations Athens and Potchefstrom corrected for the geomagnetic effect due to a shift of the cutoff rigidity are presented in Fig. 32. One can see that at some hours (coinciding with maximum decrease of the D_{st} index) the geomagnetic effect at these stations reached 6–8%. It is quite possible that this geomagnetic effect was the largest ever observed by neutron monitors in cosmic rays. Even in March 1989 it was less.

The behavior of ΔR_c obtained for November 20 demonstrates a clear latitude dependence (Fig. 33) and is very well consistent with D_{st} variation. The maximum changes of the geomagnetic threshold are observed in this case at unusually low latitudes corresponding to a geomagnetic cutoff rigidity of about 8 GV.

15.3. Long-Periodic CR Variations

On October 29–31 the counting rate of neutron monitors dropped down to so low level that had not been observed since June 1991. This is true both for hour-averaged and mean daily data. So deep modulation could not but have an effect also in long-periodic variations of cosmic rays. In addition, one should take into account that, when in the beginning of November giant active regions 10484, 10486, and 10488 left the visible part of the solar disk, solar activity did not disappeared; it was displaced to the invisible side of the Sun. The coronographs *SOHO*/LASCO observed large solar mass ejections from the opposite to us solar side on November 4, 6, 10, 11, and 12. These ejections produced interplanetary disturbances and modulated cosmic rays.

Let us look at monthly averaged data (Fig. 34). In all last cycles of solar activity (excluding may be the 20th which was generally rather weak) one can see two minima of intensity of galactic cosmic rays: the first minimum takes place when the maximum of the sunspot number is reached and the second (deeper) minimum in a couple of years. In the 21st cycle a well pronounced second GCR minimum was detected in July 1982, and in the 22nd it took place in June–July 1991. In the current cycle the first minimum was observed in July 2000. We had to wait for the second minimum for 3 years and 4 months (considerably longer than in the preceding cycles), until we observed it in November 2003. It turned out to be not so deep as in 1991, but again significantly deeper than the first minimum. The CR modulation in the 23rd cycle is deeper than in the 21st cycle (let alone 20th), and the intensity remains at a low level already for more than 4 years (since the end of 1999). One can notice that the minimum of CR intensity in odd cycles is longer than in even cycles. A.N. Charakhchyan and T.N. Charakhchyan were the first who pointed to this circumstance. Now it is explained taking into account the Hale's cycle in the global field of the Sun and the role of magnetic drift in CR propagation. Apparently, at the moment (the beginning of 2004) we are at the end of this minimum and the phase of recovery of GCR intensity will begin in the nearest months.

As a result of this consideration of the ground-based CR measurements one can conclude that the events occurred in cosmic rays in October and November 2003 deserve to be called the most outstanding in the 23rd solar cycle. At that time we observed the longest series of ground level enhancements of solar cosmic rays, the most significant series of Forbush effects, the lowest CR intensity, the largest Forbush effect, and the strongest magnetospheric effects in cosmic rays. The Forbush effect of October 29 and geomagnetic effect on November 20 are the largest not only in the current cycle, but in the entire history of ground-based observations of cosmic rays. In this cycle the Sun reserved its greatest surprises for the phase of decline. However, this used to be observed before. The brightest example was in August 1972.

15.4. Measurements of Ionizing Radiation in the Atmosphere

For many years practically everyday measurements of ionizing radiation in the Earth's atmosphere are carried out in Lebedev Physical Institute from sea level up to altitudes of 30–35 km [37]. In the end of October and in the beginning of November 2003 the precipitation of solar protons with energies above 100 MeV was observed in the stratosphere of the polar regions (Murmansk region and Mirny observatory, Antarctica). The radiation background in the stratosphere was substantially enhanced to altitudes of ~15 km (residual atmo-

spheric pressure ~120 g/cm^2), while at altitudes of 30–35 km (residual pressure ~12–5 g/cm^2) the fluxes of charged particles increased by a factor of 10–20. Figure 35 presents the results of measuring the omnidirectional fluxes of charged particles in the atmosphere of Murmansk region (68°57′N, 33°03′E) during the events of October–November 2003. The measurements were carried out using a gas-discharge counter with a wall thickness of 50 mg/cm^2 of steel. The radiation background enhancements shown in the figure were caused by solar protons with energies 100–600 MeV. The fluxes and energy spectra of these protons converted to the atmosphere boundary well agree with the spacecraft data from the side of lower energies. At higher energies they are well consistent with the fluxes of more than 500 MeV protons estimated from the data of the Apatity neutron monitor.

16. POSSIBLE SCENARIO OF EVENTS ON THE SUN AND IN THE HELIOSPHERE IN OCTOBER–NOVEMBER 2003

The observations considered above together with other data confirm the well known conclusions about nonpotentiality and complex dynamic character of the FPAR (flare-productive active region) magnetic field, i.e., that strong and highly variable electric currents flow here. For example, in observations of *TRACE*, *SOHO*/EIT, *SOHO*/LASCO, and *Coronas-F* twisted loops in magnetic field arcades are visualized in the corona before ejection, when eruptive prominences elevate, and in the coronograph field of view. For the limb event of November 4, 2003 one can estimate the current value in the coronal electrojet as 1 TA using the degree of twisting for observed loop structures in the arcades and measured magnetic fields at the feet of arcs. The development of this flare and CME was accompanied by a complication of the whole structure and by the appearance of a large number of well discernible dynamic details, i.e., by turbulence of plasma and magnetic field. However, the role played by these processes is not, apparently, of prime importance in this case, since one clearly deals with dynamics of larger-scale magnetic fields and plasma structures with higher and variable free energy. Preliminary estimates show that in this case there is an energy cascade directed from the largest scales of order of geometrical dimensions and lifetime of the global complexes of coronal holes and active regions to the side of smaller and higher-variable scales, and not vice versa. In other words the energy cascade is rather direct than inverse. This implies a strong delocalization of the energy-carrying region during this event.

The coronal mass ejections and solar flares originate because of a local and sufficiently fast conversion of free energy into plasma motion and electromagnetic emission. As was mentioned earlier, these phenomena are neither in cause-effect relations nor independent of each other. In reality, they represent two sides, two energy channels of a single dissipative process supported by free energy available in the solar atmosphere. In the context of radiation magnetic hydrodynamics one can make a clear quantitative distinction between these two energy channels in the amount of power and energy. The dimensionless parameter V_e, the ratio of corresponding powers can serve as a convenient quantitative measure (so-called "velocity–emission" ratio). If the energy of plasma motion dominates, the process has the features of a coronal ejection ($V_e \gg 1$). If, on the contrary, the emission energy prevails, one deals with a flare-like event ($V_e \ll 1$). However, in many cases $V_e \sim 1$, and then both phenomena accompany each other. They develop being interrelated, practically simultaneously and jointly. To some extent both channels are concurrent between themselves on the Sun. In addition, other channels of dissipation of free energy play an important role, for example, the thermal flows that are transferred mainly by electrons along the field into lower and colder parts on the solar atmosphere. A certain, usually lesser fraction of energy is spent for the development other kinetic processes (including acceleration of suprathermal tails in the distribution function of charged particles and formation of numerous small-scale irregularities) and quickly variable processes (including convective and wave disturbances in the upper solar atmosphere). There are no doubts that, generally, direct energy cascades prevail in the solar atmosphere, since free energy in different forms is delivered from the interiors of the Sun to be emitted into open space mainly in the form of emission. However, inverse energy cascades undoubtedly take place and play important role in the redistribution of free energy and in the formation of dynamic structures in the solar atmosphere. The spectral region near 5-min oscillations in the photosphere can serve as an example. The ratio and balance between the direct and inverse energy cascades on the Sun still are studied insufficiently well.

The second important remark can be made that any adequate description of physics of the processes involved is possible only taking into account the transport of energy, momentum, and mass in considered open systems with their complex space-time structure of corresponding flows. In this case the conceptions of equilibrium and stability of isolated system can serve as useful idealization only in the simplest cases, as well as models of replenishment from above, below, or from side of the considered segment. In general, the main difficulty is that there are no sufficient observational data in order to separate such isolated system and thus to localize the consideration of causes and effects. In the future, for quantitative estimation of the degree of openness of one or another morphological element it is convenient to use so-called Triest numbers which represent the ratios of internal, external, and connecting flows of mass, momentum, and energy.

In order to describe the process of propagation of energetic particles, especially in those cases when the

mean free path of particles is comparable or large in comparison with the scale of magnetic structures considered, it is important to have an idea about topology of the interplanetary magnetic field. The long magnetic loops have long been known to exist in the heliosphere. Some of these loops have both ends on the Sun being extended far beyond the Earth's orbit. Observations of anisotropy of cosmic rays allow one to discover manifestations of such a loop structure of the disturbed magnetic field in the CR anisotropy in the heliosphere and in the events considered.

Let us estimate the intensity of electric field and current in the heliosphere electrojet on October 29 near the Earth's orbit. For order-of-magnitude estimates we assume that the solar wind velocity is 1 Mm/s, magnetic field strength is 20 nT, and the duration of crossing the electrojet is about 10 h. Hence, it follows that the transverse dimension of the electrojet is of order of 0.1 AU, the total current in it is about 1 GA, and the induction electric field in the solar wind is of order of 20 V/m. In this case, the unscreened electromotive force on the magnetosphere size about 40 Earth's radii across comprises about 5 MV. Inside the magnetosphere this external electric field is screened because of charge separation and finite resistance, which results in the field reduction by, roughly speaking, about an order of magnitude.

The interplanetary magnetic disturbance in this event has the form of a not quite regular wave train of three and even more periods of oscillations with increasing duration of these periods from 1–2 h in the beginning of the train up to a day in its end, with several crossings of zero and maxima in the north-south magnetic field component. Such a structure, apparently, was initiated near the Sun and formed on the path in the interplanetary space due to dynamic processes of compression on the leading edge and rarefaction on the trailing edge of a propagating disturbance. The short-period component of the variable electric field, external with respect to the Earth's magnetosphere, causes substorm intensifications, and three longest oscillations clearly manifest themselves in the indices of global geomagnetic activity. Every turn of the magnetic field to the south for a time of several hours is accompanied by the development of a new magnetic storm main phase, while the turn to the north terminates this development. The importance of processes of intensification and turns of the magnetic field due to free energy of plasma in the heliosphere is illustrated by Fig. 36, where, as an example, the results of calculation of a "drapery" of the interplanetary magnetic field around a supersonic coronal mass ejection are presented [3].

The observational data obtained at the moment allow us to make some general conclusions about the physical nature of the considered processes and some of their parameters. The flares and CMEs are the phenomena accompanying each other. They develop spontaneously and simultaneously as two observational manifestations of a single dissipative process in the solar atmosphere. In the course of this process at altitudes of about 10 Mm and higher the induction electric field is generated and exists for a time of order of ten minutes. This field is directed along the major axis of the arcade of magnetic loops with a length of order of some tenths of a gigameter. The electric field strength reaches 10 V/m, and effective electromotive force is of order of a few gigavolts. In these fields plasma transfers electric currents of order of several teraampers and drifts upwards with velocities of tens to many hundreds of kilometers per second. These rough estimates in general correspond to commonly assumed typical values of total power and dissipated energy in upper layers of the solar atmosphere during strong flares and CMEs. Separate groups of particles can be accelerated in this case to ultimately high energy which is admissible by the available electromotive force. This plasma and electrodynamic process in its entirety has locally well-pronounced nonlinear character with a great number of details which are complicated and even more rapidly variable. As far as the events under discussion are concerned the estimates presented here are rough and preliminary, though they are based on the totality of observational data. We emphasize that the estimate of recuperated free energy coming back to the lower layers of the solar atmosphere cannot be done reliably enough at the moment. It requires more accurate measurements of the parameters of plasma and emission. It is important to notice that not a single parameter but a whole hierarchy of controlling dimensionless parameters exists. They are interrelate temporal and spatial scales between themselves in different combinations, which jointly make the phenomena observed so complex and diverse, the more so because the laminar and turbulent structures coexist and are intermittent in space. The time of flight on the altitude scale determines the basic duration of CME development at a given altitude, however, in addition to this inertial scale, other factors also play important role.

The variations of electric currents and magnetic fields on time scales of hours or days deep inside the Sun under the photosphere is a cause of origination of the induction electric field. This is observed as a quick emergence in active regions of a new magnetic flux with a strength of some hundred gauss and more. The process encompasses not only active regions but their neighborhood too, where it looks as more delocalized, large-scale, and linear in its character. It goes without saying that in addition to inductions electric fields the potential electric fields are also developed. They are directed predominantly along the magnetic field, unlike the induction fields that originate and act across the field. Together, they form the common electric circuit of a solar flare and CME. The filed-aligned electric currents close the global circuit of induction currents, which are in this sense a visible prime cause of phenomena under consideration. To make clear the struc-

ture and dynamics of this circuit remains to be a topical problem.

The disposition and evolution of active regions demonstrate the global asymmetry on the Sun. In turn, they are controlled by more long-term variations of convective heat flows. These variations are much smaller in their relative amplitudes; however, their reservoir of free energy is enormous, and it serves as a main source of all observable manifestations of solar activity, including variations of luminosity, flares, and CMEs. In this sense, it is exactly here where one should search for a deeper prime mover of the phenomena under study.

The "heat engine" of the Sun is closely related to convective and radiation transfer of free energy in the solar interior, which proceeds basically at low Mach–Alfven numbers, i.e., at a relatively small involvement of the magnetic field. The solar "dynamo" in this sense is a product rather than prime cause of solar activity. The latter in this broader meaning is understood as a fundamental property of a star with relatively small variability of energy release and transfer in its interiors against the background of much greater steady energy flux supported by nuclear fusion processes in gravitationally confined core of the Sun. From this point of view the phenomena considered on the Sun are an example of a complex self-organization in a non-equilibrium open physical system with the fluxes of free energy and mass. The "magnetic degree of freedom" from this standpoint is subordinate and controlled by other, more powerful global processes. However, locally in some areas and at some time intervals this degree of freedom can be predominant over others, which is the case during flares. Here, we deal with all manifestations of well-known general laws of physics, characteristic for nonlinear processes with dissipation.

Thus, in flares and CMEs one can clearly trace a chain of energy transfer from the global to smaller scales and from slow variations to rapid changes. Simultaneously, there exists an inverse concurrent process: merging and dissipation of small and quickly variable structures with the formation of new large-scale and slowly varying irregularities. The very existence of hot solar corona as a whole can serve as simple and pictorial evidence of the importance of the inverse energy cascade. In other words, the situation is typical for unsteady and inhomogeneous turbulent states. As is known, the quantitative dynamical description of turbulent processes and forecasting their development are strongly limited by a number of circumstances related to the great number of possible degrees of freedom and to the difficulty to control them. Therefore, to study the prospects of forecasting the solar and heliospheric processes seems to be a topical scientific and applied problem.

At present, one can say little about the probability of appearance of extremely strong events of the type of those observed in October–November 2003 in the future solar activity or about the a posteriori probability in the past, since the level of our real knowledge in this area remains to be obviously insufficient. Observationally, we are dealing with a small amount of data about rare phenomena. For this reason they are not treatable statistically. Theoretically, there are difficulties in understanding, describing, and modeling the driving forces and energy sources of these processes. Nevertheless, in many respects the legendary solar flare observed by Carrington on September 1–2, 1859 together with a subsequent geomagnetic storm [31], situation in August 1972, and the phenomena of October–November 2003 considered in this paper have much common and similar in their nature and parameters. However, they do not exhaust all potential possibilities in this respect and surprises of the Sun. Further investigations of extreme events on the Sun, in the heliosphere, and in the magnetosphere seem to be interesting and important both in practical and theoretical aspects.

17. CONCLUSIONS

(1) We have collected and analyzed the new data about extremely strong manifestations of solar and heliospheric activity in October and November 2003. These manifestations turned out to be record in the values of a number of parameters.

(2) In addition to many well known phenomena, in the flare of October 29 a strong polarization of hard X-ray emission was discovered for the first time. It could be associated with bremsstrahlung of sufficiently narrowly directed electron beams at the tops of loop and arc structures in the solar atmosphere during the flare. The gamma ray and neutrons emissions were detected.

(3) The year 2003 corresponds to the phase of decline of the 23rd solar cycle determined using the smoothed number of solar flares. However, in addition to 11-year cycle there are clear cyclic and irregular variations of comparable amplitudes in many manifestations of solar and heliospheric activity on the time scales shorter than several years, several months, and even days. The variations on a large temporal scale (from one cycle to another) are equally strong.

(4) Manifestations of a global asymmetry of the Sun in the period under consideration are revealed and investigated. They are caused by the process in the solar interior. They are visible in the solar atmosphere and heliosphere as partially recurrent events due to rotation of the Sun.

(5) The strongest quickly variable and localized processes of the release of free energy in the solar atmosphere reveal themselves as coronal mass ejections and accompanying solar flares, which can be immediately observed and are related to each other by a single physical cause: dissipation of free energy. This energy is delivered from under the photosphere layers of the Sun and from accumulating reservoirs in the upper atmosphere, where it is redistributed between plasma and

electromagnetic fields, including the energy of detectable particles and radiations.

(6) The situation on the Sun and in the heliosphere in October–November 2003 was complicated and strongly disturbed. It is characterized by numerous events and processes comparable in intensity, densely located in space and time, and not always permitting to be considered as isolated because of nonlinear plasma and electrodynamic interactions between them.

(7) The strong geomagnetic storms in October–November 2003 were caused by the coronal mass ejections produced as a result of this nonstationary conditions on the Sun. CMEs carried to the Earth the fast plasma streams with sufficiently strong and prolonged magnetic fields of favorable southern orientation in the heliosphere.

ACKNOWLEDGMENTS

The work is partially supported by the Russian Foundation for Basic Research (RFBR, projects 02-02-16201, 02-02-17272, 03-02-16049, 03-02-16591, 04-02-16131, and 04-02-16736). It is also supported by the Ministry of Industry and Science of Russian Federation (Stable Contract 40.0221.1.1105 and grants NSh 477.2003.2, NSh 1455.2003.2, and NSh 2046.2003.2), and by the programs "Nonstationary Processes in Astronomy" of Russian Academy of Sciences, "Solar Wind" (program no. 18 of Division of Physical Sciences of RAS), "Universities of Russia" (grant 1877-04), and INTAS 03-51-6206. The authors also thank V.N. Oraevsky for a large contribution to the *Coronas* project. We are grateful to all persons and institutes presenting to our disposal the data of satellite and ground-based observations on the Internet, and to the staff of all cosmic ray stations whose data were used in this paper: Alma-Ata, Apatity, Barentsburg, Erevan, Irkutsk, Magadan, Moscow, cape Shmidt, Novosibirsk, Norilsk, Tixie, Yakutsk, Athens, Calgary, Climax, Haleakala, Hermanus, Junffraujoch, Kiel, Larc, Lomnitcky Stit, McMurdo, Oulu, Potchefstrom, Rome, Sanae, Tsumeb, Kergelen, and Terra Adelie. The authors also thank the collaborations *SOHO*/EIT and *SOHO*/LASCO for permission to use their data. The work of Russian cosmic ray stations is partially supported by RFBR grants 03-07-90389 and 04-02-16763, and US stations are supported by NSF grant ATM-0000315. K. Kudela thanks the APVT agency of Slovakia for support under the project 0259.

REFERENCES

1. Zastenker, G.N., Temnyi, V.V., D'Uston C., and Bosqued J.M., The Form and Energy of the Shock Waves from the Solar Flares of August 2, 4, and 7, *J. Geophys. Res.*, 1978, vol. 83, no. 3, pp. 1035–1041.
2. Cliver, E.W. and Hudson, H.S., CMEs: How Do the Puzzle Pieces Fit Together?, *J. Atmosph. and Solar-Terr. Phys.*, 2002, vol. 62, p. 1071.
3. Romashets, E., Vandas, M., and Nagatsuma, T., Evolution of Geoeffective Disturbances in Interplanetary Space, *Proc. Space Weather Workshop: Looking towards a European Space Weather Space Programme*, 2003, ESTEC, The Netherlands, pp. 59–62.
4. *Preliminary Report and Forecast of SOLAR – GEOPHYSICAL DATA*, Space Environment Services Center, Boulder, Colorado, USA: SESC PRF, 1991, 823, 824, p. 1.
5. Bothmer, V., Veselovsky, I.S., Dmitriev, A.V., *et al.*, Solar and Heliospheric Reasons for Geomagnetic Perturbations during the Growth Phase of the Solar Cycle 23, *Solar System Research*, 2002, vol. 36, pp. 498–505.
6. Yermolaev, Yu.I. and Yermolaev, M.Yu., Statistical Relationships between Solar, Interplanetary, and Geomagnetic Disturbances, 1976–2000: 3, *Kosm. Issled.*, 2003, vol. 41, no. 6, pp. 574–584.
7. Panasyuk, M.I. *et al.*, Magnetic Storms in October 2003, *Kosm. Issled.*, 2004, vol. 42, Present Issue.
8. Veselovsky, I.S., Heliospheric Electrojets: Their Structure and Magnetospheric Impacts, *Proc. 10th European Solar Physics Meeting*, ESA, SP-506, 2002, pp. 37–40.
9. Zhukov, A.N., Veselovsky, I.S., Clette, F., *et al.*, Solar Wind Disturbances and Their Sources in the EUV Solar Corona, *Solar Wind Ten*, Velli, M., Bruno, R., and Malara, F., Eds., AIP CP 679, Melville, New York: 2003, pp. 711–717.
10. Nusinov, A.A., Ionosphere as a Natural Detector for Studying Long-Term Variations in Fluxes of Solar Geoeffective Radiation, *Geomagn. Aeron.*, 2004, vol. 34, no. 5 (in press).
11. Zhitnik, I.A., Bougaenko, O.I., Delaboudiniere, J.-P., *et al.*, SPIRIT X-ray Telescope/Spectroheliometer Results, *Proc. of the 10th European Solar Physics Meeting*, ESA SP, 2002, vol. 506, pp. 915–918.
12. Oraevskii, V.N. and Sobel'man, I.I., Complex Studies of Solar Activity onboard the *Coronas-F* Satellite, *Pis'ma Astron. Zh.*, 2002, vol. 28, pp. 457–467.
13. Chertok, I.M. and Grechnev, V.V., Large-Scale Activity in Eruptive Events of October–November 2003, submitted for publication in *Astron. Zh.*, 2004.
14. Grechnev, V.V., Kuzin, S.V., Slemzin, V.A., and Chertok, I.M., Solar Eruptive Events of October–November 2003 by Data of the EUV Complex SPIRIT aboard of the *CORONAS-F* Satellite, *Space Weather*, 2004.
15. Chertok, I.M. and Grechnev, V.V., Large-Scale Canalized Dimmings Caused by Coronal Mass Ejections on the Sun, *Astron. Zh.*, 2003, vol. 80, pp. 162–174.
16. Chertok, I.M. and Grechnev, V.V., Large-Scale Dimmings Caused by Coronal Mass Ejections on the Sun according to the Data of SOHO/EIT in Four Lines of Extreme UF-Range, *Astron. Zh.*, 2003, vol. 80, pp. 1013–1025.
17. Bogod, V.M. and Tokhchukova, S.Kh., Specific Features of Microwave Radiation of Active Regions Generating Strong Solar Flares, *Pis'ma Astron. Zh.*, 2003, vol. 29, no. 4, pp. 305–316.
18. Gorgutsa, R.V., Gnezdilov, A.A., Markeev, A.A., and Sobolev, D.E., An Upgrade of the IZMIRAN's Digital Radio Spectrograph: First Results, *Astron. Astrophys. Transactions*, 2001, vol. 20, pp. 547–549.

19. Gorgutsa, R.V., Sobolev, D.E., Fomichev, V.V., and Chertok, I.M., An Eruptive Event with a Fast Drifting Radio Burst of Type II, in *Aktivnye protsessy na Solntse i zvezdakh* (Active Processes on the Sun in Stars), Sankt-Peterburg: St. Petersb. Gos. Univ., 2002, pp. 28–32.
20. Chertok, I.M., Fomichev, V.V., Gnezdilov, A.A., *et al.*, Solar Radio Emission in Extreme Events of October–November 2003 by IZMIRAN Data, *Space Weather*, 2004 (in press).
21. Thomson, N.R., Rodger, C.J., and Dowden, R.L., Ionosphere Gives Size of Greatest Solar Flare, *Geophys. Res. Lett.*, 2004, vol. 31.
22. Kaufmann, P., Raulin, J.-P., Gimeĭnez de Castro, C.G., *et al.*, A New Solar Burst Spectral Component Emitting Only in the Terahertz Range, *Astrophys. J.*, 2004, vol. 603, pp. L121–L124.
23. Denisov, Yu.I., Kuznetsov, S.N., Logachev, Yu.I., *et al.*, Hard X-ray Emission of Solar Flares in the Second Half of 2001: Preliminary Results of an Experiment with the SPR-N Instrument onboard the *Coronas-F* Station, *Astron. Vestn.*, 2003, vol. 37, p. 127.
24. Tindo, I.P., Ivanov, V.D., Mandel'shtam, S.L., *et al.*, Discovery of Polarization of X-ray Emission of Solar Flares, *Kosm. Issled.*, 1971, vol. 9, p. 116.
25. Coburn, W. and Boggs, S.E., Polarization of the Prompt Gamma-Ray Emission from the Gamma-Ray Burst of 6 December 2002, *Nature*, 2003, vol. 423, p. 415.
26. Lopez, R.E., Baker, D.N., and Allen, J., Sun Unleashes Halloween Storm, *EOS*, 2004, vol. 85, no. 11, pp. 105–108.
27. Mitrofanov, I.G., Litvak, M.L., Kozyrev, A.S., *et al.*, A Search for Water in Martian Soil Using the Data of Global Mapping of Neutron Fluxes Measured by the Russian Instrument HAND onboard the NASA Project 2001 Mars Odyssey, *Astron. Vestn.*, 2003, vol. 37, no. 5, pp. 400–412.
28. Shea, M.A. and Smart, D., A Summary of Major Solar Proton Events, *Solar Physics*, 1990, vol. 127, pp. 297–320.
29. Dorman, L.I., Smirnov, V.S., and Tyasto, M.I., *Kosmicheskiye luchi v magnitnom pole Zemli* (Cosmic Rays in the Earth Magnetic Field), Moscow: Nauka, 1971.
30. Belov, A.V., Eroshenko, E.A., Oleneva, V.A., *et al.*, What Determines the Magnitude of Forbush Decreases?, *Adv. Space Res.*, 2004, vol. 27, pp. 625–630.
31. Tsurutani, B.T. *et al.*, The Extreme Magnetic Storm of 1–2 September, 1859, *J. Geophys. Res.*, 2003, vol. 108(A7).
32. Dvornikov, V.M., Sdobnov, V.E., and Yudina, M.V., Mechanism of Cosmic Ray Modulation by Regular Electromagnetic Fields of the Heliosphere, *Astron. Vestn.*, 2004 (in press).
33. Dvornikov, V.M. and Sdobnov, V.E., Variations in the Rigidity Spectrum and Anisotropy of Cosmic Rays at the Period of Forbush Effect on the 12–25 July, 1982, *Intern. J. Geomagn. Aeron.*, 2002, vol. 3, no. 3, pp. 217–228.
34. Debrunner, H., Flueckiger, E., von Mandach, H., and Arens, M., Determination of the Ring Current Radii from Cosmic Ray Neutron Monitor Data for the 17 December 1971 Magnetic Storm, *Planet. Space Sci.*, 1979, vol. 27, pp. 577–581.
35. Flueckiger, E.O., Smart, D.F., and Shea, M.A., On the Effect of Magnetospheric Current Systems on Cosmic Ray Cutoff Rigidities, *Proc. 17th ICRC, Paris*, 1981, vol. 4, pp. 244–247.
36. Baisultanova, L., Belov, A., and Yanke, V., Magnetospheric Effect of Cosmic Rays within the Different Phases of Magnetic Storms, *Proc 24-th ICRC*, 1995, vol. 4, pp. 1090–1094.
37. Charakhch'yan, A.N., Investigation of Intensity Fluctuations of Cosmic Rays in Stratosphere Caused by Processes on the Sun, *Usp. Fiz. Nauk*, 1964, vol. 83, no. 1, pp. 35–62.